Central Time-of-Flight Counter Performance Details

D.S. Carman, Jefferson Laboratory

report-aug15.tex

August 31, 2015

Abstract

This document highlights the performance of the CTOF counters based on the initial cosmic ray studies. The data were investigated in order to make recommendations on which scintillation bars need to be resurfaced due to surface quality issues.

1 Overview

This document contains a series of plots, both "higher level" and "lower level", to highlight the performance of the individual CTOF counters based on the initial cosmic ray studies in the CTOF cosmic ray test stand. The goal of this report is to show the level of performance of the counters and make recommendations on which scintillation bars need to be resurfaced due to surface quality issues. For this purpose a counter "quality factor" has been defined based on comparisons with a "good" reference counter. The recommendation for which counters to resurface are based on those counters with the lowest quality factor.

In the CTOF cosmic ray test stand the counters are positioned on their sides in vertical stacks. There are six storage carts, each containing eight counters. Within each cart the counters are separated by ≈21 cm. The counters are aligned relative to each other to better than ±0.5 cm in all dimensions. The data shown here were collected using a so-called triplet trigger, defined by the logical OR over all consecutive groups of 3 counters. A counter satisfied its part of the triplet trigger with coincident signals from both the upstream and the downstream PMTs above threshold. For the first cart, containing counters #1 → #8 the trigger definitions are given by:

C1 = 1U · 1D	C2 = 2U · 2D
C3 = 3U · 3D	C4 = 4U · 4D
C5 = 5U · 5D	C6 = 6U · 6D
C7 = 7U · 7D	C8 = 8U · 8D

$$\begin{aligned}\text{TRIGGER}_{\text{CART\#1}} &= (C1 \cdot C2 \cdot C3) + (C2 \cdot C3 \cdot C4) + (C3 \cdot C4 \cdot C5) \\ &\quad + (C4 \cdot C5 \cdot C6) + (C5 \cdot C6 \cdot C7) + (C6 \cdot C7 \cdot C8)\end{aligned}$$

The global triplet trigger is then defined as:

$$\begin{aligned}\text{TRIGGER} &= \text{TRIGGER}_{\text{CART\#1}} + \text{TRIGGER}_{\text{CART\#2}} + \text{TRIGGER}_{\text{CART\#3}} + \\ &\quad \text{TRIGGER}_{\text{CART\#4}} + \text{TRIGGER}_{\text{CART\#5}} + \text{TRIGGER}_{\text{CART\#6}}.\end{aligned}$$

The global trigger rate summed over all counter triplets is roughly 2 to 3 Hz.

The anode signals from the PMTs are run to 90/10 signal splitters. The 90% signal outputs are connected to Ortec 934 CFDs and to CAEN V1290a high resolution (25 ps LSB) TDCs. The 10% signal outputs are connected to the JLab FADCs. Furthermore, all PMTs were fully gain-matched by adjusting the high voltage settings to put the muon peak in the average ADC spectrum in a particular channel (channel 5000).

2 Higher-Level Plots

The higher-level plots are the extracted resolutions from the counters as a function of coordinate (as reconstructed from the TDC time difference measurements) and as a function of the ADC pulse height. These results are still a work in progress given the ongoing optimization of the time-walk settings of the CFDs. The time resolution for each counter is extracted by comparing its average hit time to the average hit time measured by the other two counters of the triplet. The detailed approach is to define a time residual given by:

$$\begin{aligned}t^m_{res} &= t_m - \frac{1}{2}(t_t + t_b) \\ &= \frac{1}{2}(t^U_m + t^D_m) - \frac{1}{2}\left[\frac{1}{2}(t^U_t + t^D_t) + \frac{1}{2}(t^U_b + t^D_b)\right],\end{aligned}$$

where the subscripts m, t, and b represent the middle, top, and bottom counters of a triplet respectively. For the case where the counter is on the top or bottom of the vertical stack in a given cart, the residual definition becomes either:

$$\begin{aligned}t^t_{res} &= t_t - \frac{1}{2}(t_m + t_b - \Delta L/c) \\ t^b_{res} &= t_b - \frac{1}{2}(t_t + t_m - \Delta L/c),\end{aligned}$$

respectively. Here $\Delta L/c$ accounts for the path length difference between the middle of the reference counter and the mid-point between the other two counters used to compute the residual. From these residual definitions, the counter resolution can be expressed in terms of the width of this residual time as:

$$\sigma_{counter} = \frac{2}{\sqrt{6}}\delta t_{res}. \tag{1}$$

Figs. 1 and 2 show the counter resolution as a function of the coordinate reconstructed from the TDC time difference. Figs. 3 and 4 show the counter resolution as function of the mean ADC value for the counter. These data were acquired during a week-long cosmic ray run.

2.1 Results and Interpretation

The resolutions for all counters are reasonably consistent with averages varying at the ± 10 ps level due to non-optimized time-walk settings, counter mis-alignments, and detector performance issues. Based on initial inspection of the data there was clear evidence of problems with several of the counters that were found to be due to surface crazing effects (i.e. micro-cracks) that resulted in loss of light along the counters. The signature of these effects was highly non-uniform distributions in the plots of ADC_U vs. ADC_D for the counters. To date, four of the counters have been resurfaced and repolished. These are #37, #44, #46, and #48. In these four counters the crazing effects were not uniform across the four surfaces of the scintillation bars, but were localized to relatively limited regions, typically on multiple surfaces of the bars. For counter #37 the crazing was mostly limited to one 10-in-long section on one face about the middle of the bar. For counter #44, the problems were located to a 8-in-long section that spread across the downstream end of the counter and covered two faces. For counter #46, the crazing problems were seen on multiple faces near the ends of the bar. Counter #48 wasn't in particularly bad shape to begin with, but did have a depletion near the center of the ADC correlation distribution that was initially thought to be evidence of a surface problem. Ultimately due to the presence of crazing evidence seen on all four faces of these bars, we resurfaced all four faces of each bar. This work was carried out with the counters mounted in their storage carts.

The resurfacing procedure employed a hand-held orbital sander. Sandpaper grits from 280 to 6000 (280, 400, 600, 1000, 1500, 2000, 3200, 4000, 6000) were employed using a continuous stream of water during sanding to ensure proper cooling of the scintillation material. The crazing was a surface-related property. Our estimates indicated that it was localized to within $\approx$50 μm of the surface. In order to ensure that the micro-cracks would not continue to propagate further into the scintillation bars, it is necessary to aggressively sand the scintillation bars to get below the original level of the cracks. After the re-surfacing work was completed, the bars went through a polishing phase in an attempt to return the surface to a mirror-like finish. For this task we employed hand-polishing of the bars. The first polishing phase employed a liquid polish (Novus Heavy Scratch Remover followed by Novus Fine Scratch Remover) as recommended by the scintillator manufacturer (Eljen Technologies). We then employed a polishing compound in three steps of decreasing grit (Extec 1 μm Alpha Alumina powder, Extec 0.3 μm Alpha Alumina powder, and Extec 0.05 μm Gamma Alumina powder). After each sanding or polishing step, the counter was washed down first with tap water that included Ivory liquid and then with tap water. This was necessary to remove grit and debris from the previous sanding or polishing step.

The before/after comparisons of the ADC_U vs. ADC_D distributions for the four resurfaced counters are shown in Figs. 5 and 6. The effect of the surface quality issues result in loss of light collected at the PMTs. The yellow lines shown in Figs. 5 and 6 are fixed reference lines for each counter. Clearly after the resurfacing work the light distribution is much more uniform across the bars.

Further information about the counters can be seen by comparing the coordinate reconstruction from the TDC information to that reconstructed from the ADC information before and after the resurfacing. These coordinate distributions are given by:

$$\begin{aligned} \mathrm{coor_{TDC}} &= \frac{v_{eff}}{2}(t_U - t_D) \\ \mathrm{coor_{ADC}} &= \frac{\lambda}{2}\log\left(\frac{ADC_U}{ADC_D}\right). \end{aligned}$$

The comparisons of these coordinate distributions before and after the resurfacing work for counters #37, #44, #46, and #48 are shown in Figs. 7 to 10. The surface quality issues do not result in a loss of efficiency for the counter (as seen in the uniform coordinate distributions from the TDC data), but in a loss of light. This decrease in photon statistics impacts the time resolution. The comparison of the measured time resolution vs. coordinate before and after the counter resurfacing for the four bars is shown in Fig. 11. After the resurfacing the resolution is better in all cases and is more symmetric about the middle of the counter. Note that the apparent improvements in the resolution appear somewhat modest, however after the resurfacing work the ADC distributions are much more uniform. This better enables the ADC information to be used for particle identification via the dE/dX method.

Note that in Figs. 5 to 6 there are "micro-structures" seen in the ADC distributions that show up as diagonal bands. These micro-structures do not result in a uniform distribution of ADC values. These same microstructures show up in Figs. 7 to 10 as peaks and dips in the coordinate distributions reconstructed from the FADC data. At first this was believed to be a signature of surface quality effects resulting in loss of light. However, after studying all 48 counters it is apparent that this is actually a binning effect associated with the 250 MHz clock of the FADCs. Looking at the raw ADC distributions from the FADC (see Fig. 12), there are only six samples across the ADC muon peak distribution. This sampling gives rise to a discrete ADC distribution instead of a continuous ADC distribution. In the near future we plan to study these distributions replacing one of our FADC modules with a charge integrating ADC to ensure that we understand what we are seeing in the FADC data.

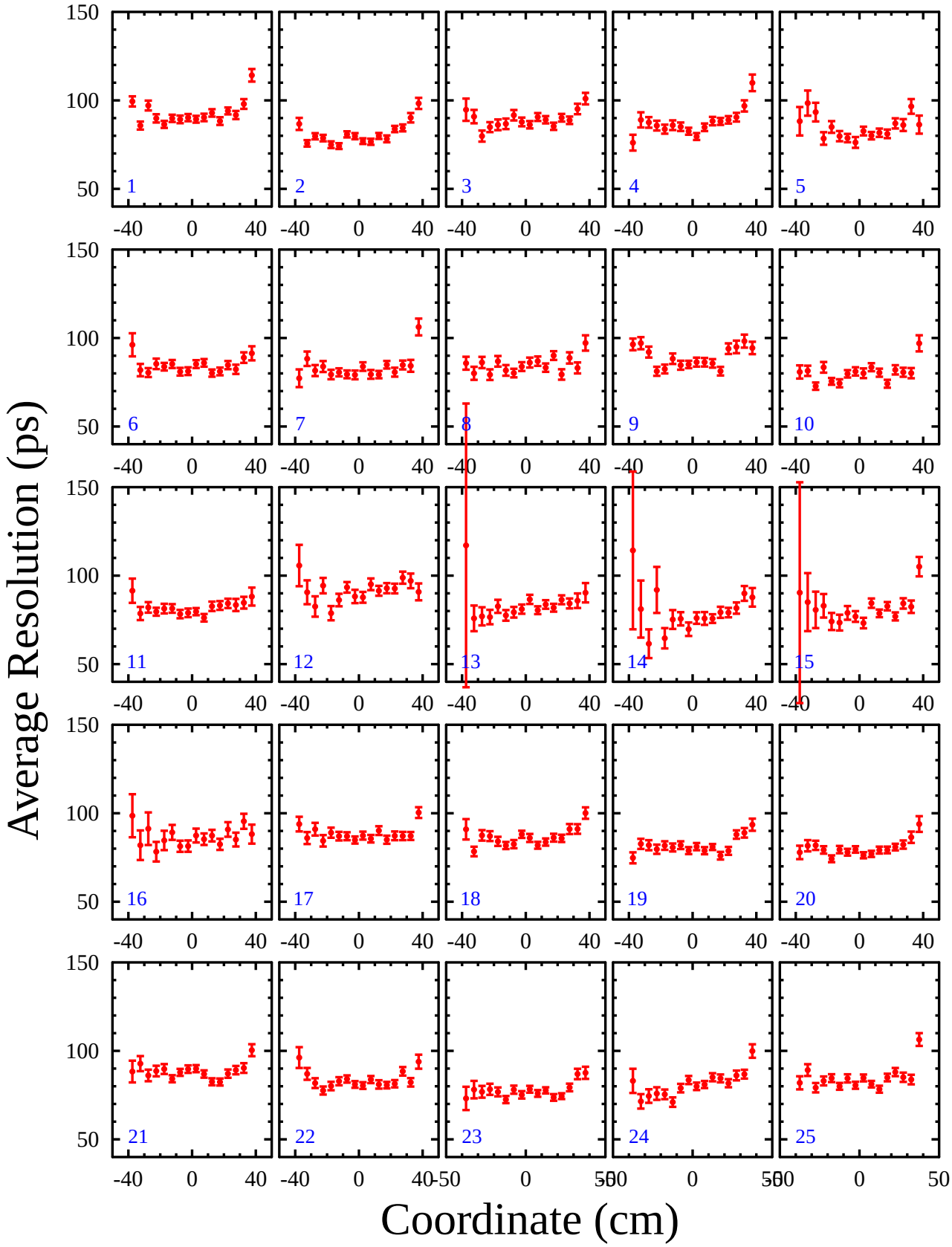

Figure 1: Measured counter resolution vs. coordinate for counters #1 to #25 from run 6387.

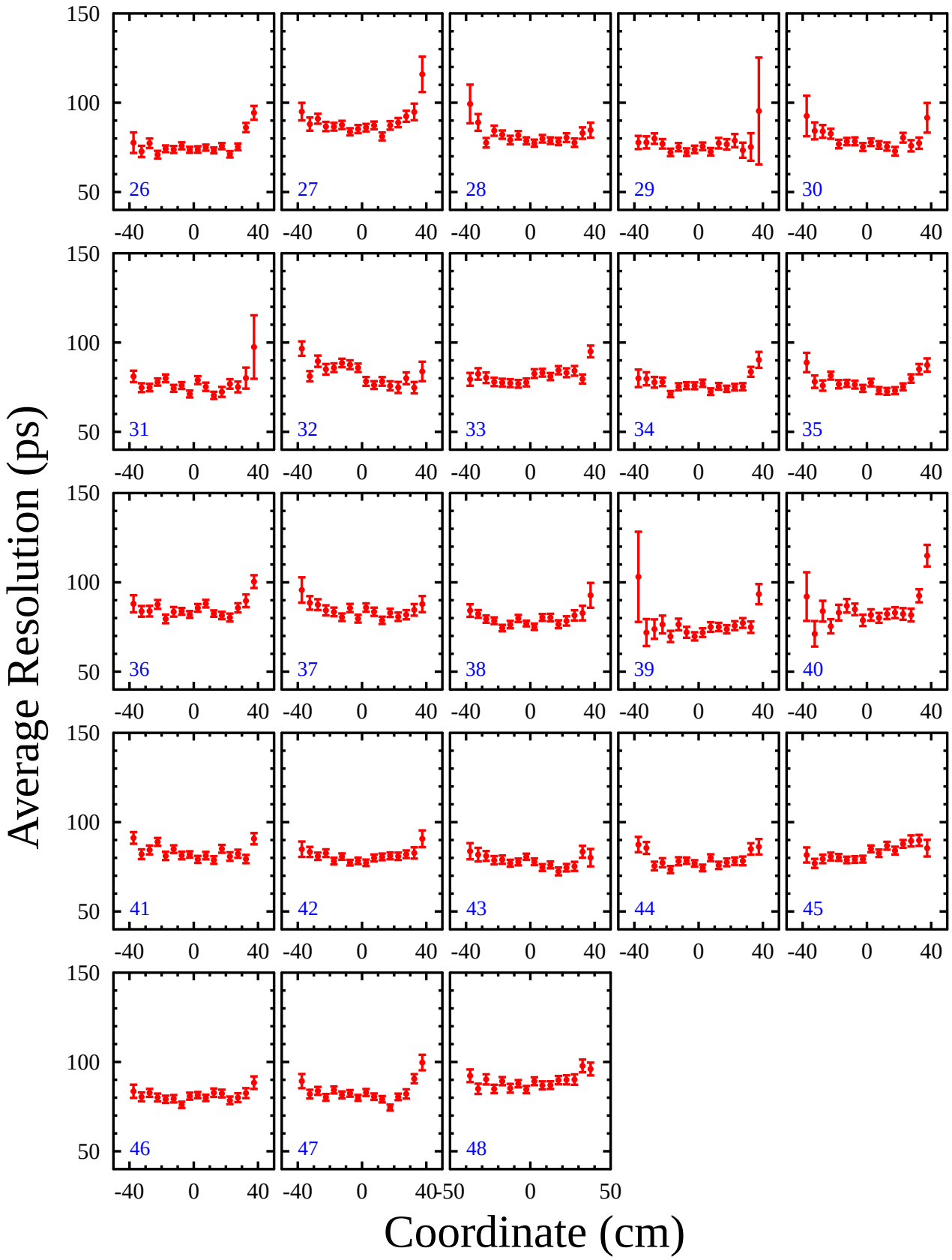

Figure 2: Measured counter resolution vs. coordinate for counters #26 to #48 from run 6387.

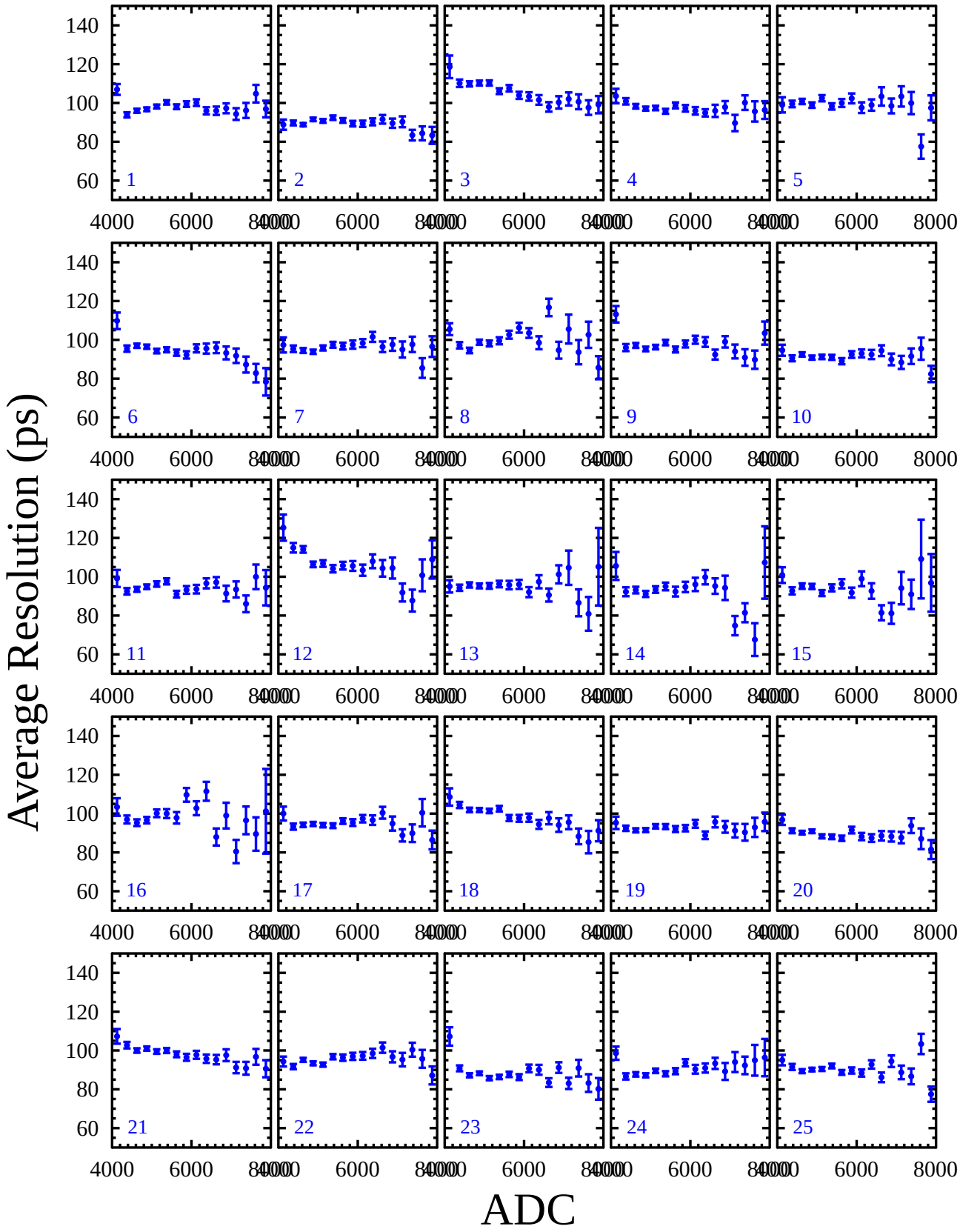

Figure 3: Measured counter resolution vs. ADC for counters #1 to #25 from run 6387.

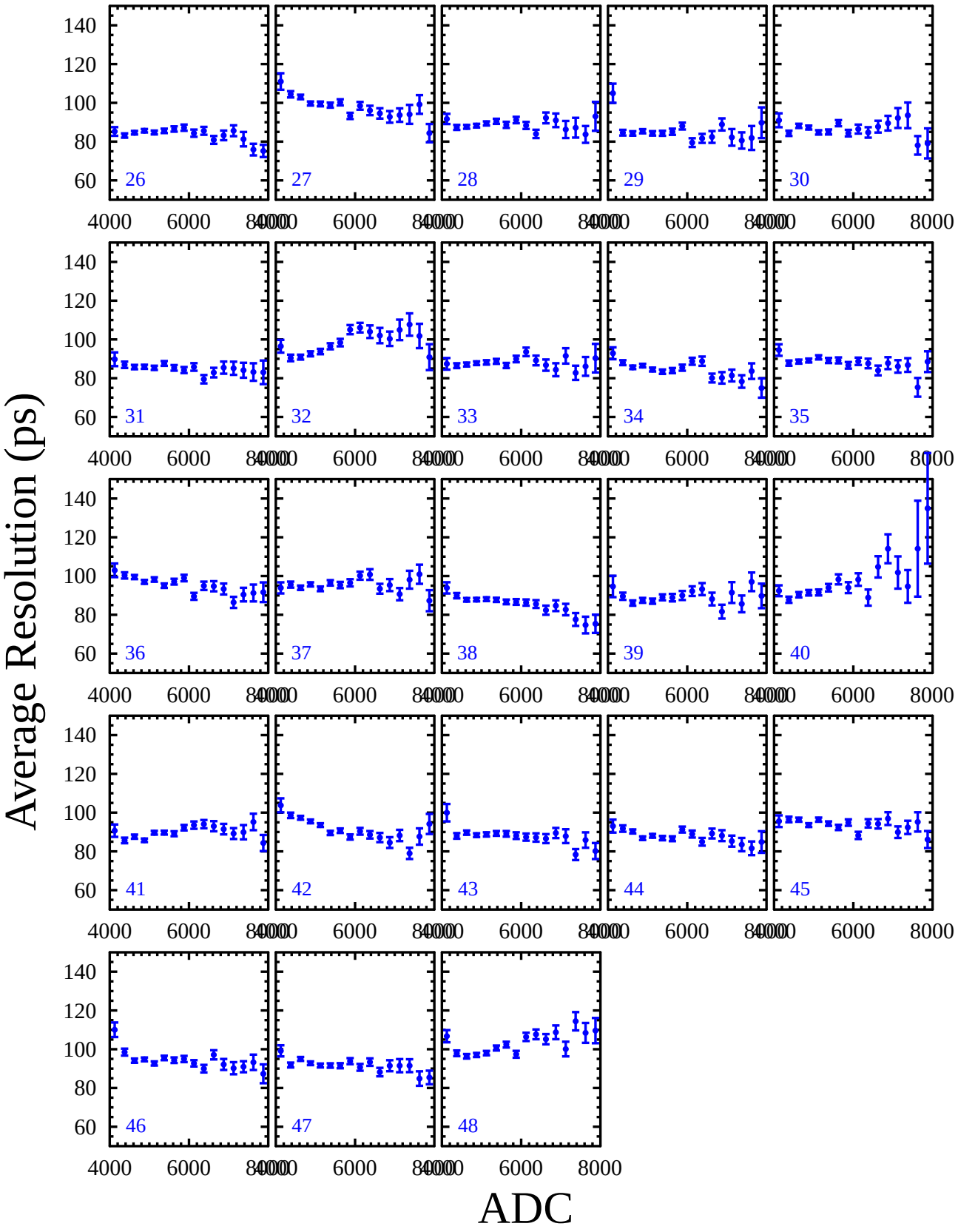

Figure 4: Measured counter resolution vs. ADC for counters #26 to #48 from run 6387.

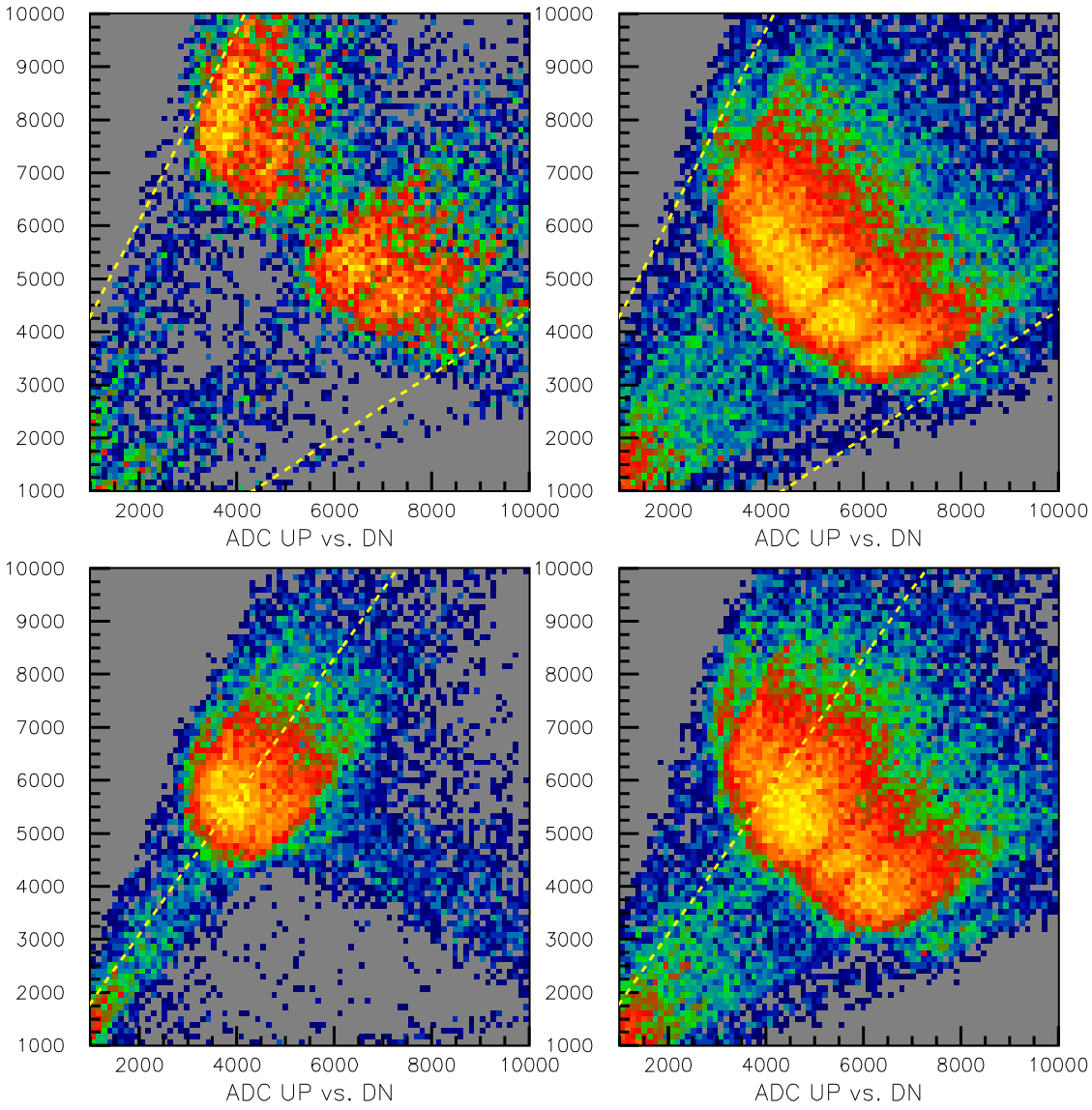

Figure 5: Plots of ADC_U vs. ADC_D for counter #37 (top) and counter #44 (bottom) before polishing (left) and after polishing (right). The yellow lines are drawn for reference and explained in the text.

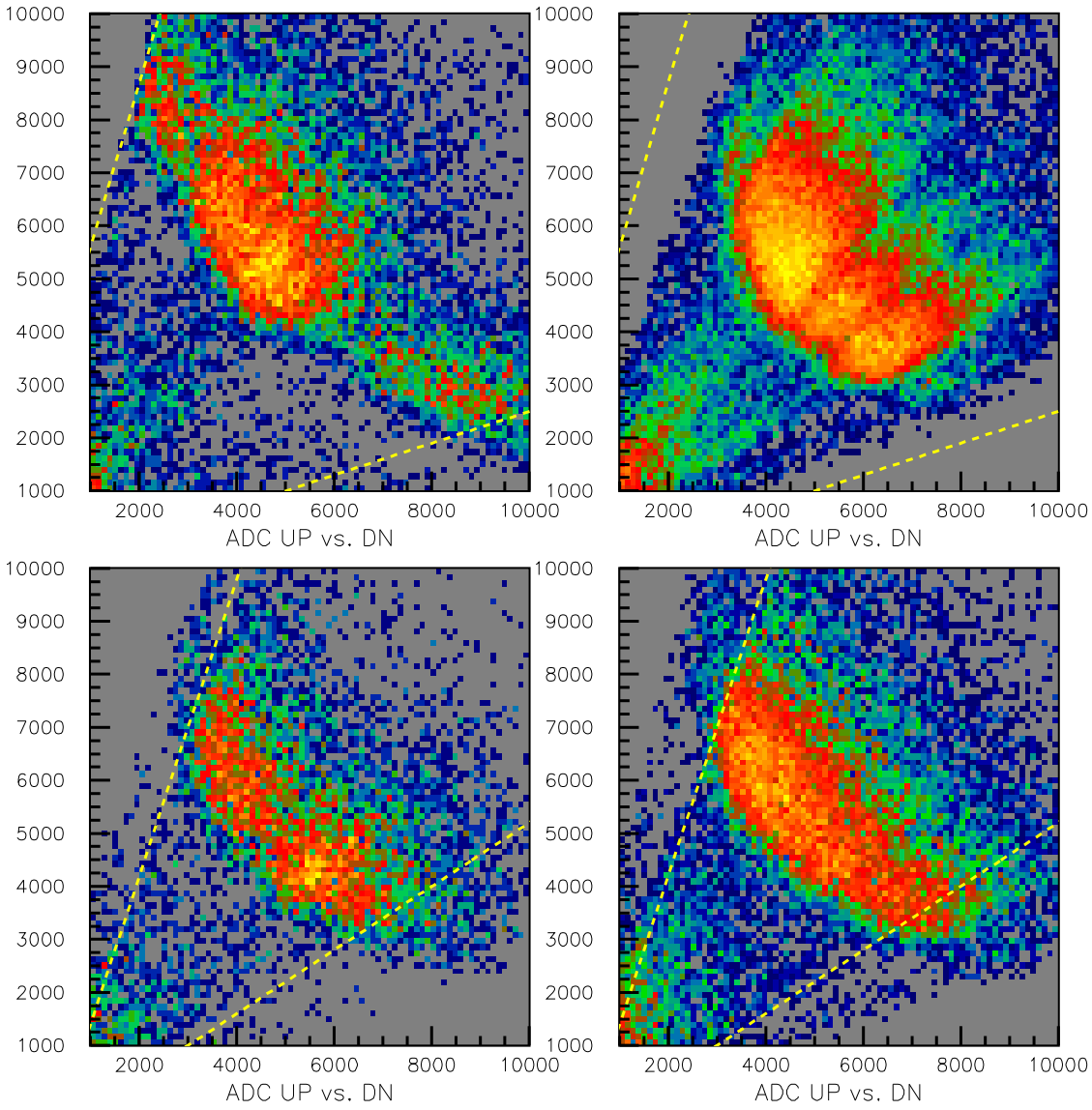

Figure 6: Plots of ADC_U vs. ADC_D for counter #46 (top) and counter #48 (bottom) before polishing (left) and after polishing (right). The yellow lines are drawn for reference and explained in the text.

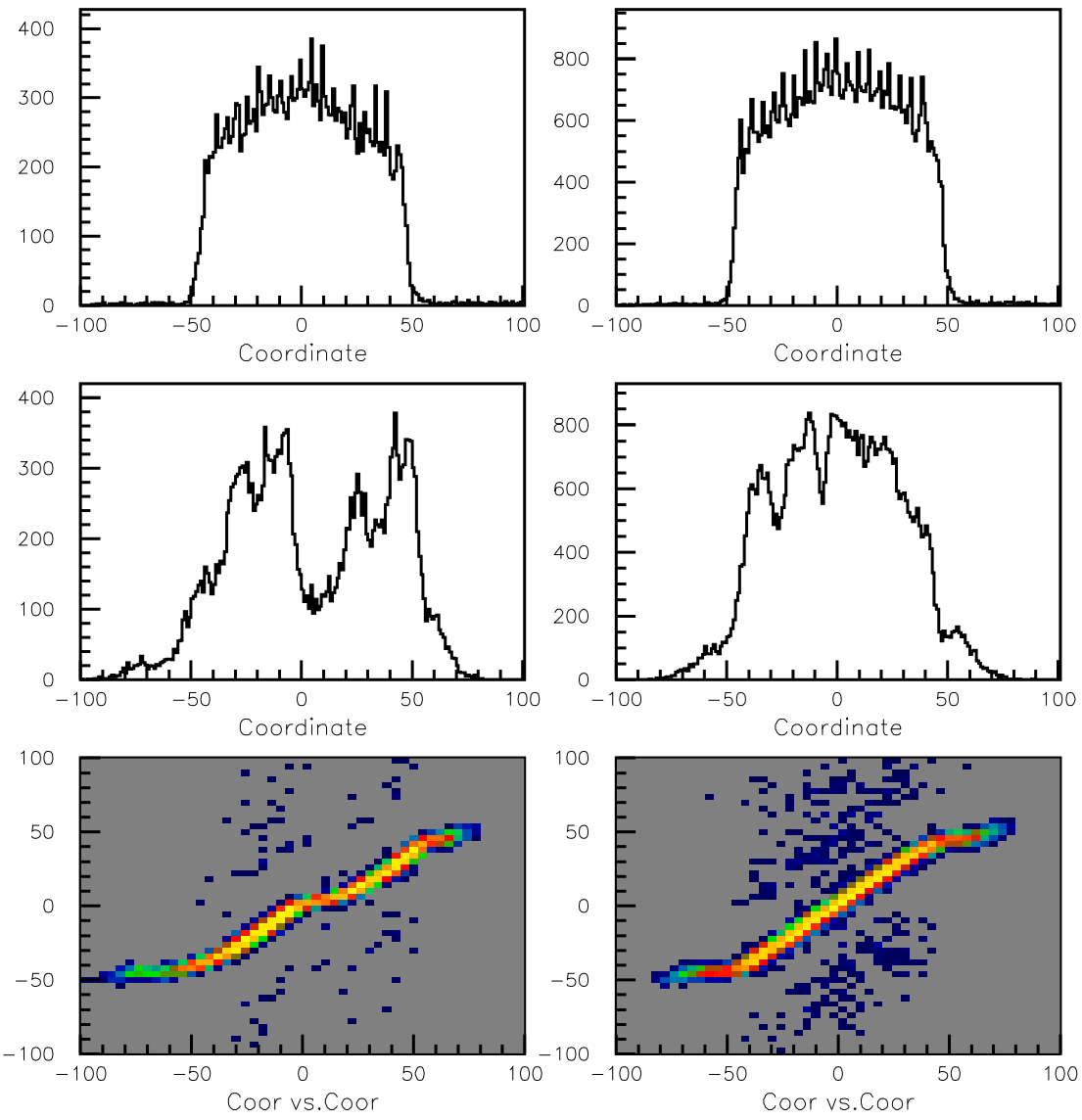

Figure 7: Counter #37. Plots of coordinate from TDC time (top), coordinate from ADC ratio (middle), and the correlation plot of coordinate (TDC) vs. coordinate (ADC) (bottom). (Left) before polishing. (Right) after polishing.

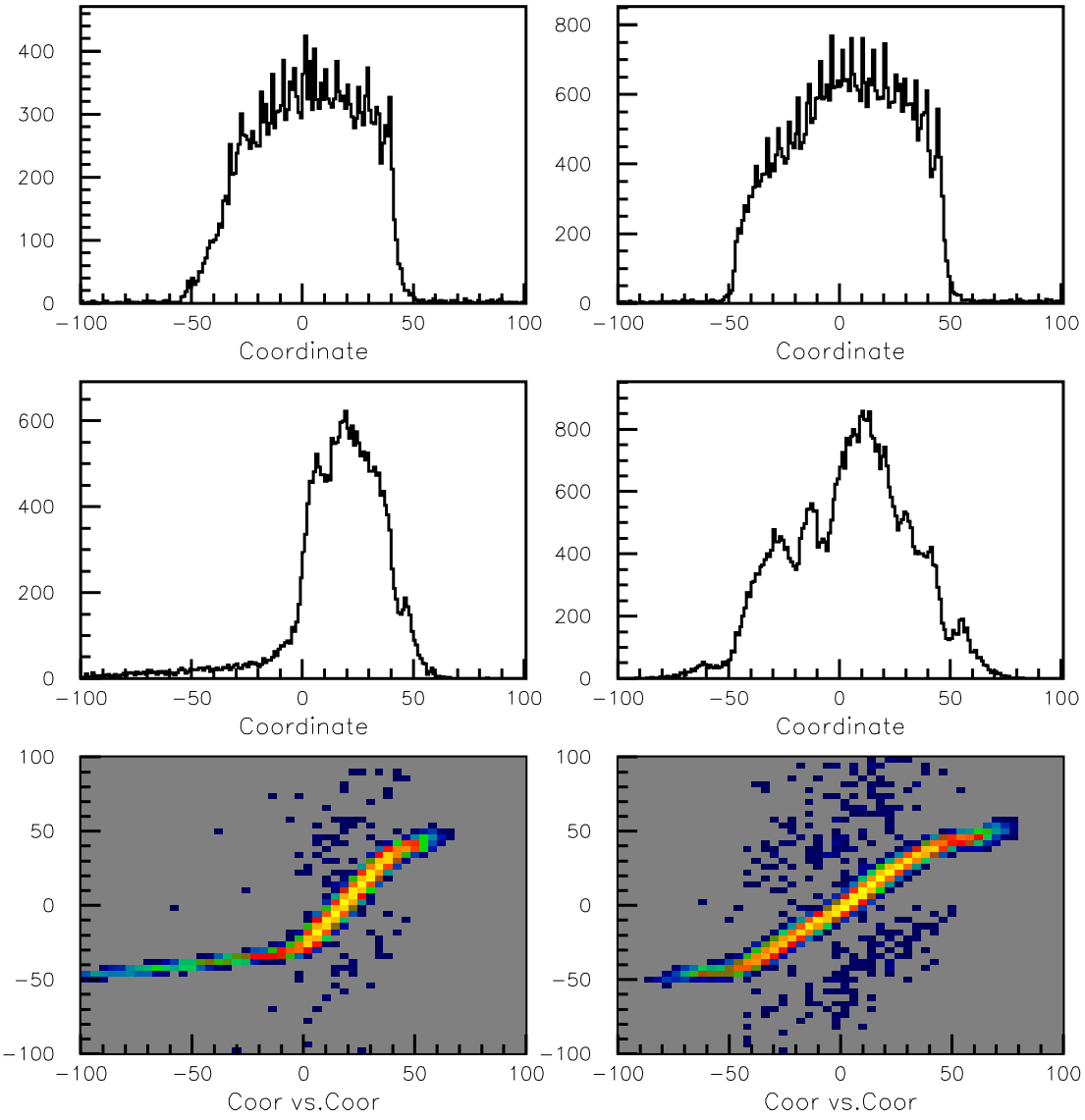

Figure 8: Counter #44. Plots of coordinate from TDC time (top), coordinate from ADC ratio (middle), and the correlation plot of coordinate (TDC) vs. coordinate (ADC) (bottom). (Left) before polishing. (Right) after polishing.

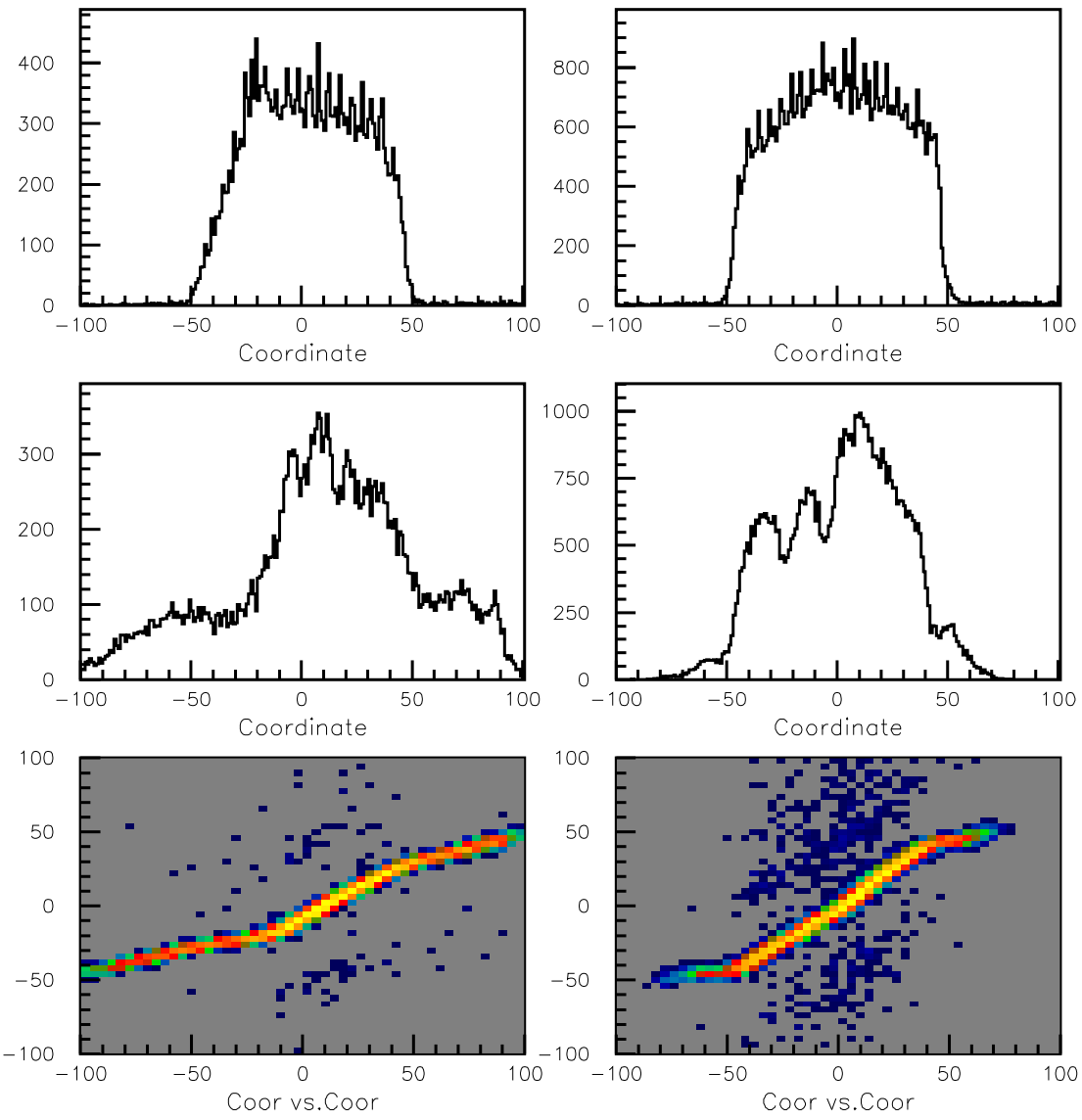

Figure 9: Counter #46. Plots of coordinate from TDC time (top), coordinate from ADC ratio (middle), and the correlation plot of coordinate (TDC) vs. coordinate (ADC) (bottom). (Left) before polishing. (Right) after polishing.

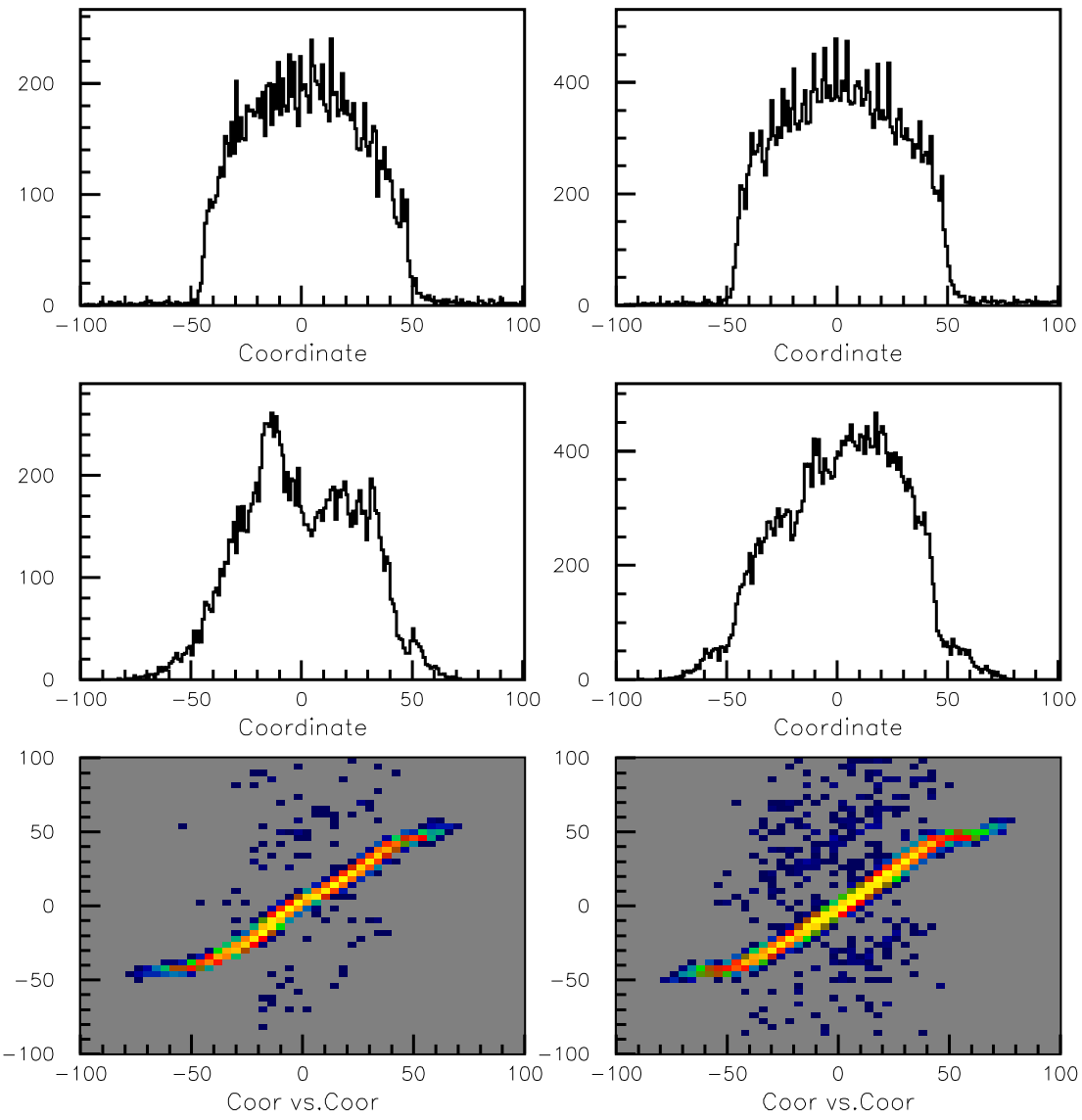

Figure 10: Counter #48. Plots of coordinate from TDC time (top), coordinate from ADC ratio (middle), and the correlation plot of coordinate (TDC) vs. coordinate (ADC) (bottom). (Left) before polishing. (Right) after polishing.

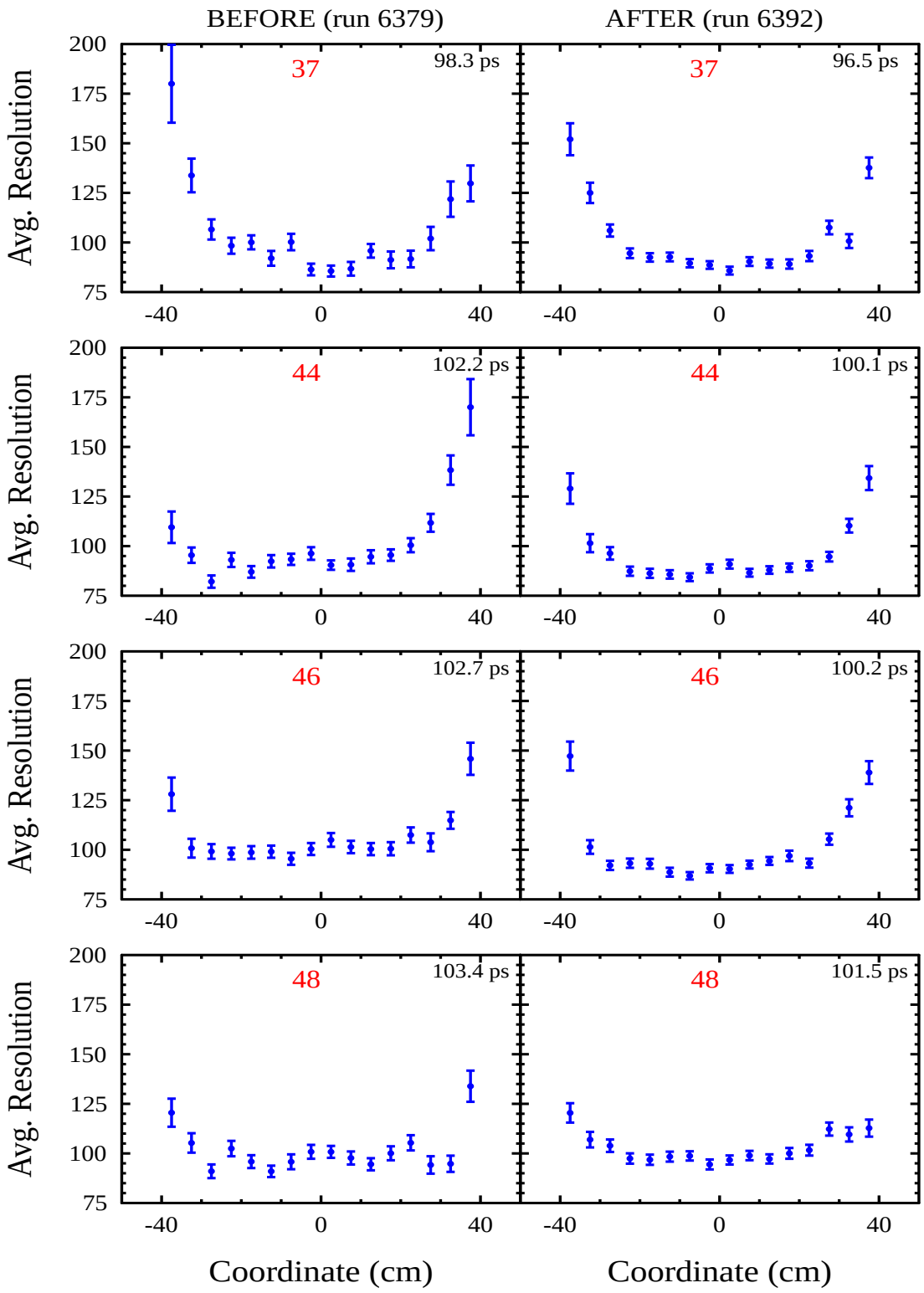

Figure 11: Plots of resolution (ps) vs. coordinate (cm) for counters #37, #44, #46, and #48 before (left) and after (right) repolishing. The number listed on the upper right of each plot gives the average resolution for the counter.

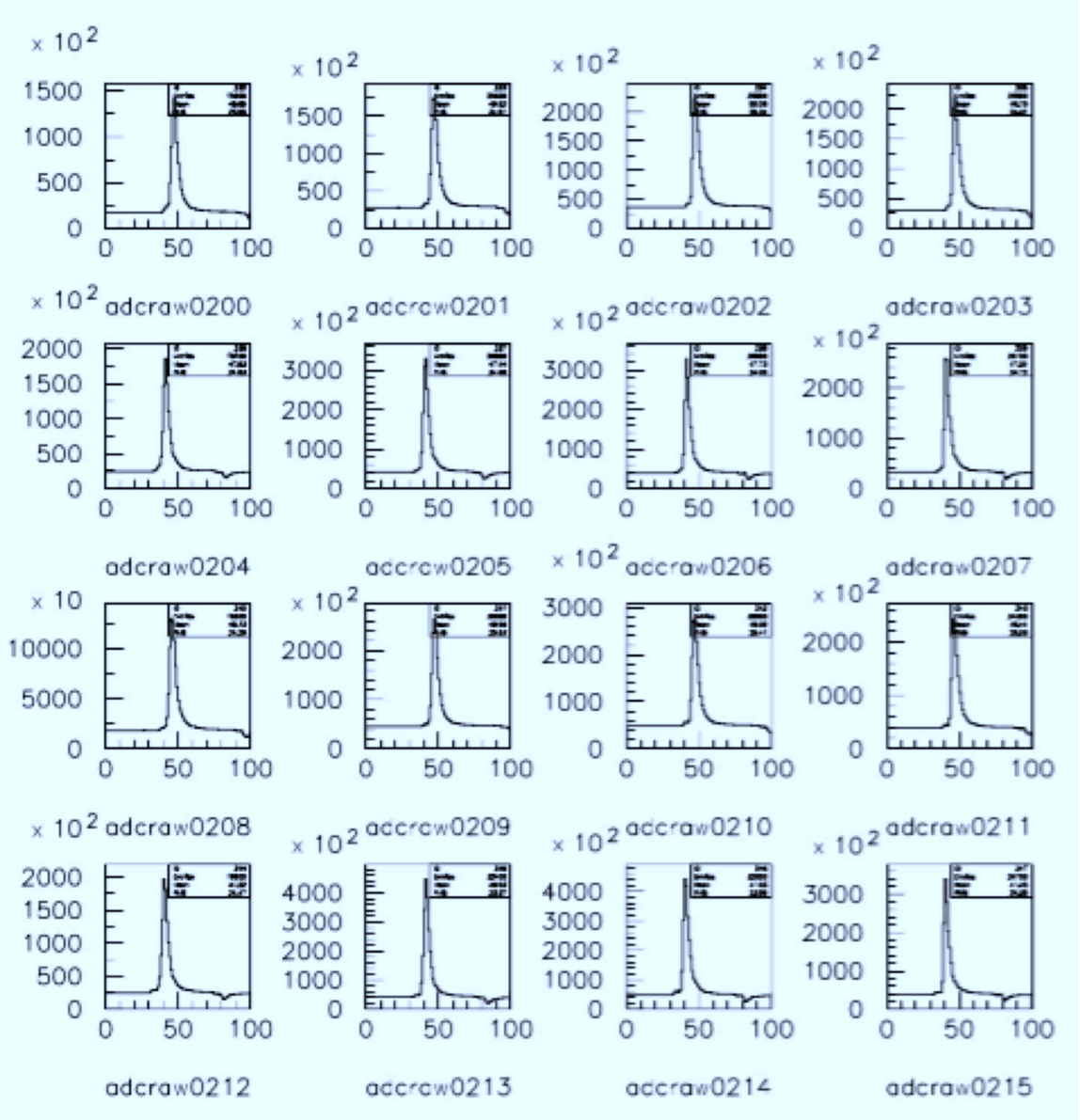

Figure 12: Distributions of the raw ADC for the counters in one FADC module showing the number of samples associated with each pulse. The bin width is given by the 250 MHz clock (4 ns bins) of the module.

3 Lower-Level Plots

In this section the lower-level plots for each counter are shown. The plots for each counter are the same five sub-figures:

- UL: Reconstructed coordinate from the TDC difference distributions.
- LL: Reconstructed coordinate from the ADC ratios (black) overlaid with a fit from the coordinate distribution of our reference "good" counter (blue).
- UR: ADC_U vs. ADC_D
- LR: ADC_U (top) and ADC_D (bottom)

Note that the regular spikes in the coordinate distribution from the TDCs are associated with the 25 ps LSB from the CAEN 1190 high-resolution TDCs. The reference counter chosen to compare against all other counters is counter #17. The fit of the ADC-based coordinate distribution from counter #17 is fit to the ADC-based coordinate distributions of all other counters. The χ^2 of these fits is used to define the counter quality factor. The data for each of the 48 CTOF counters is shown in Figs. 13 to 60. In this naming convention, counters #1 to #24 are the CTOF counters with the low-pitch angle upstream light guide design and counters #25 to #48 are the counters with the high-pitch angle upstream light guide design.

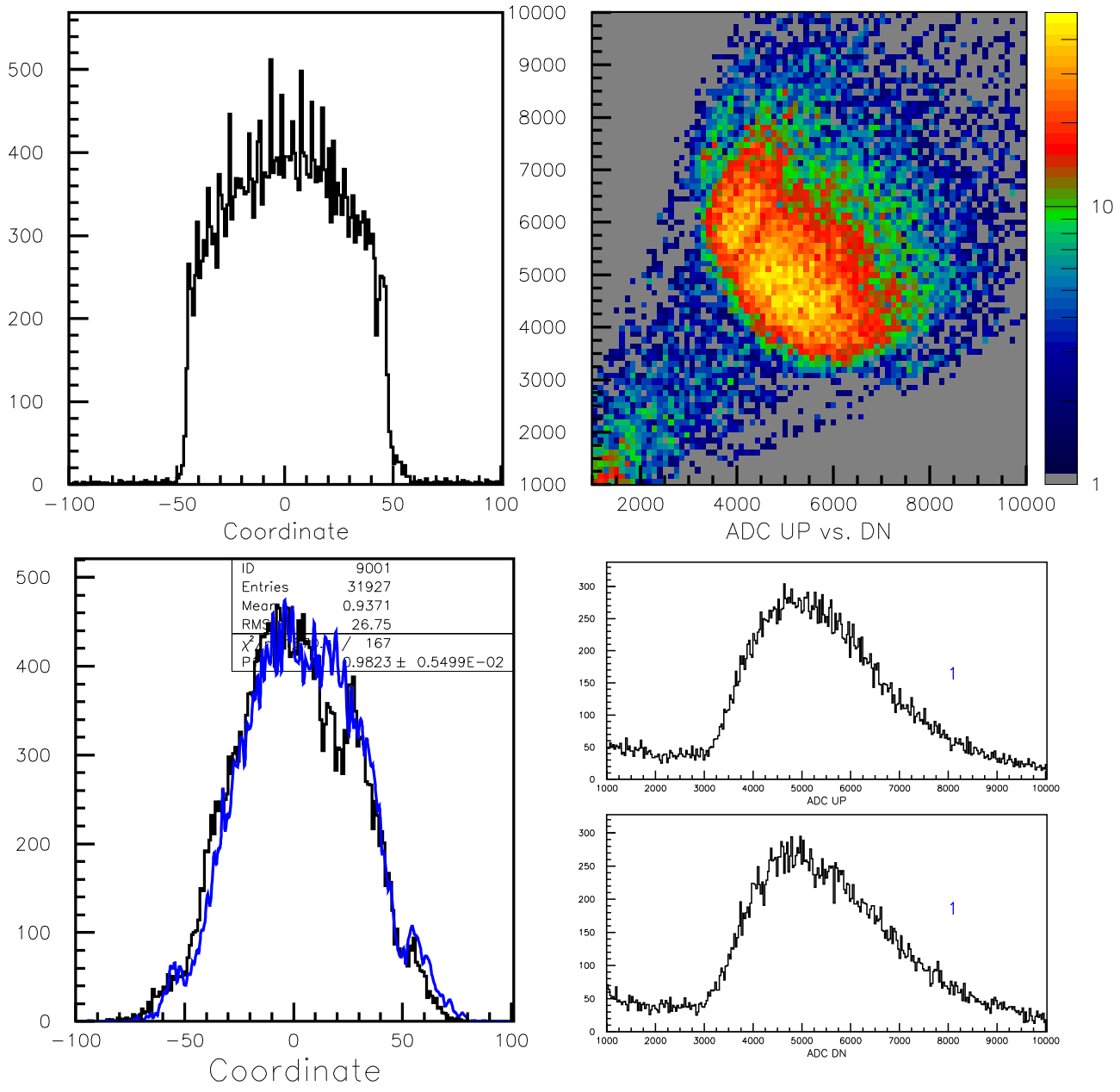

Figure 13: Data for counter #1.

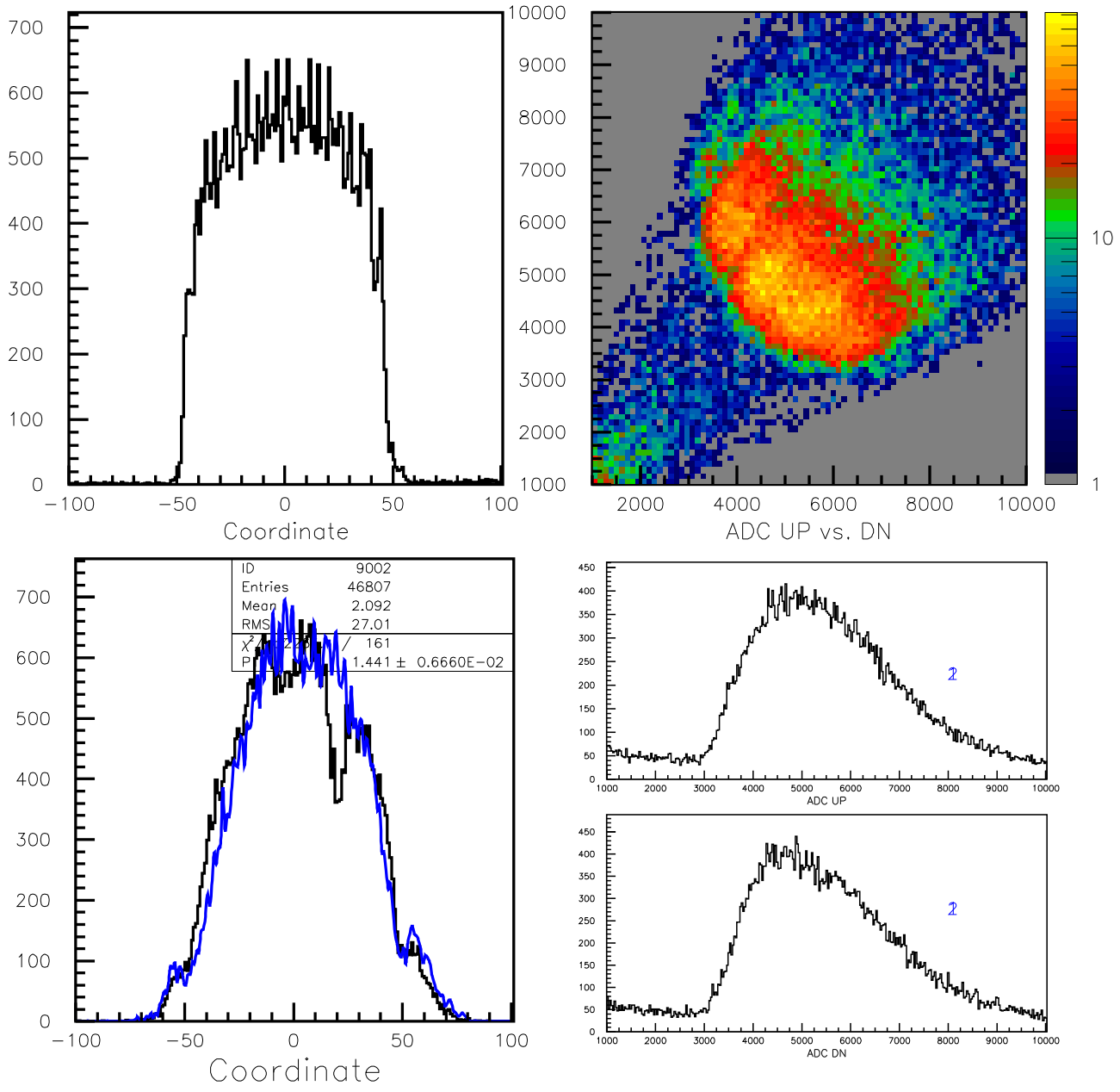

Figure 14: Data for counter #2.

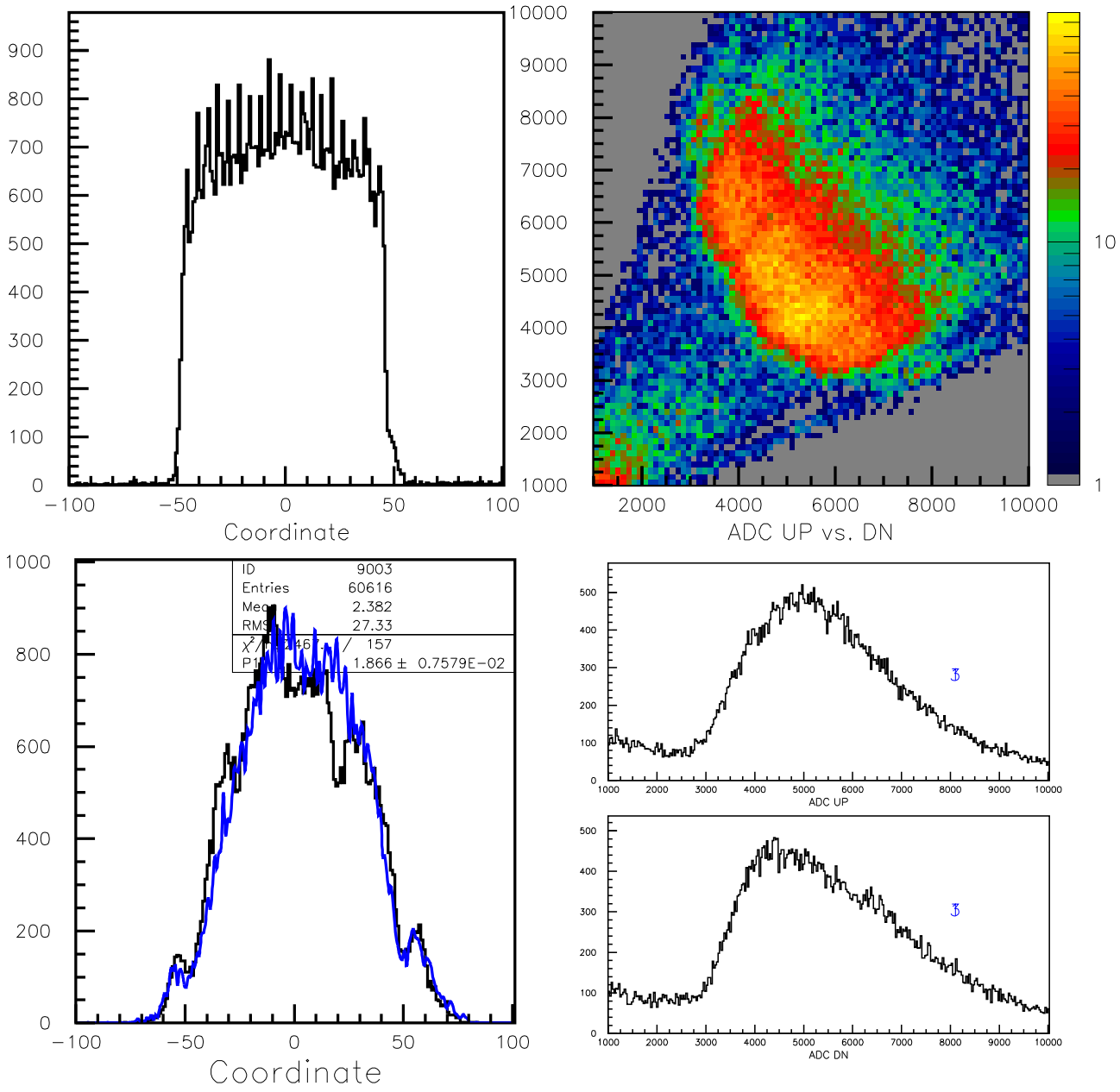

Figure 15: Data for counter #3.

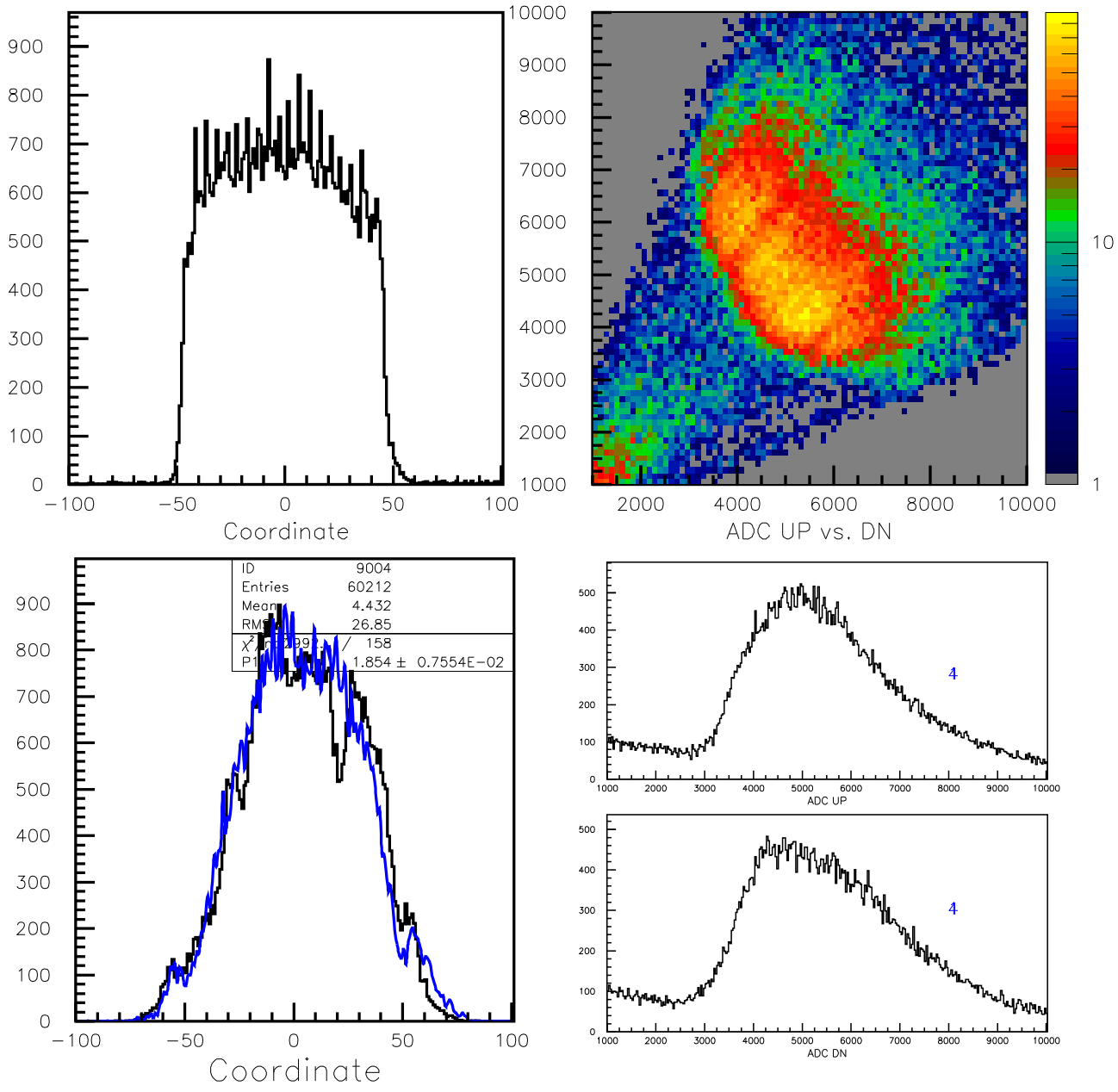

Figure 16: Data for counter #4.

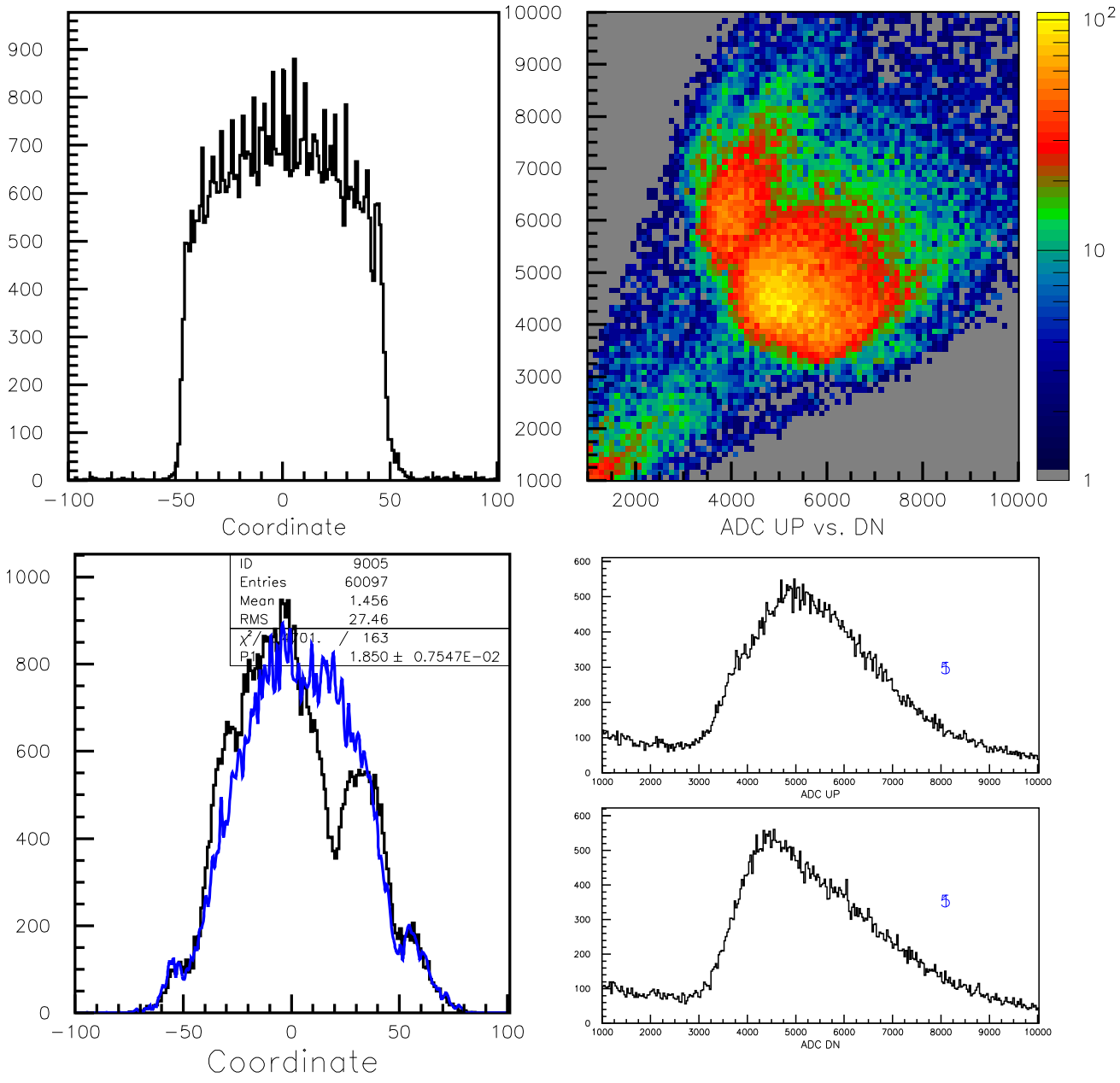

Figure 17: Data for counter #5.

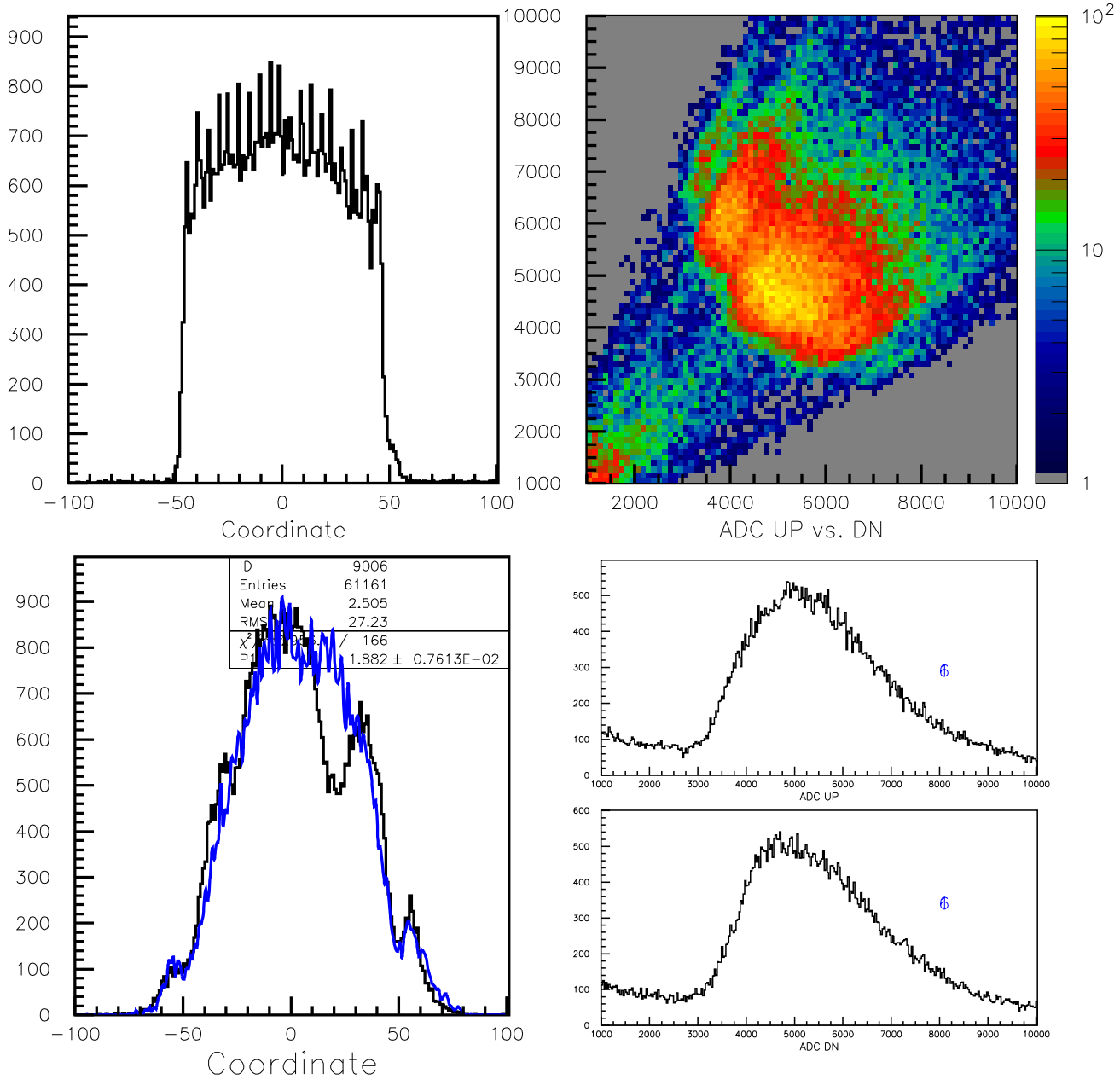

Figure 18: Data for counter #6.

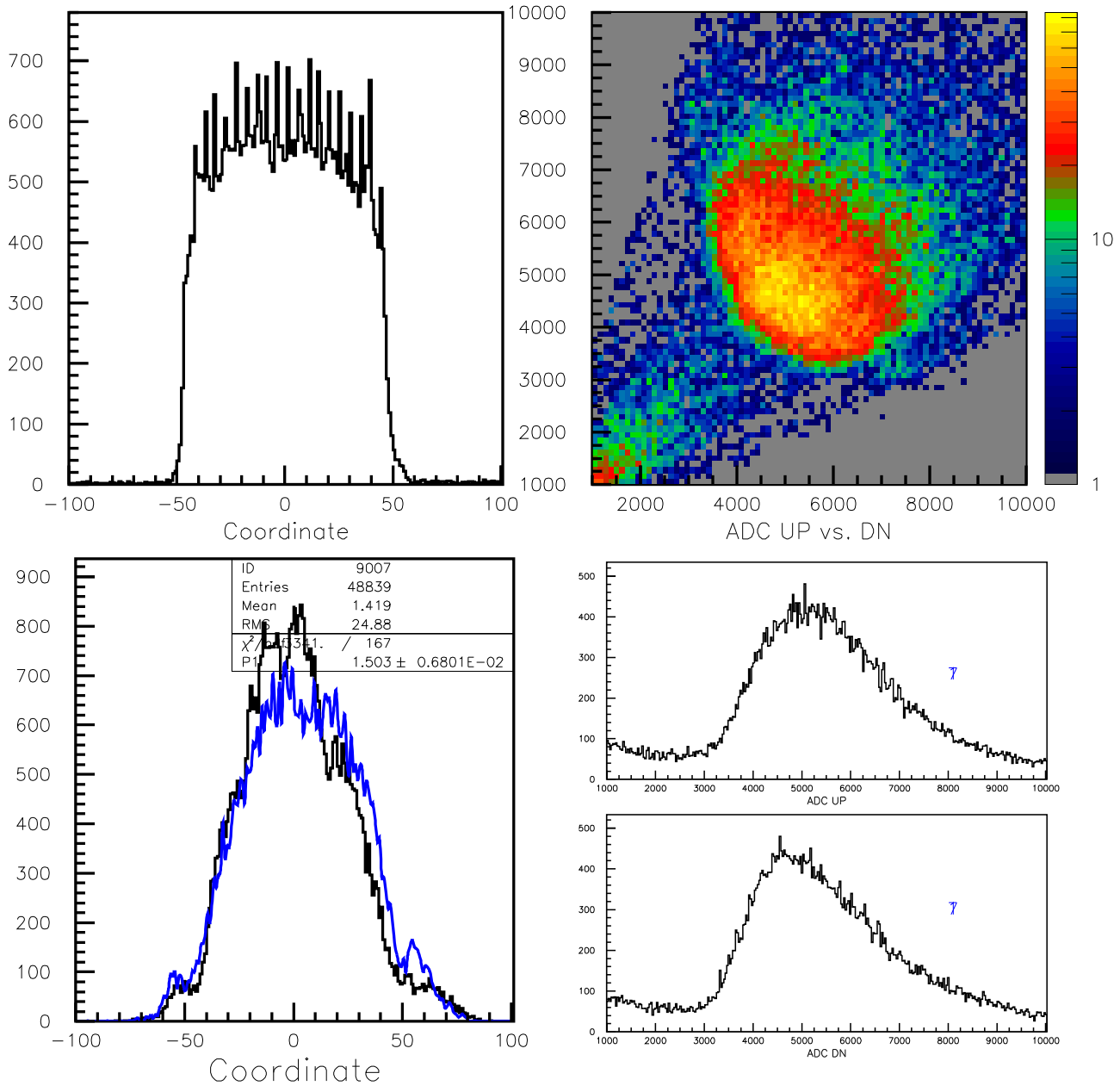

Figure 19: Data for counter #7.

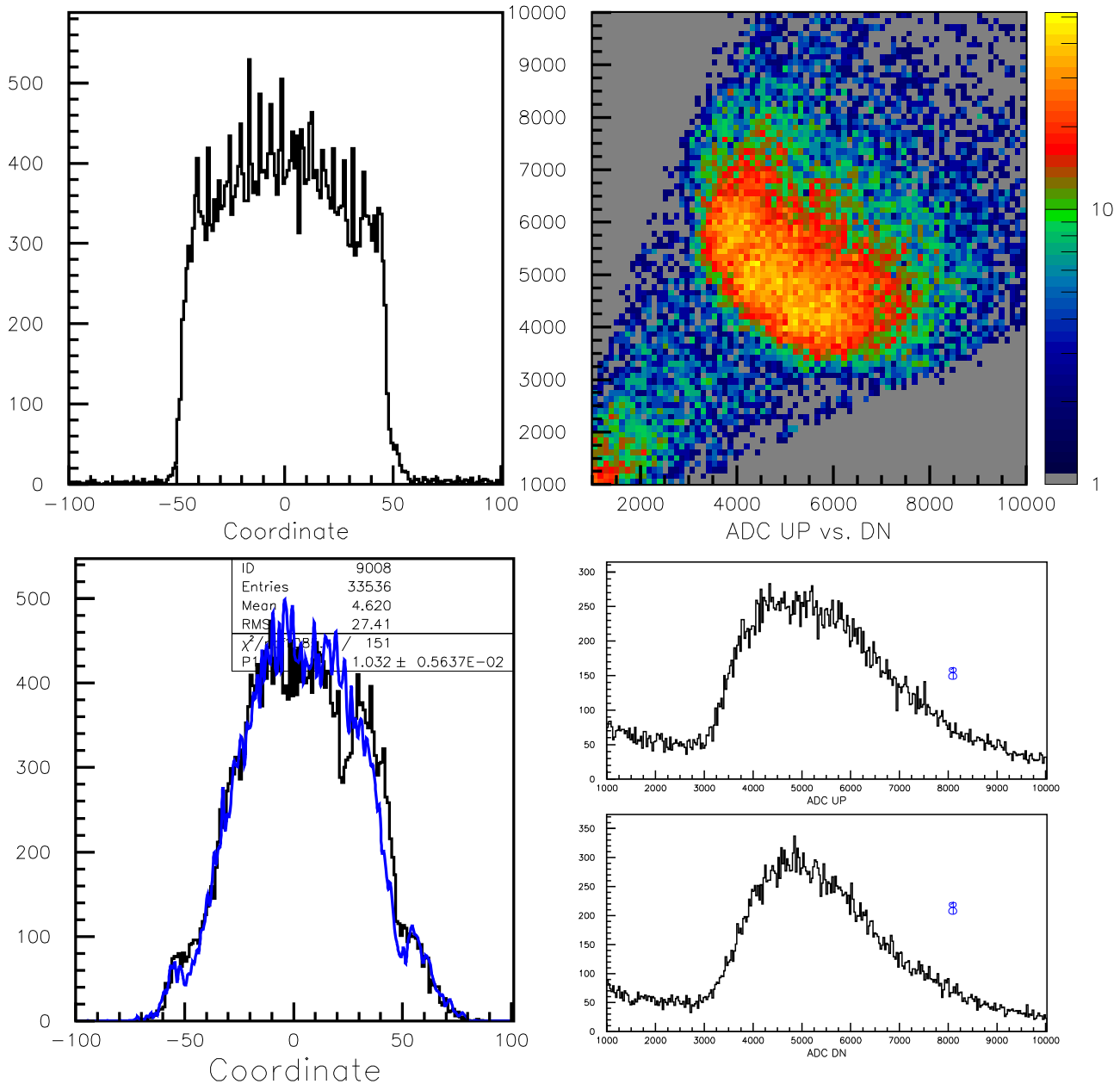

Figure 20: Data for counter #8.

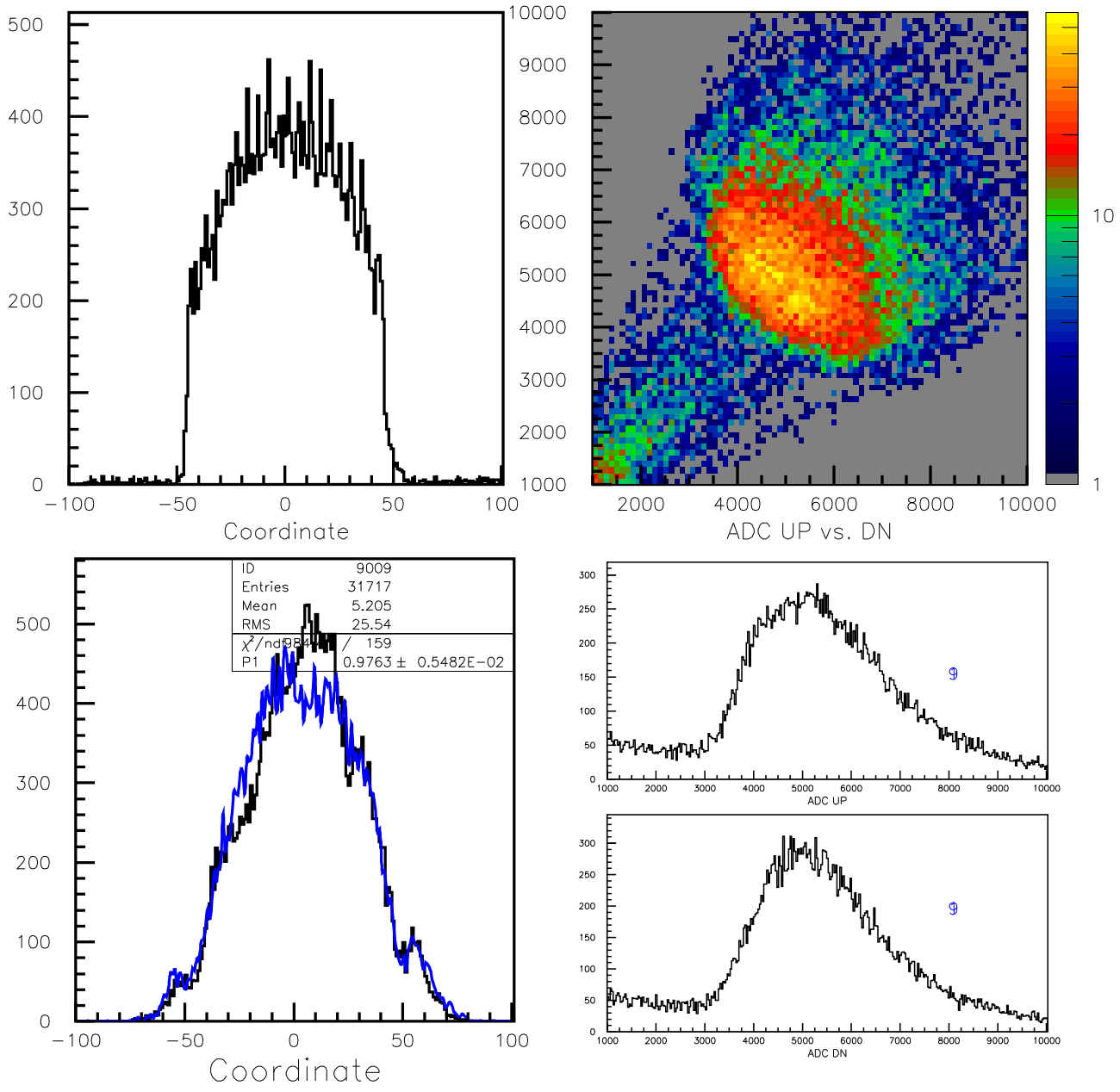

Figure 21: Data for counter #9.

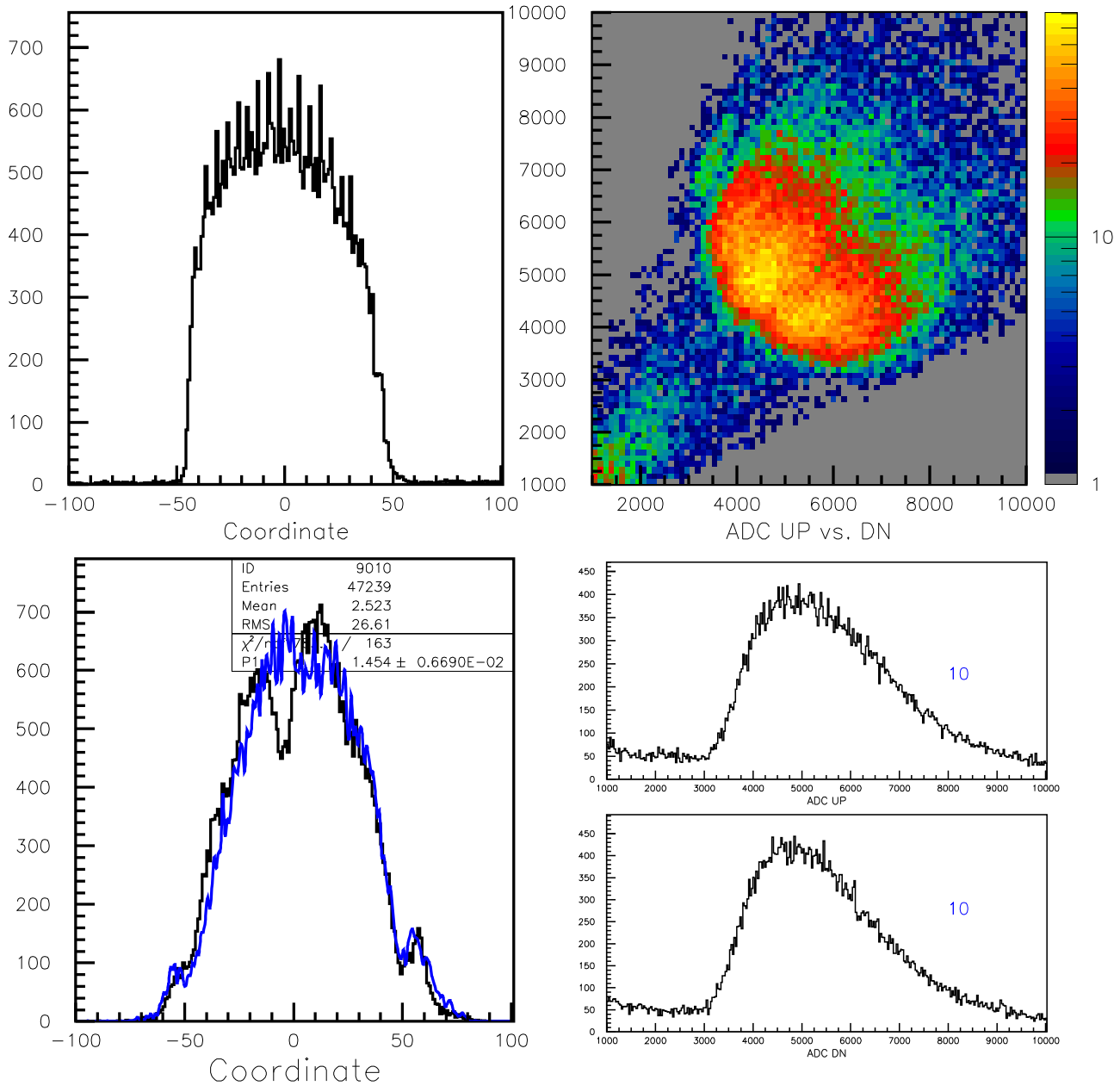

Figure 22: Data for counter #10.

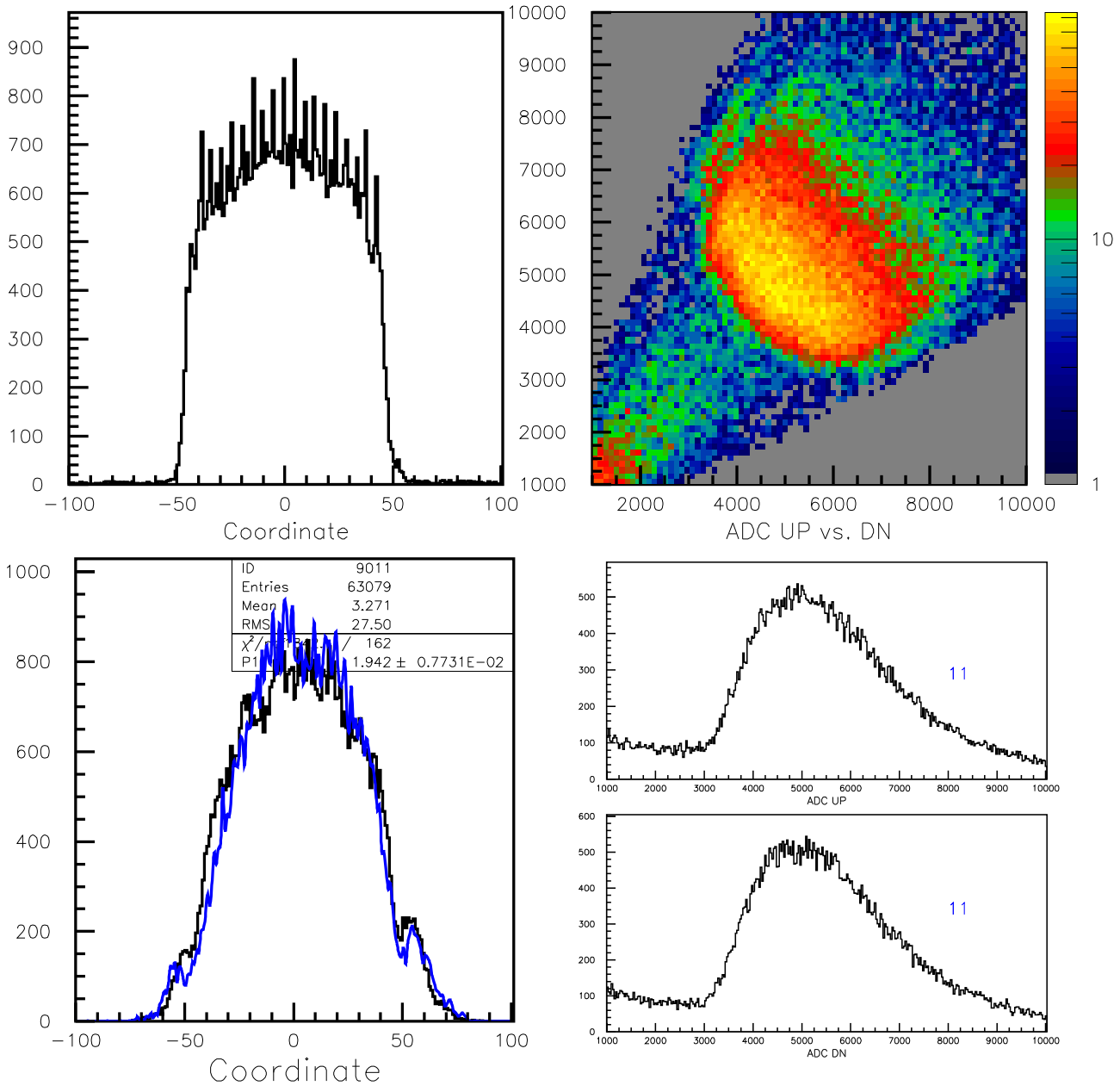

Figure 23: Data for counter #11.

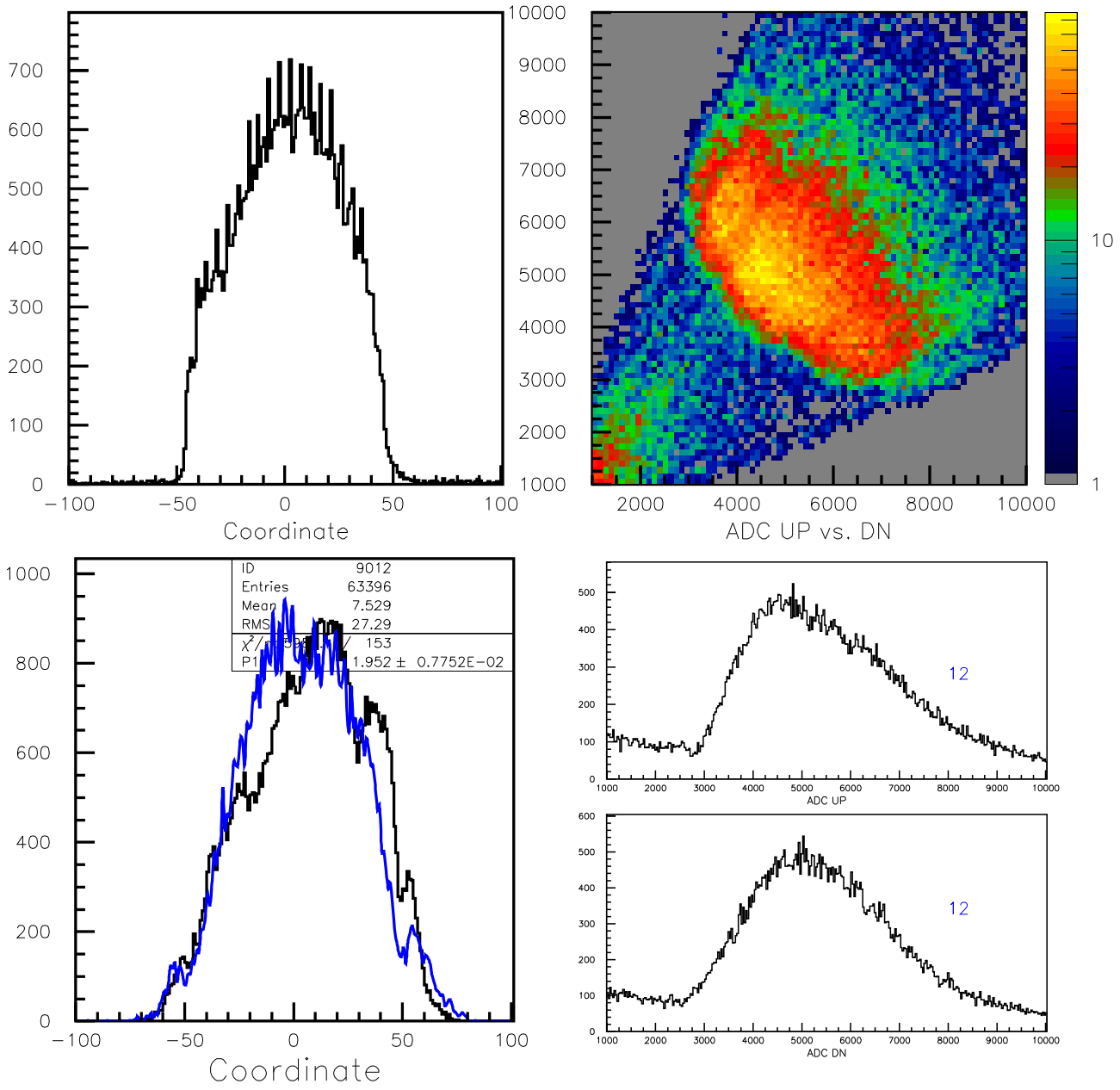

Figure 24: Data for counter #12.

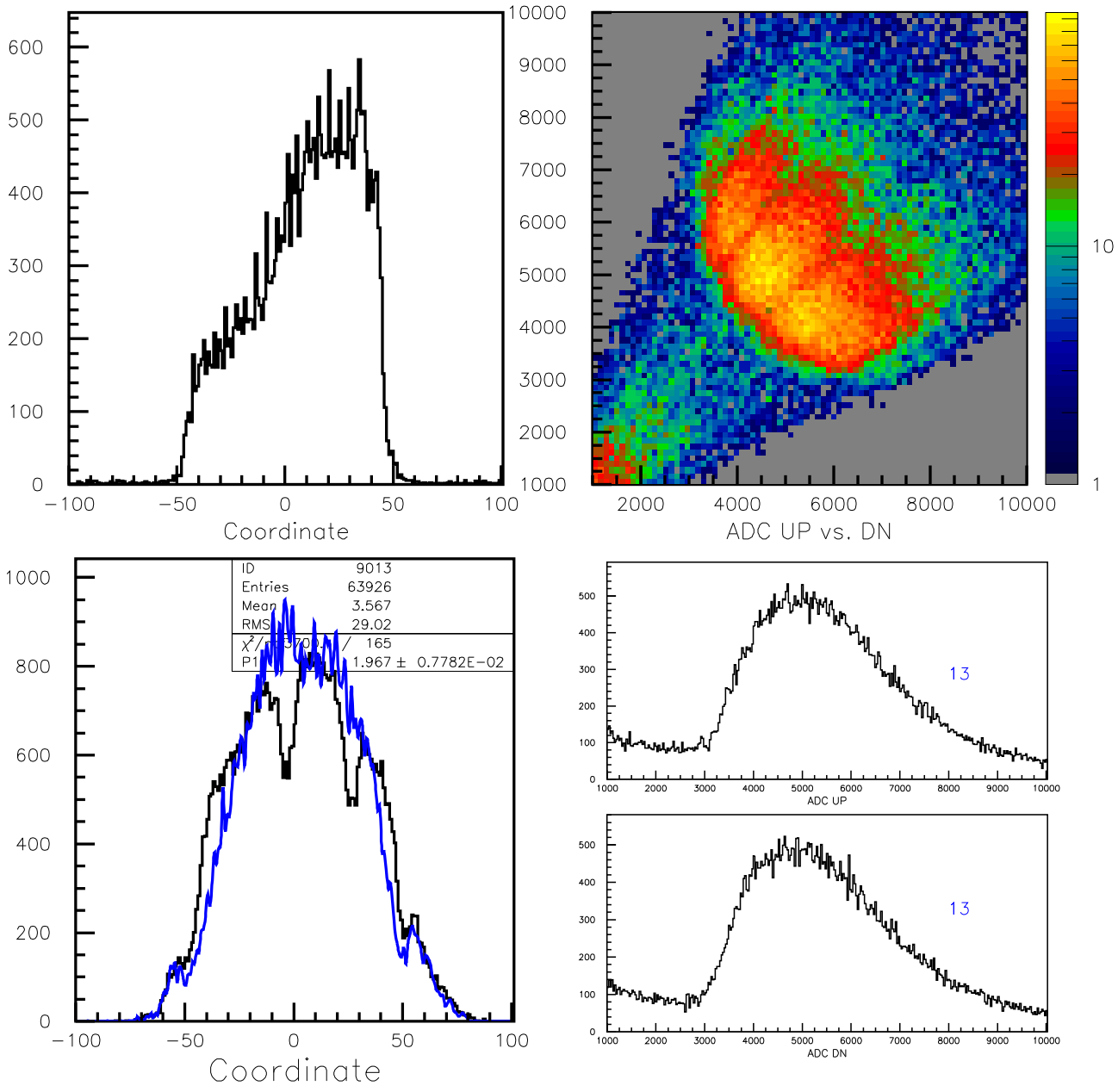

Figure 25: Data for counter #13.

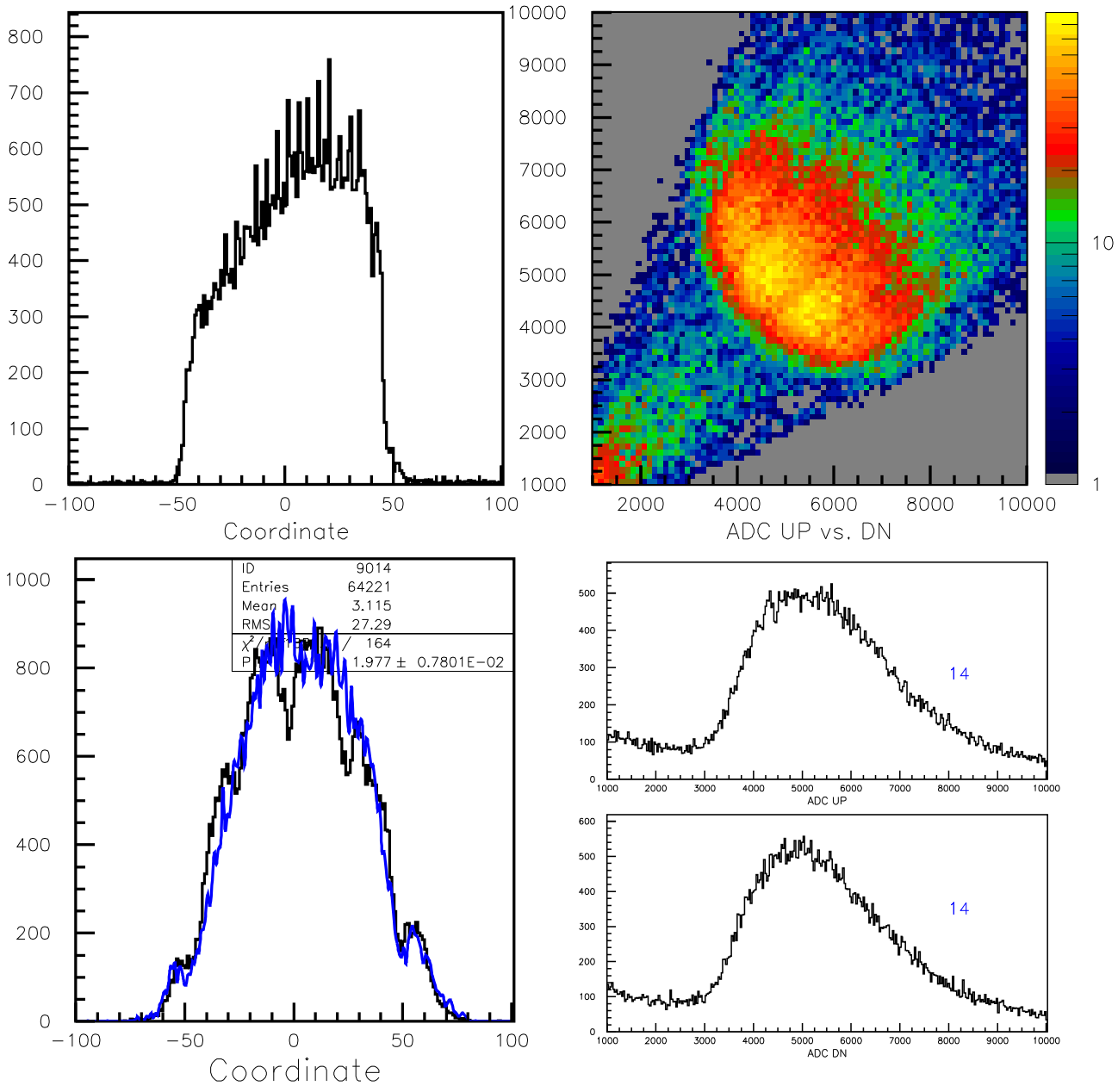

Figure 26: Data for counter #14.

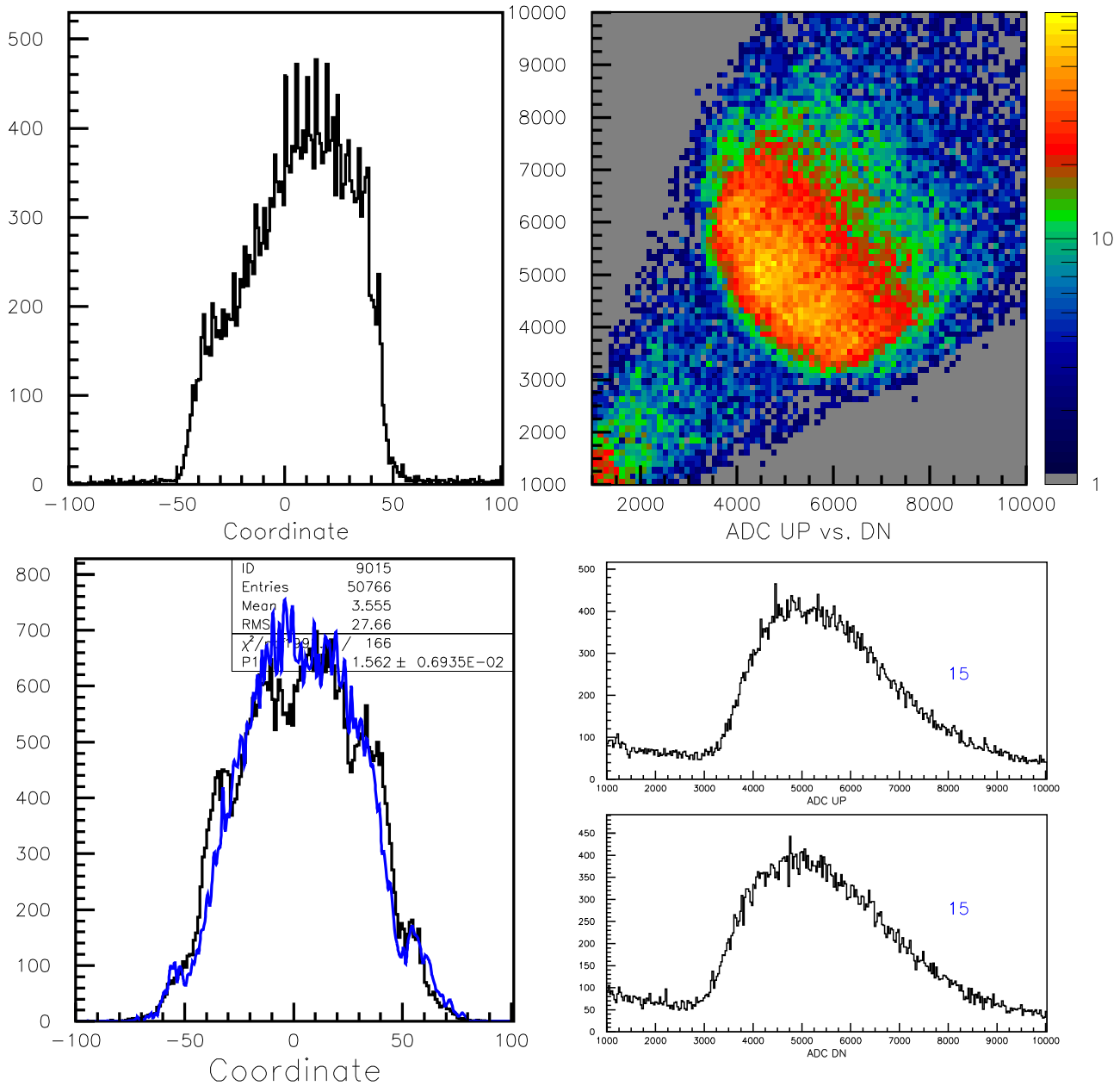

Figure 27: Data for counter #15.

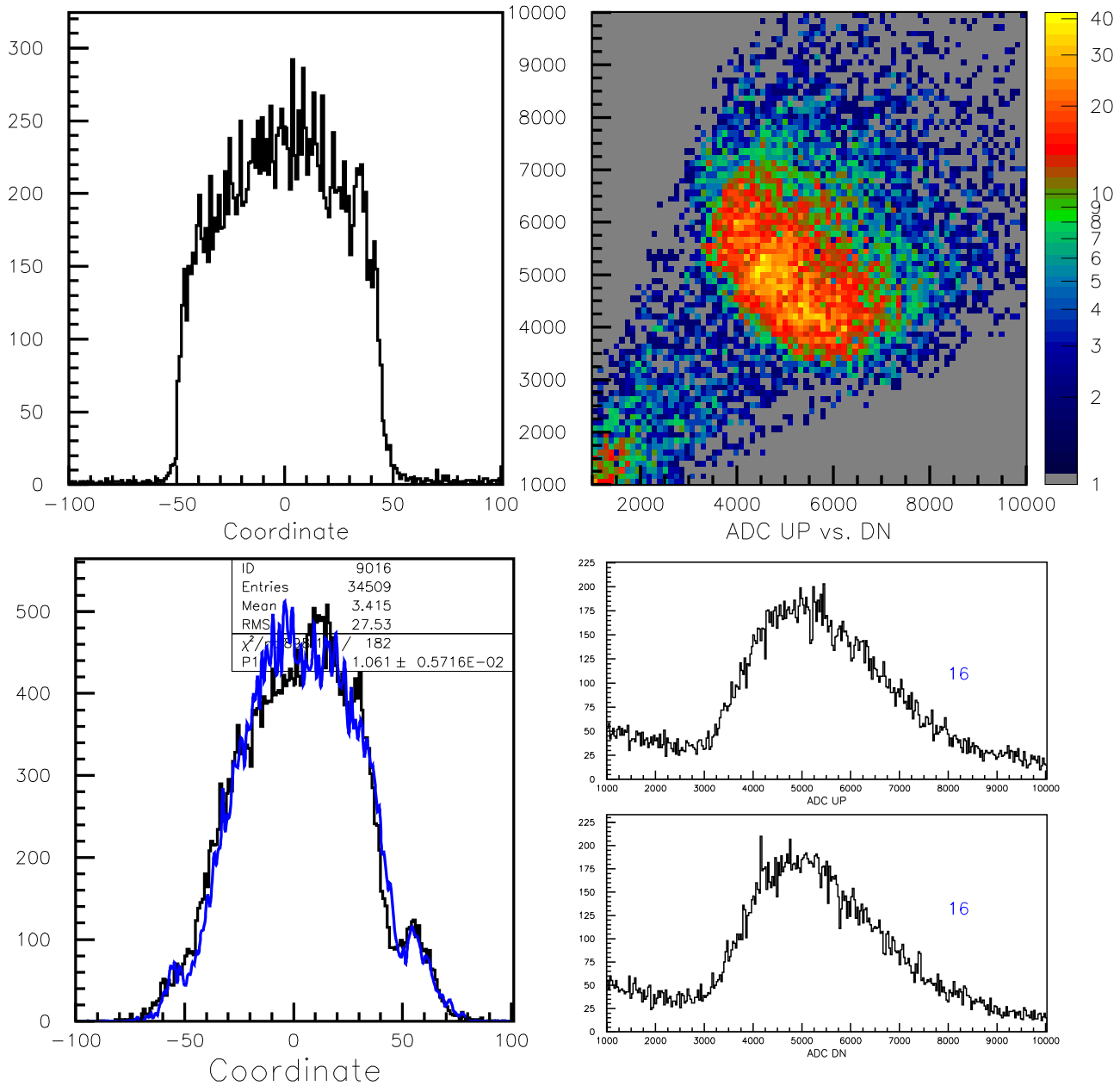

Figure 28: Data for counter #16.

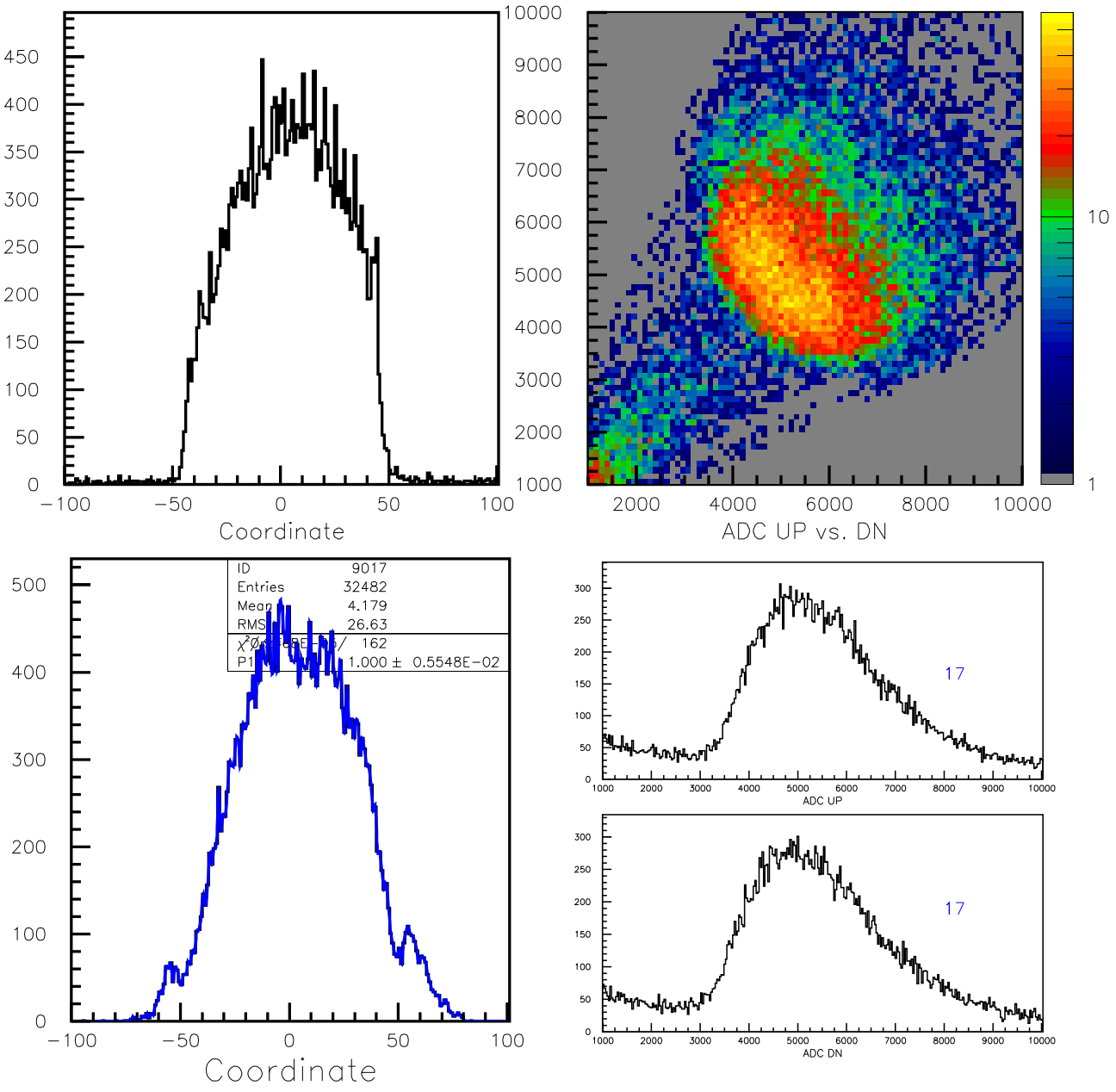

Figure 29: Data for counter #17.

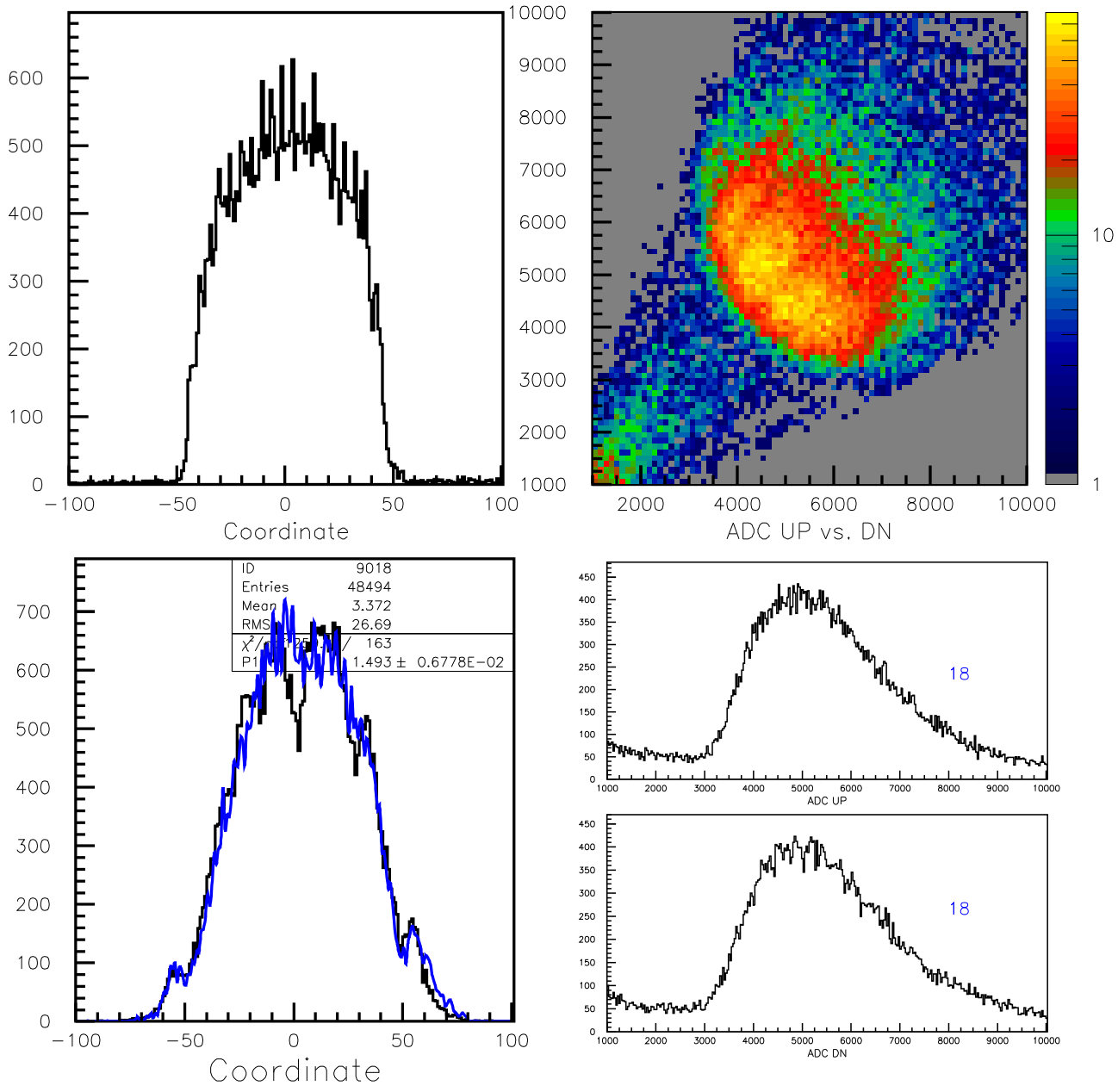

Figure 30: Data for counter #18.

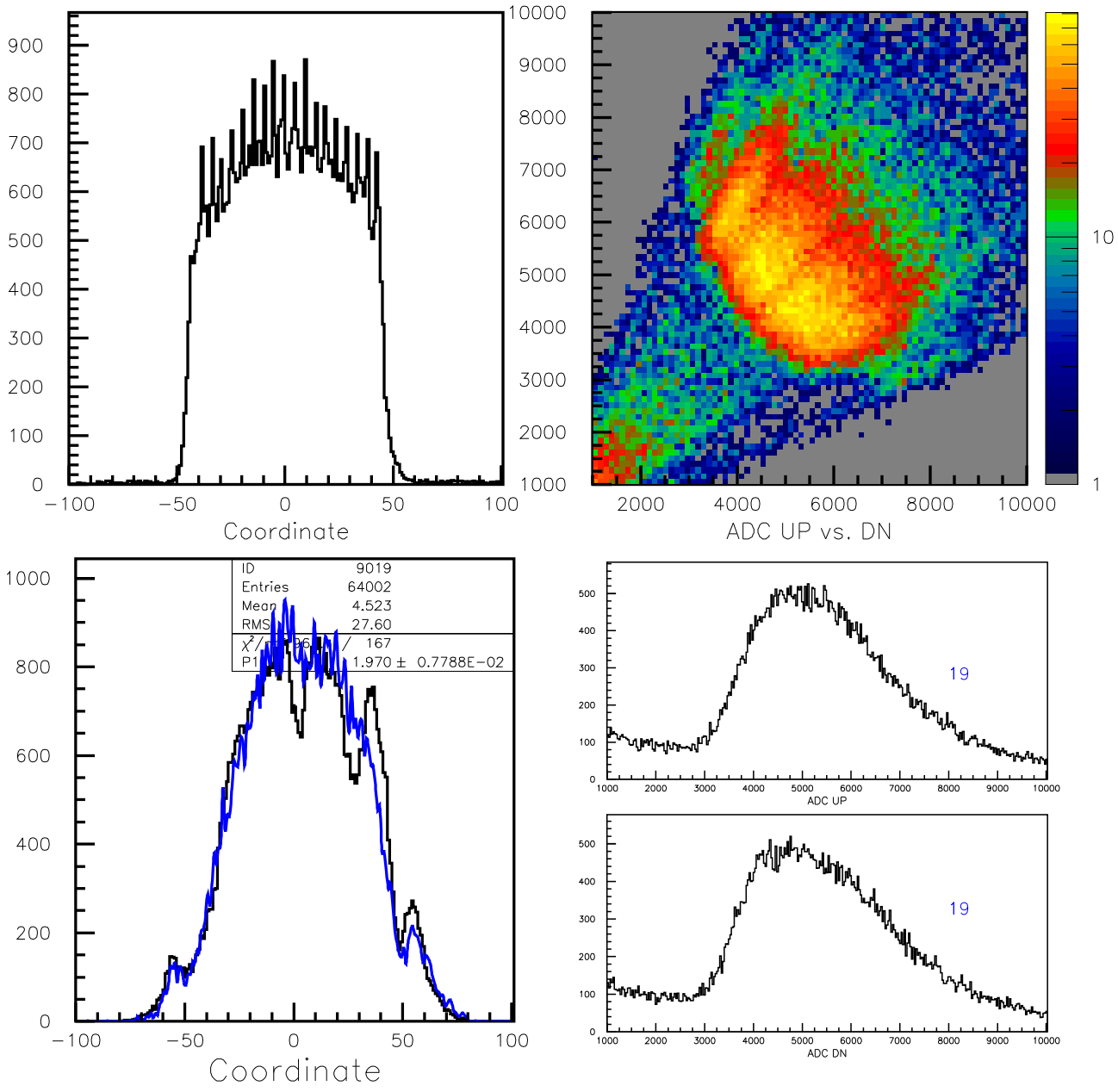

Figure 31: Data for counter #19.

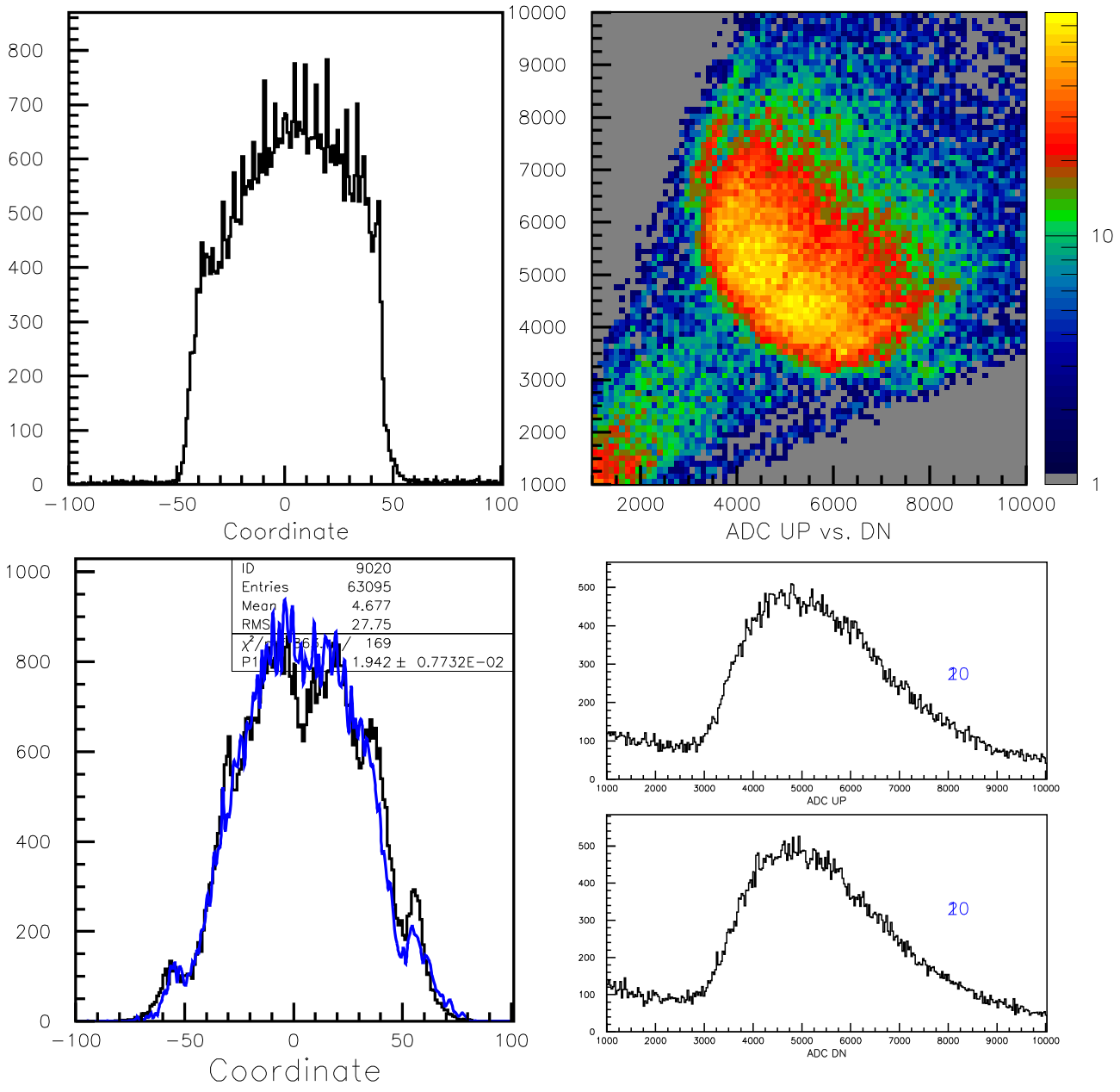

Figure 32: Data for counter #20.

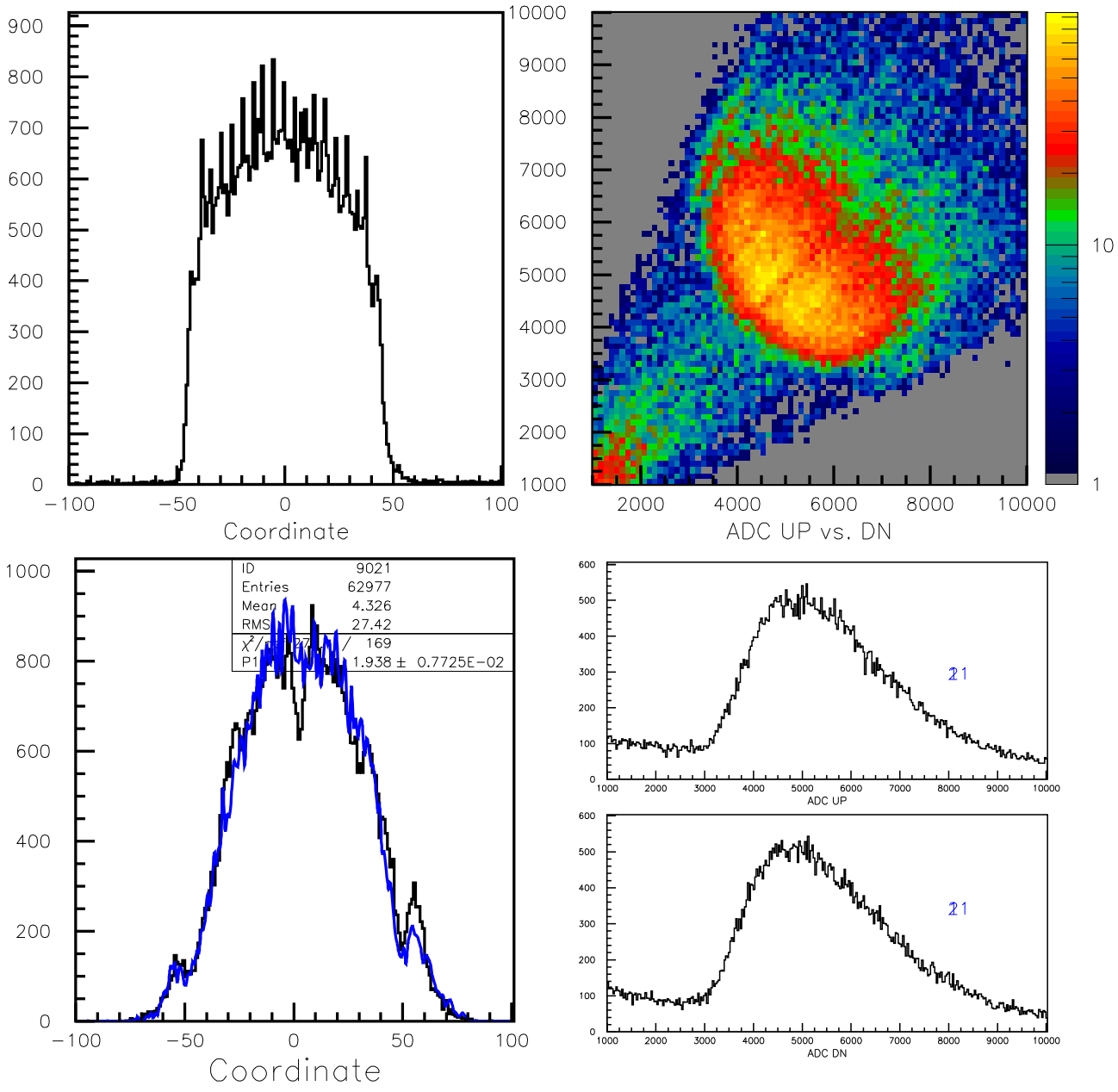

Figure 33: Data for counter #21.

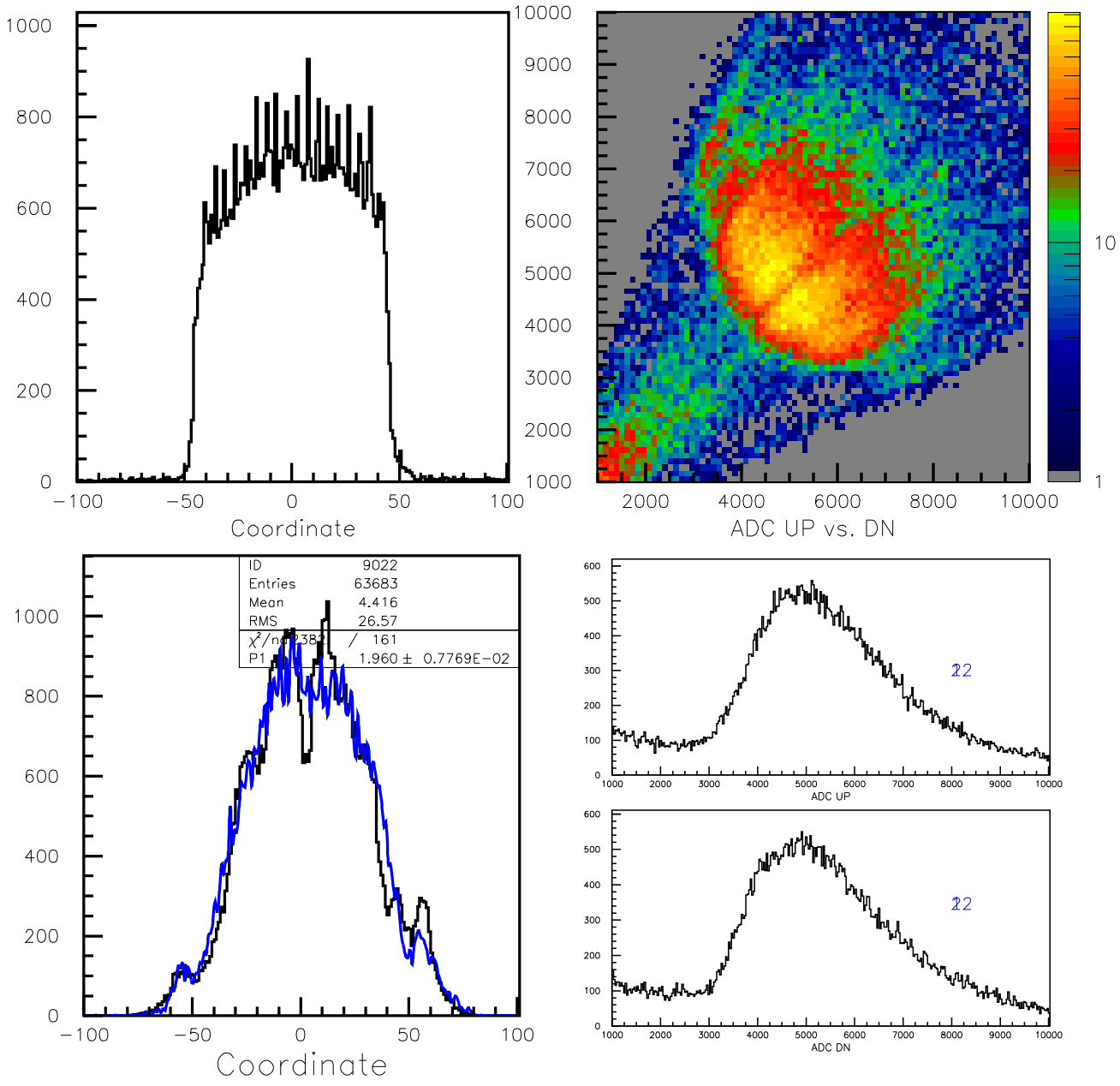

Figure 34: Data for counter #22.

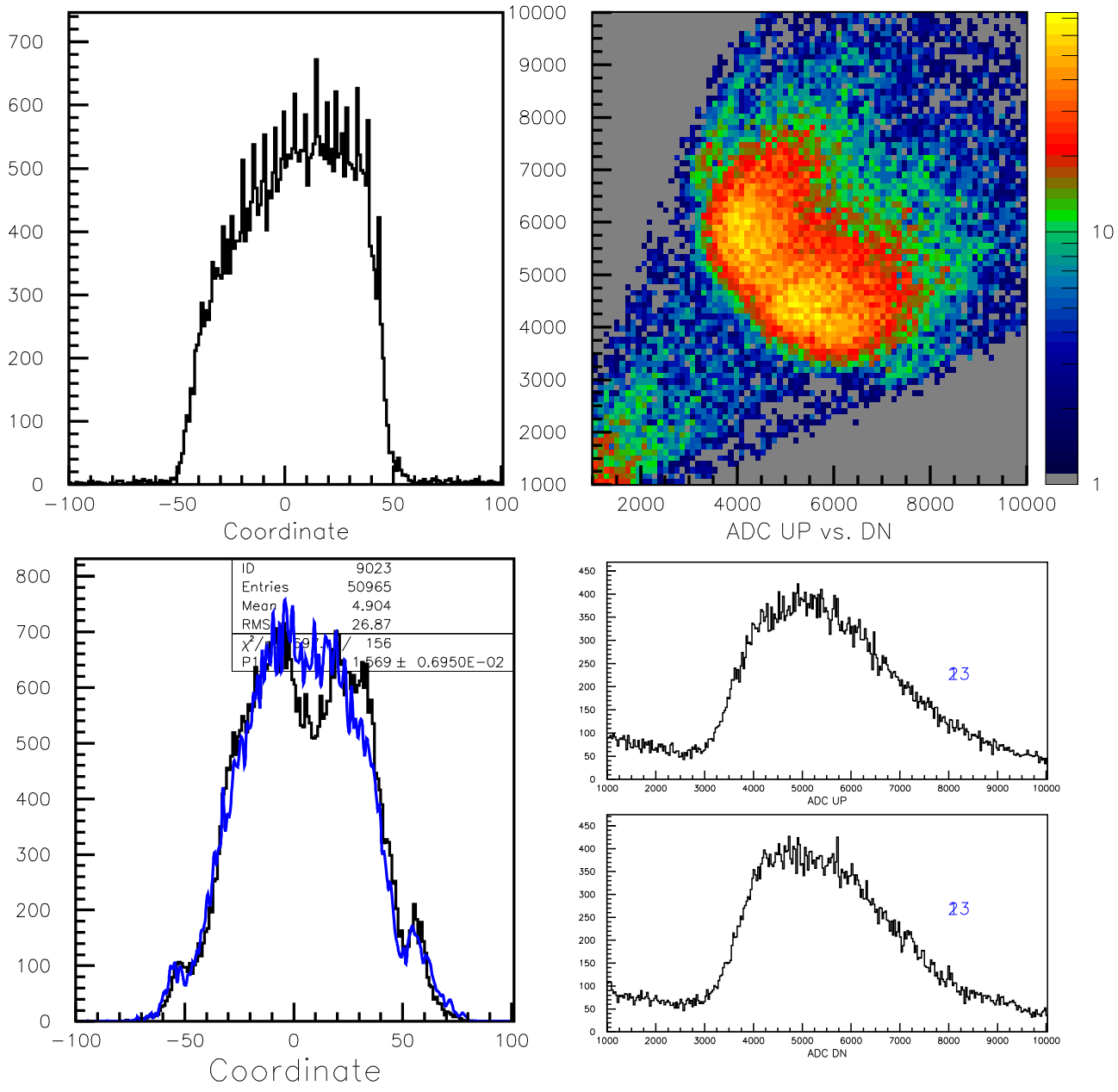

Figure 35: Data for counter #23.

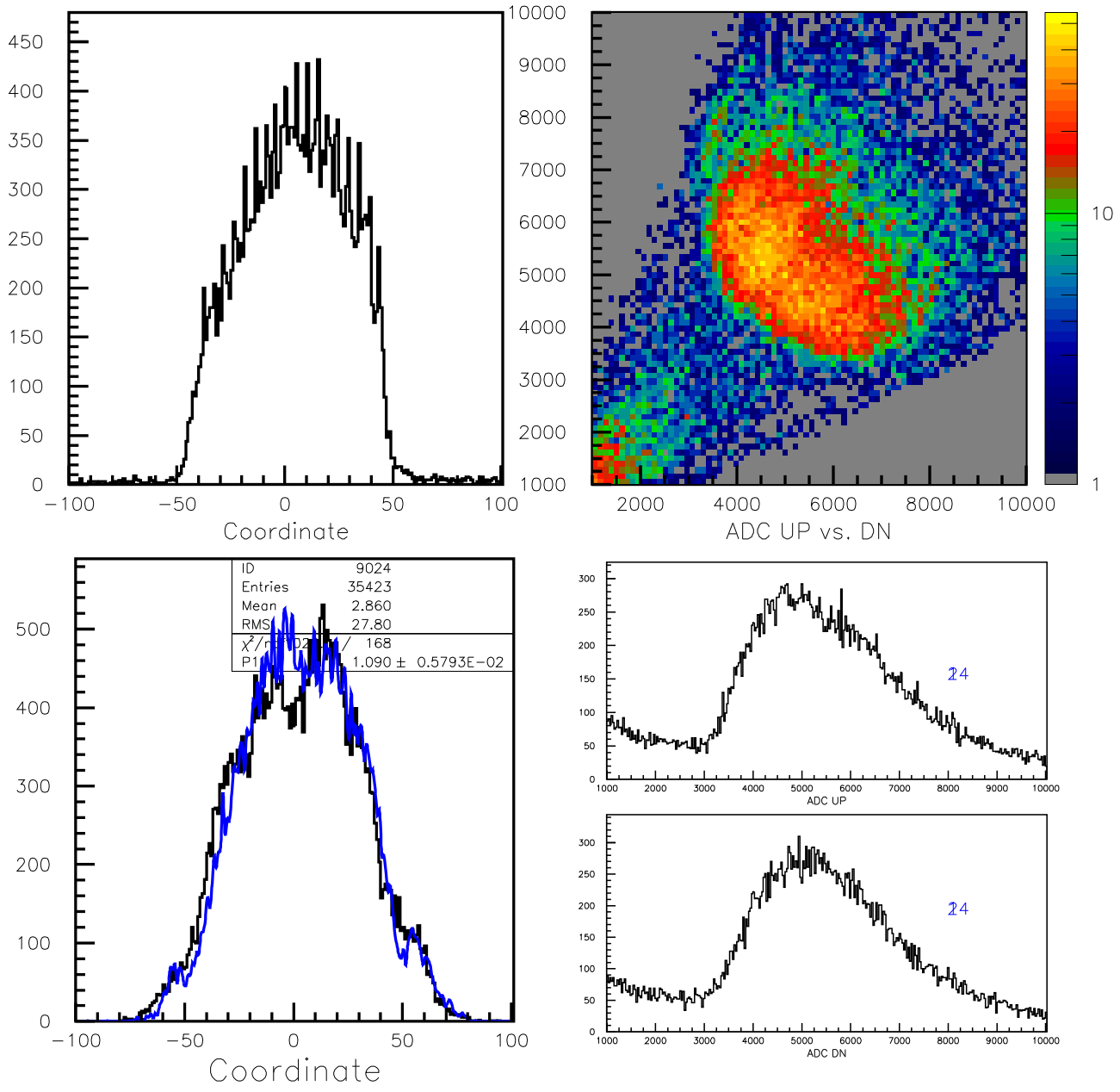

Figure 36: Data for counter #24.

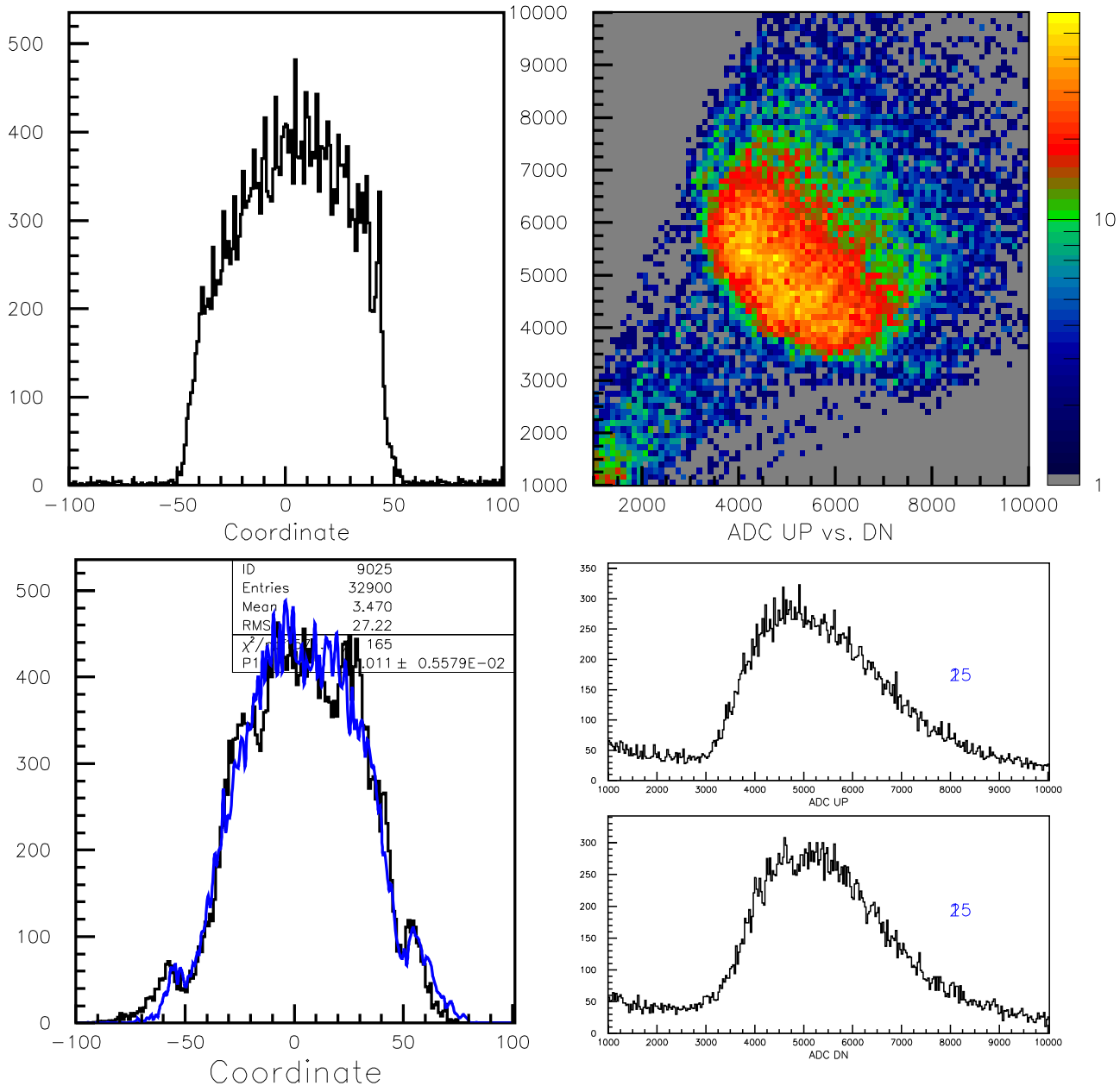

Figure 37: Data for counter #25.

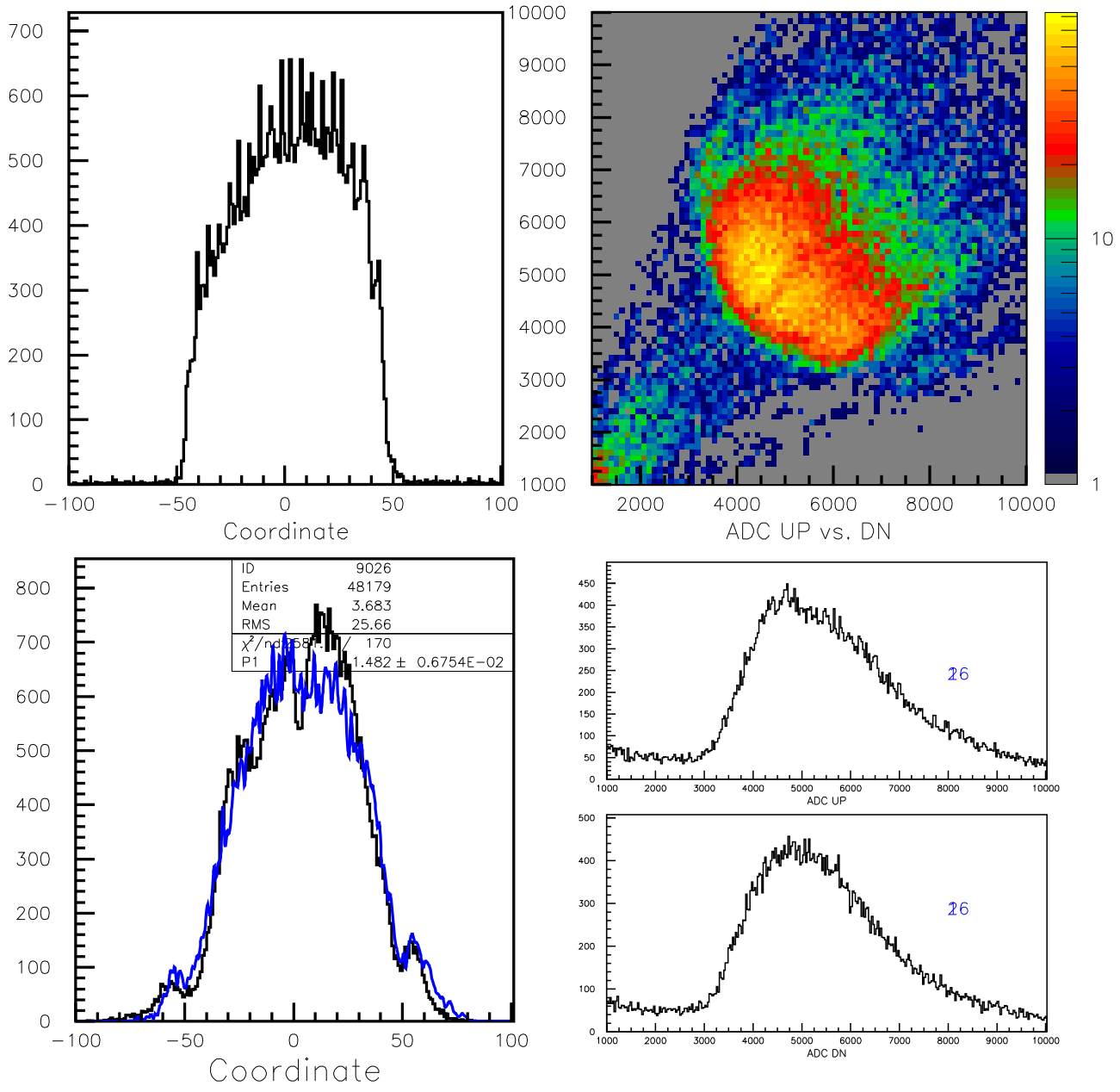

Figure 38: Data for counter #26.

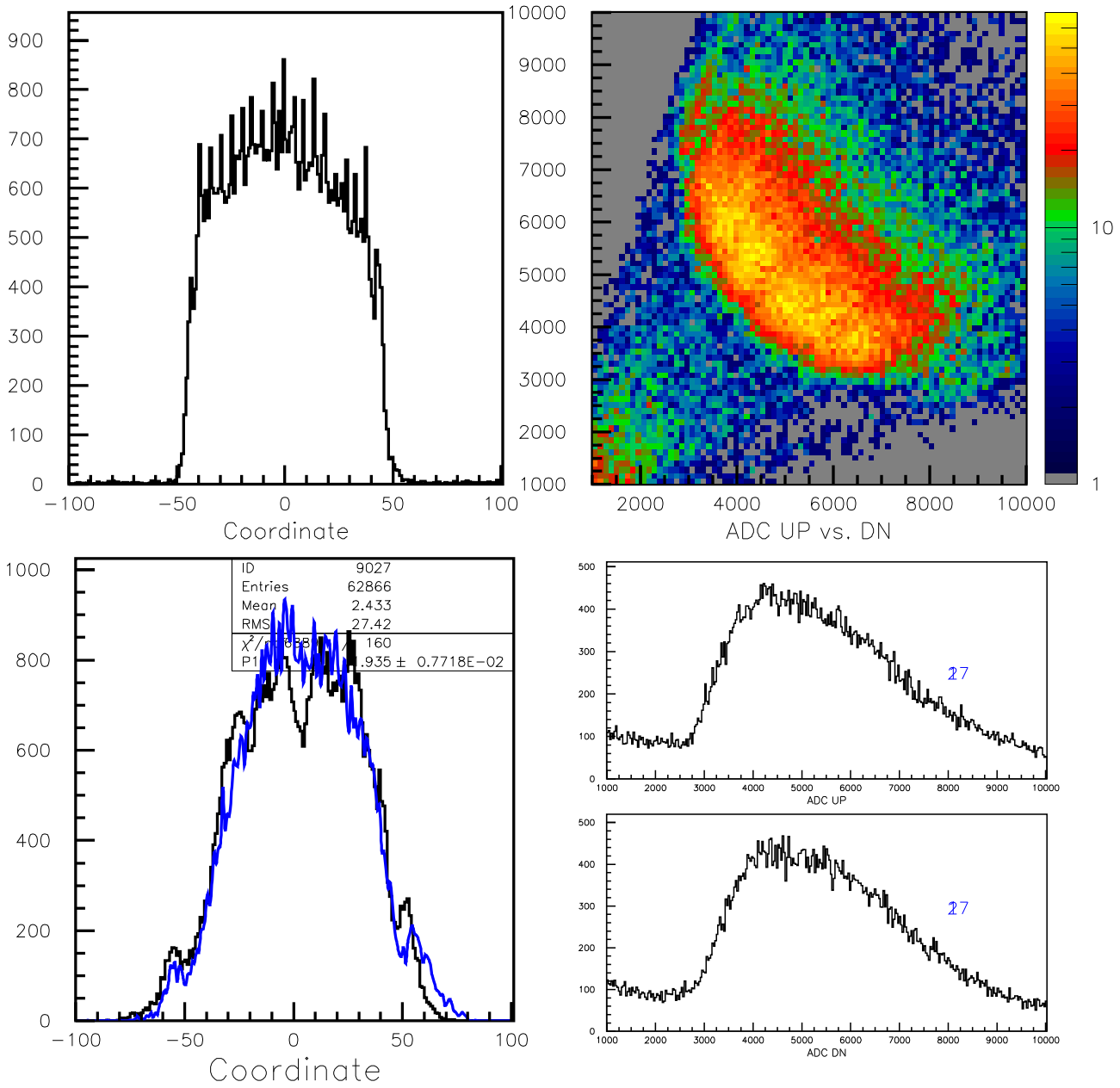

Figure 39: Data for counter #27.

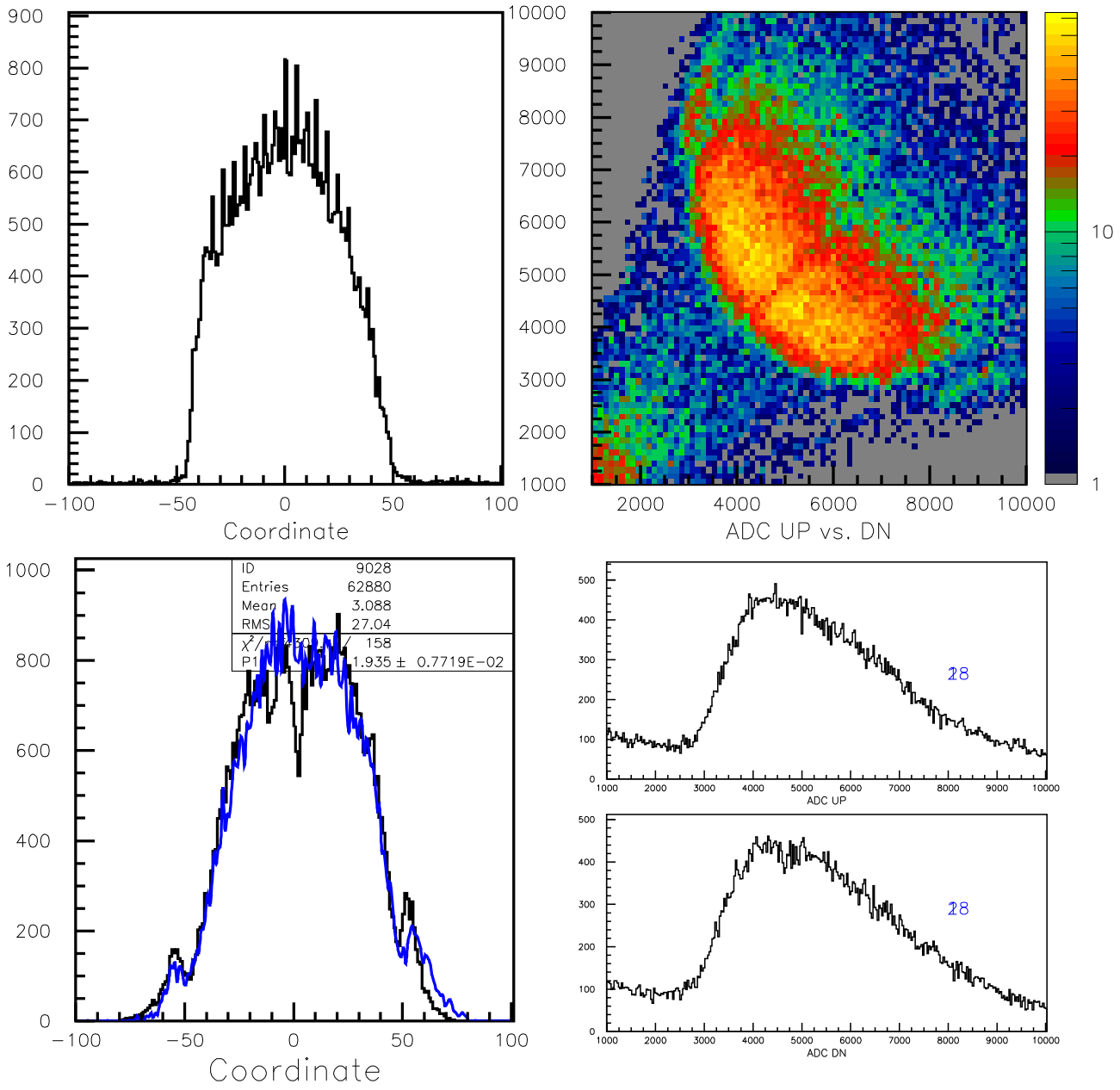

Figure 40: Data for counter #28.

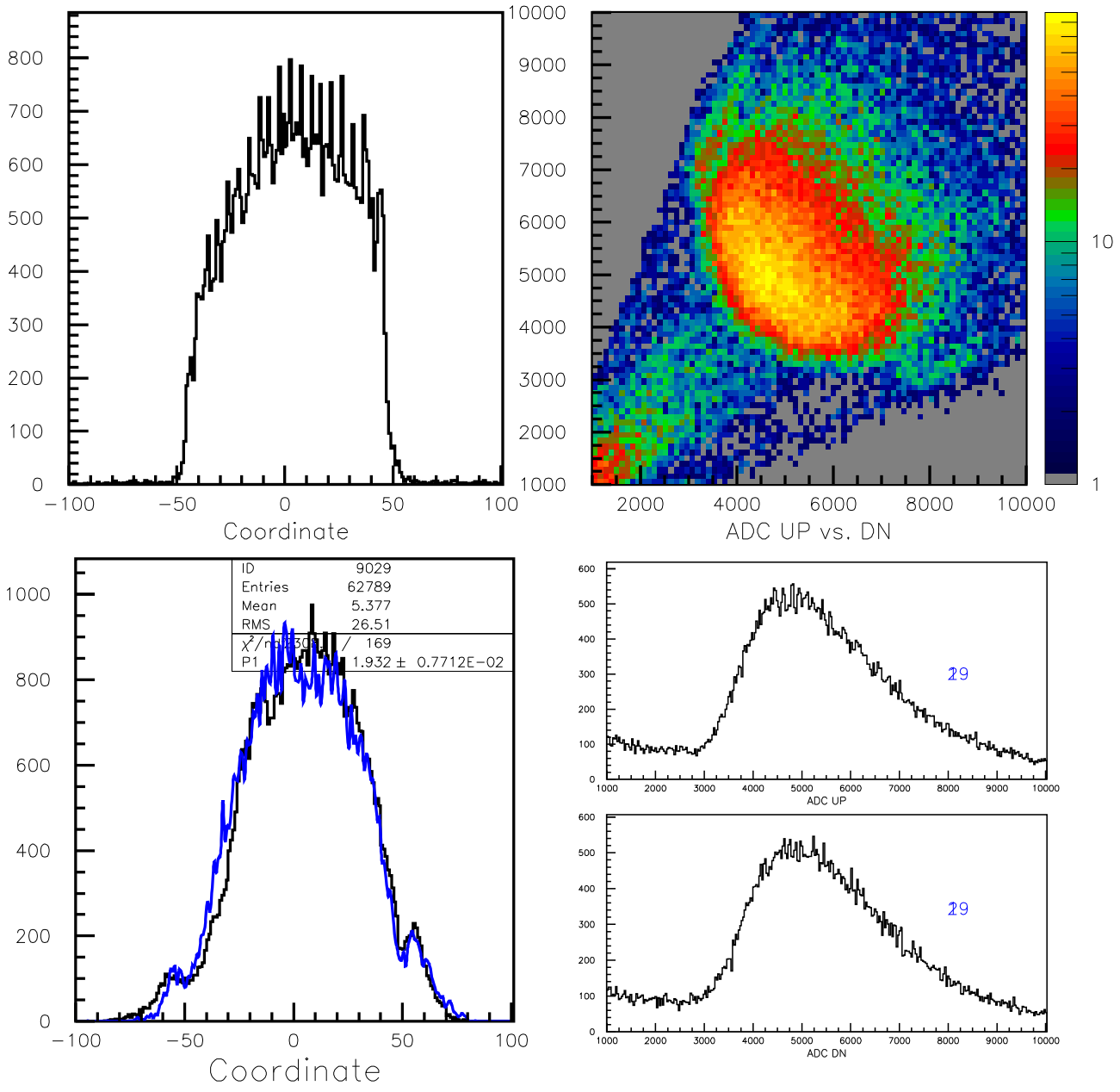

Figure 41: Data for counter #29.

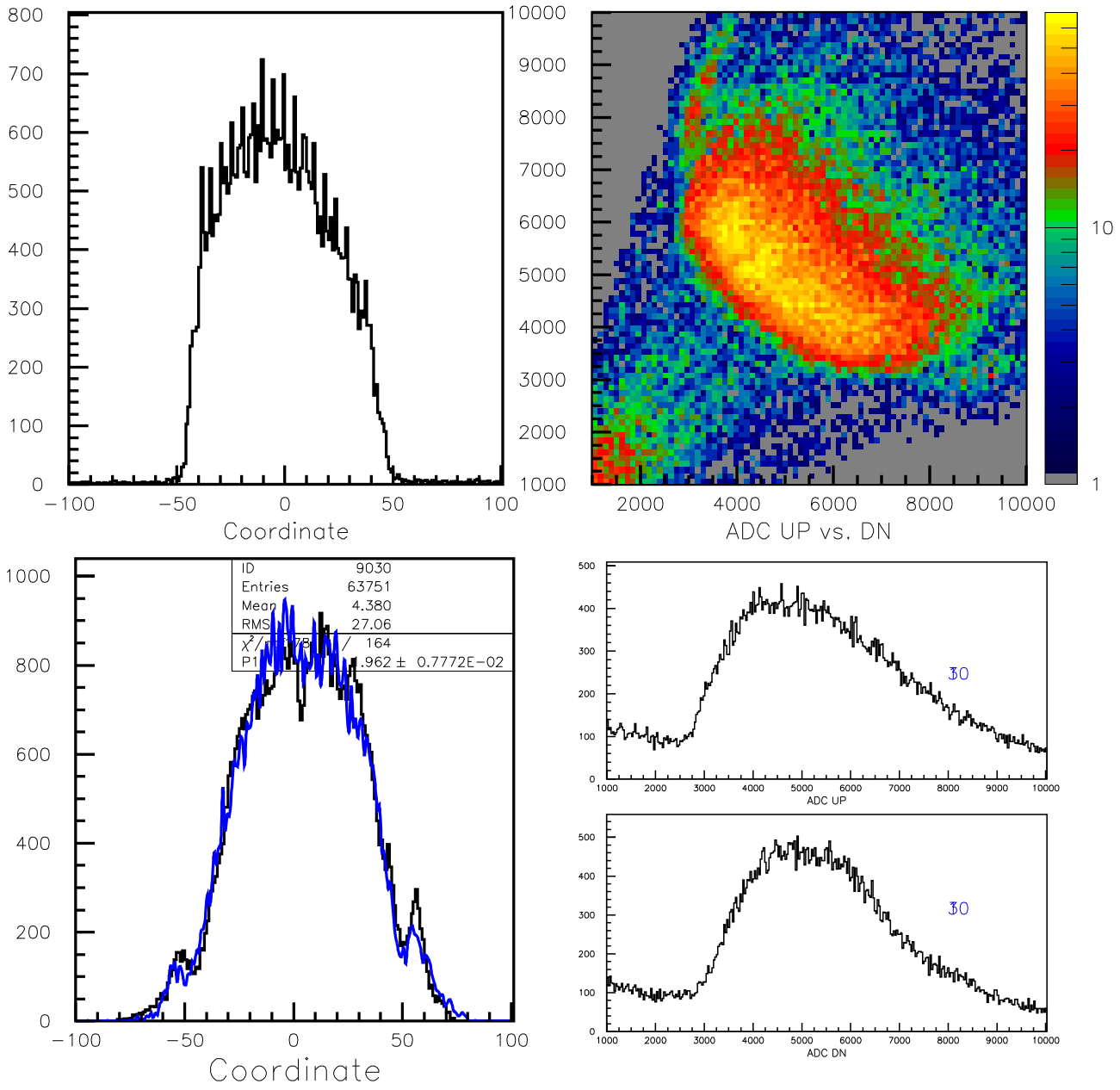

Figure 42: Data for counter #30.

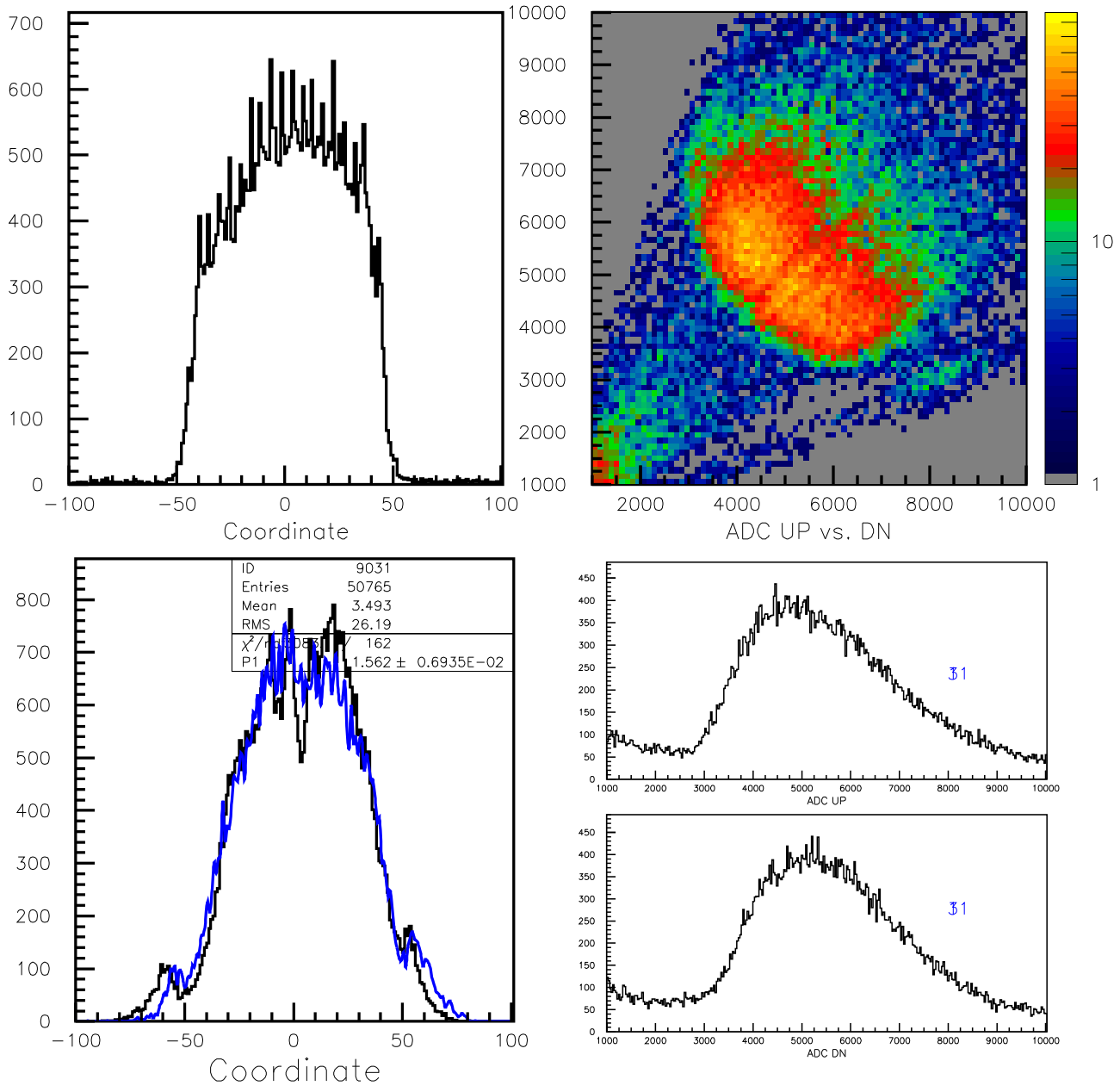

Figure 43: Data for counter #31.

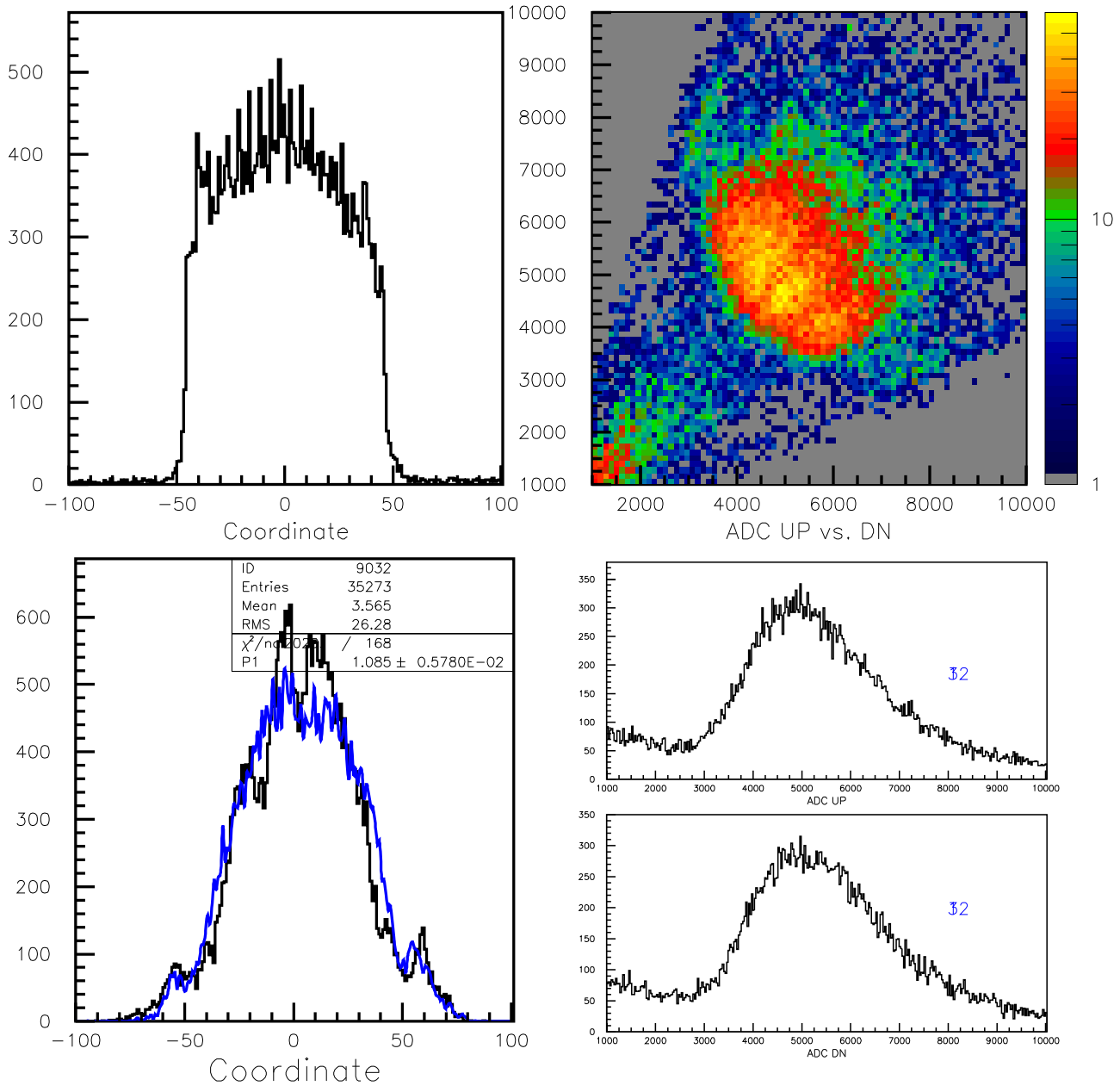

Figure 44: Data for counter #32.

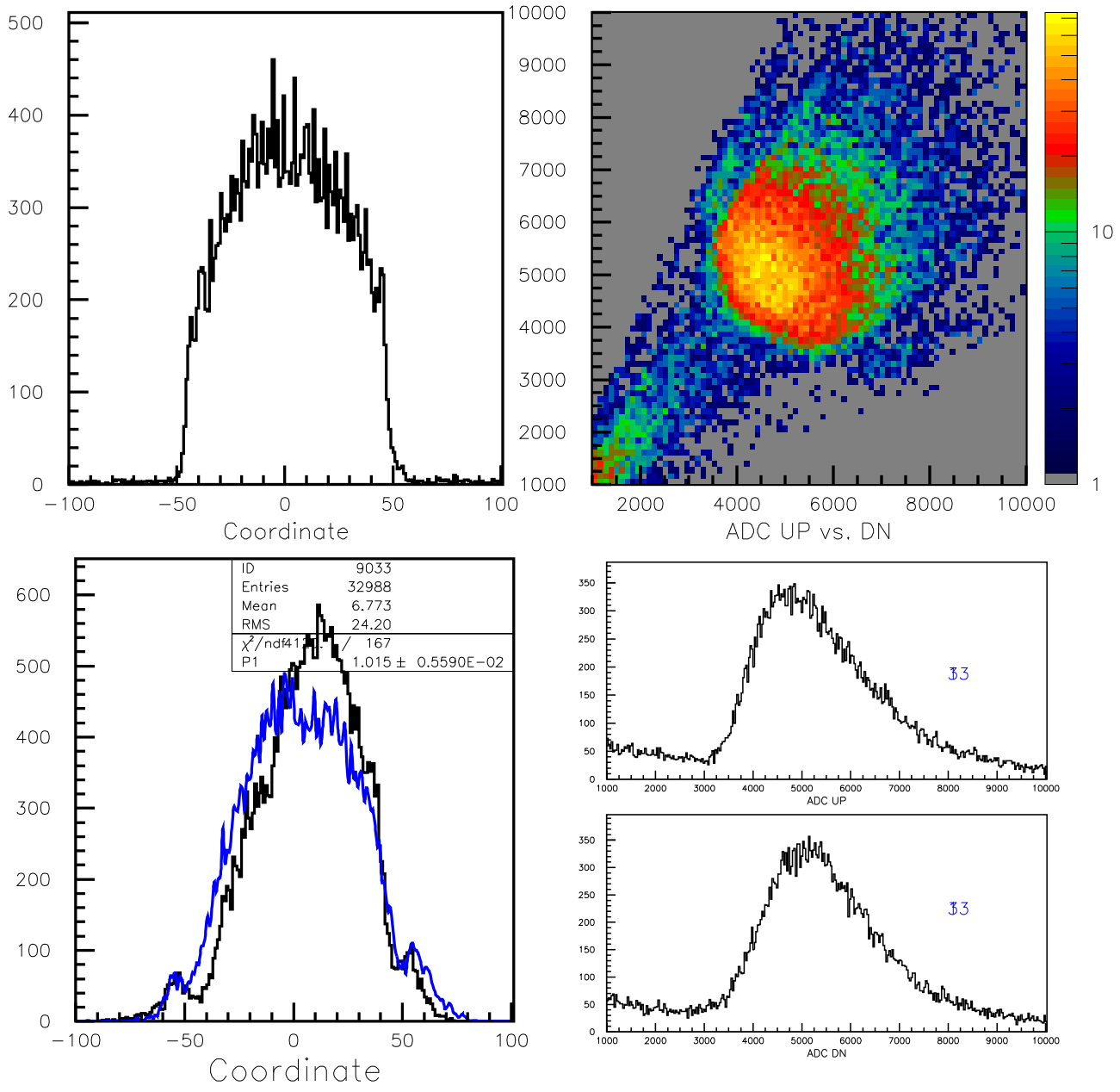

Figure 45: Data for counter #33.

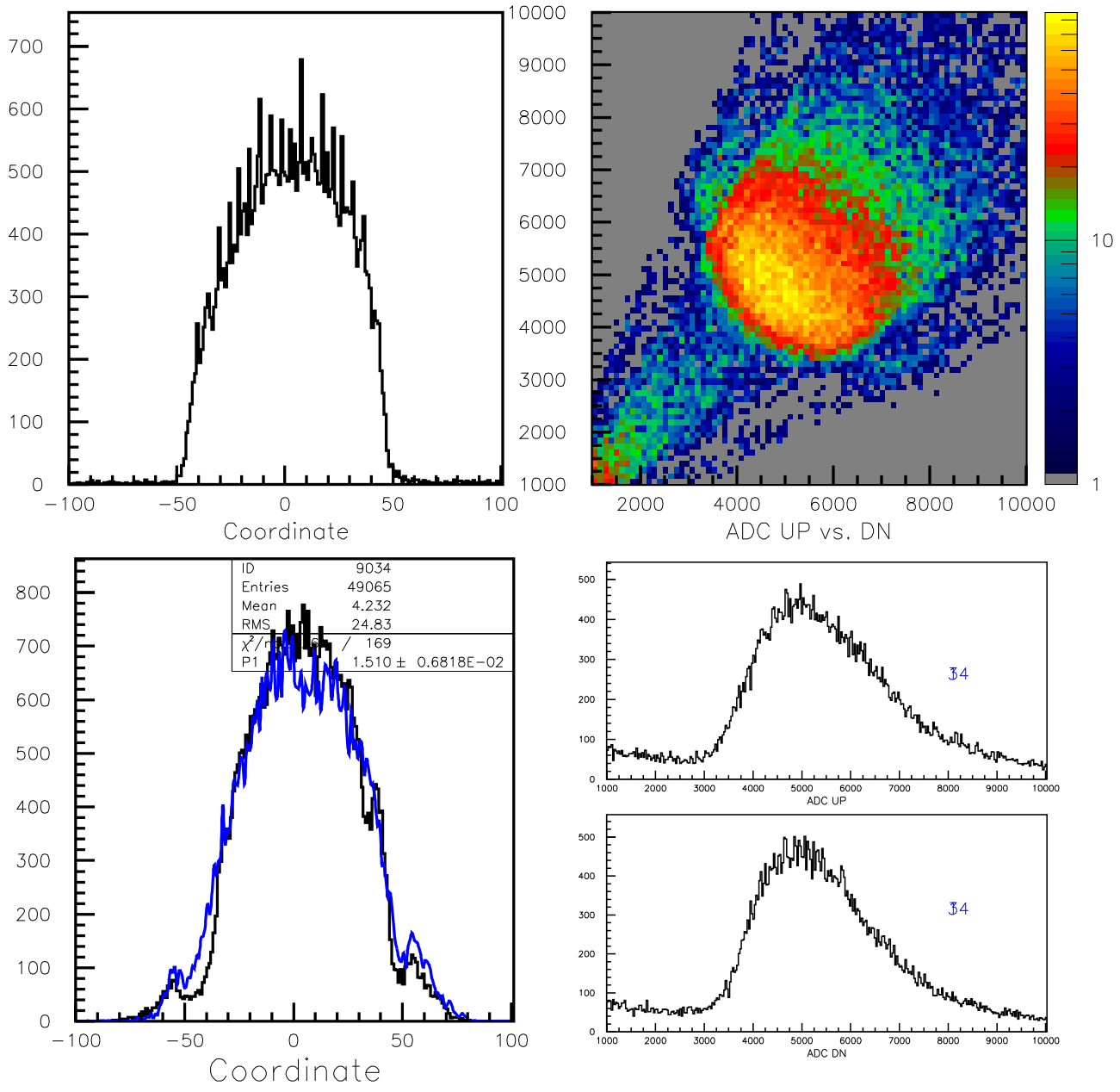

Figure 46: Data for counter #34.

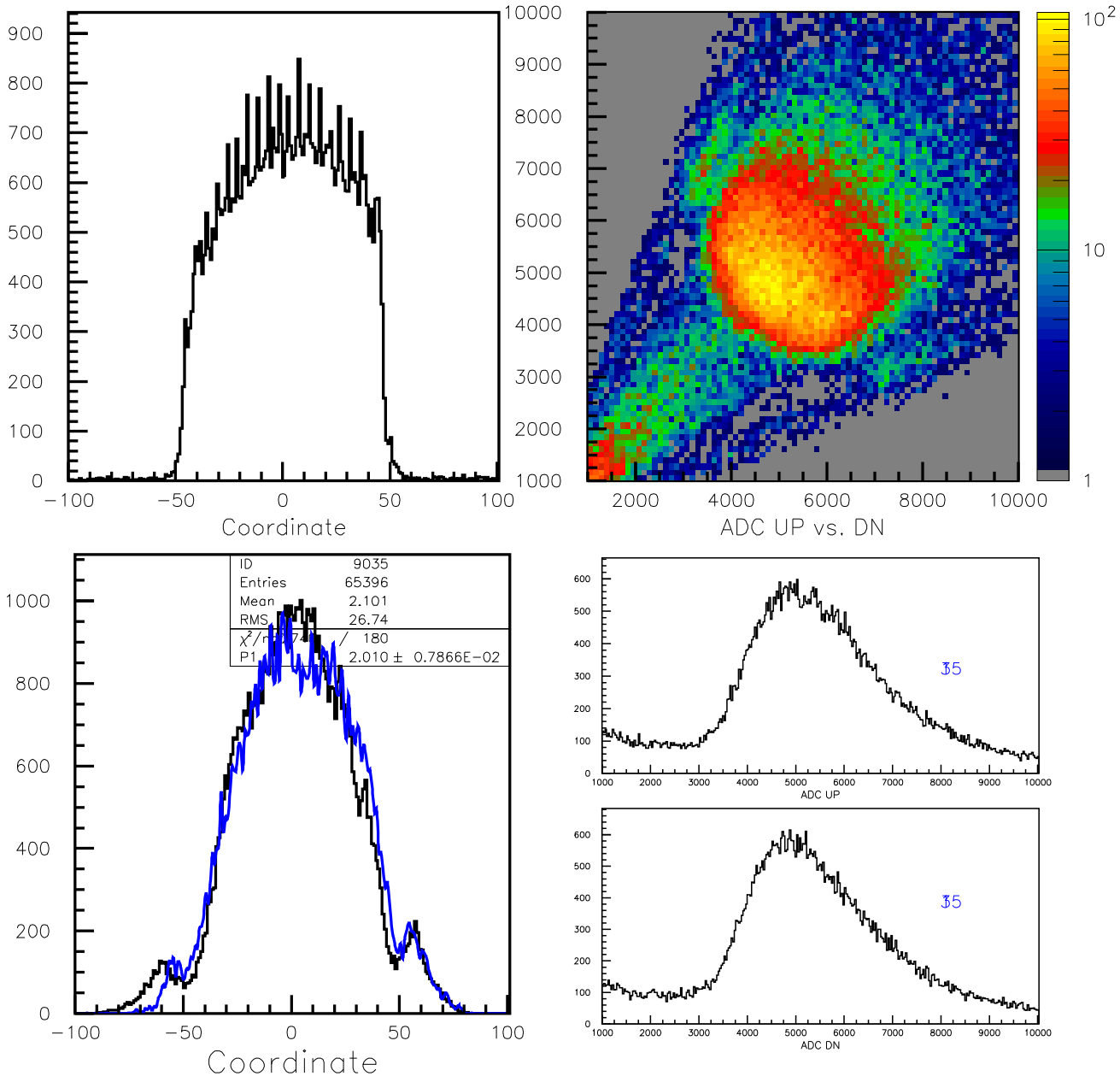

Figure 47: Data for counter #35.

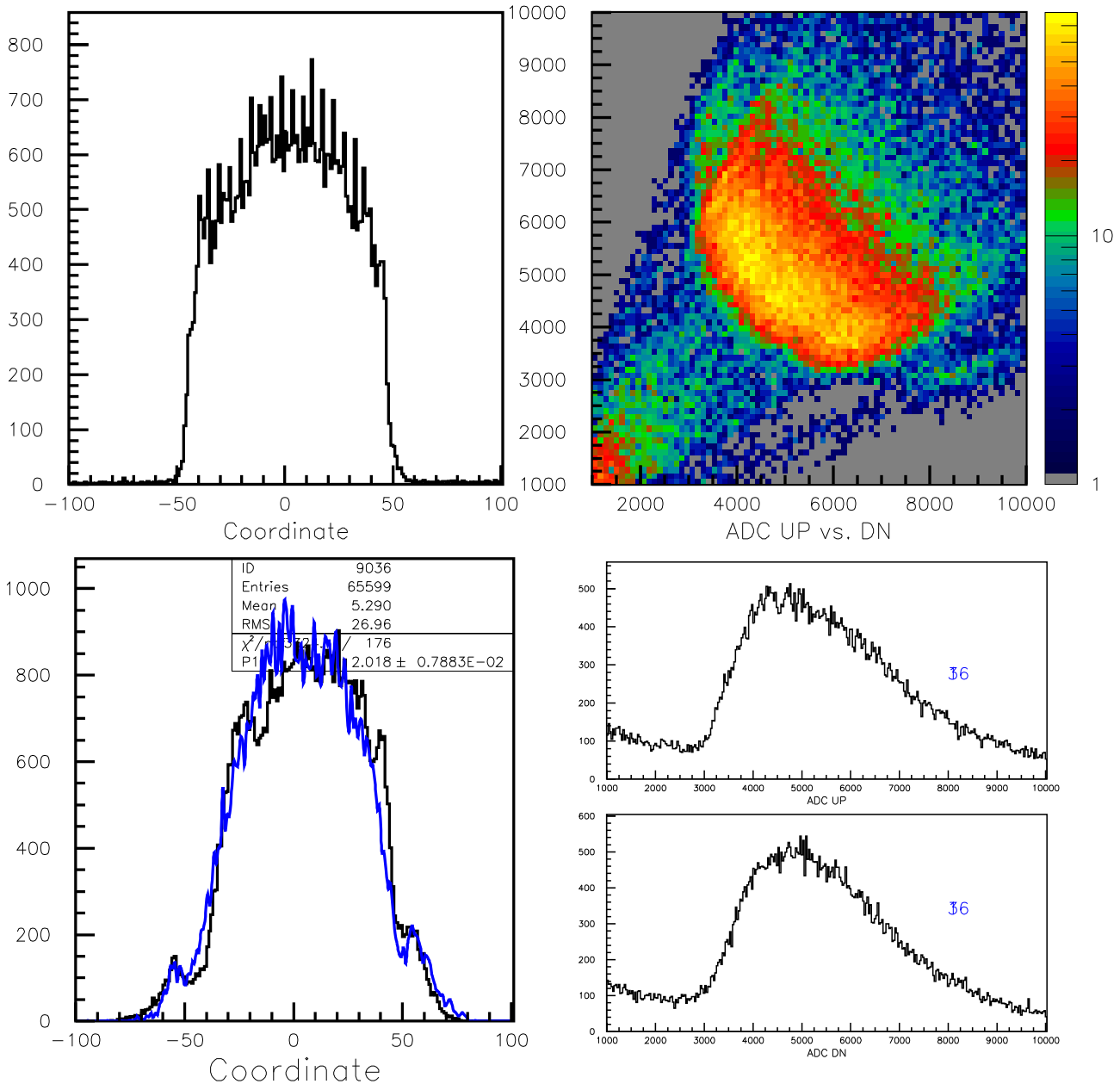

Figure 48: Data for counter #36.

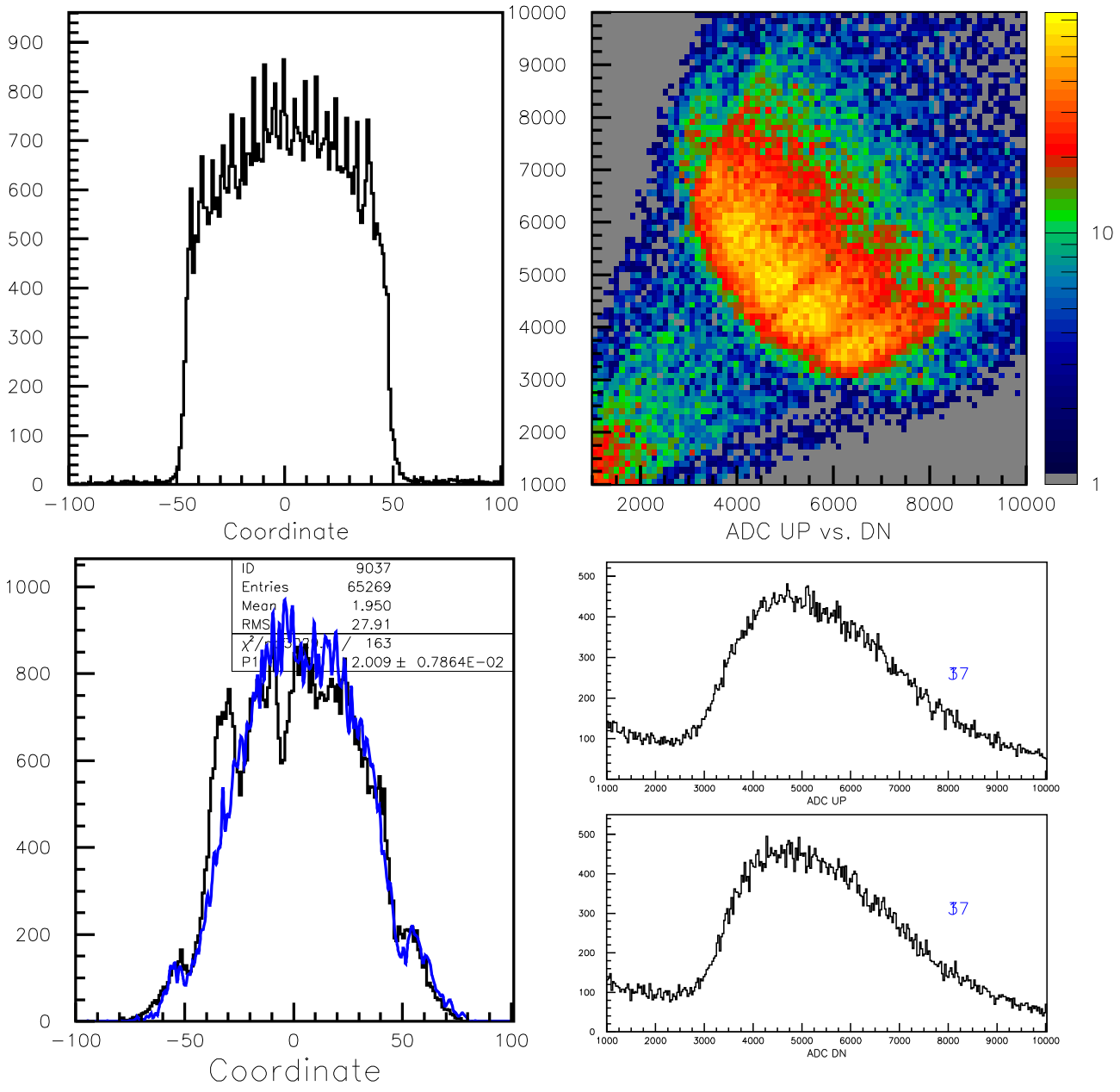

Figure 49: Data for counter #37.

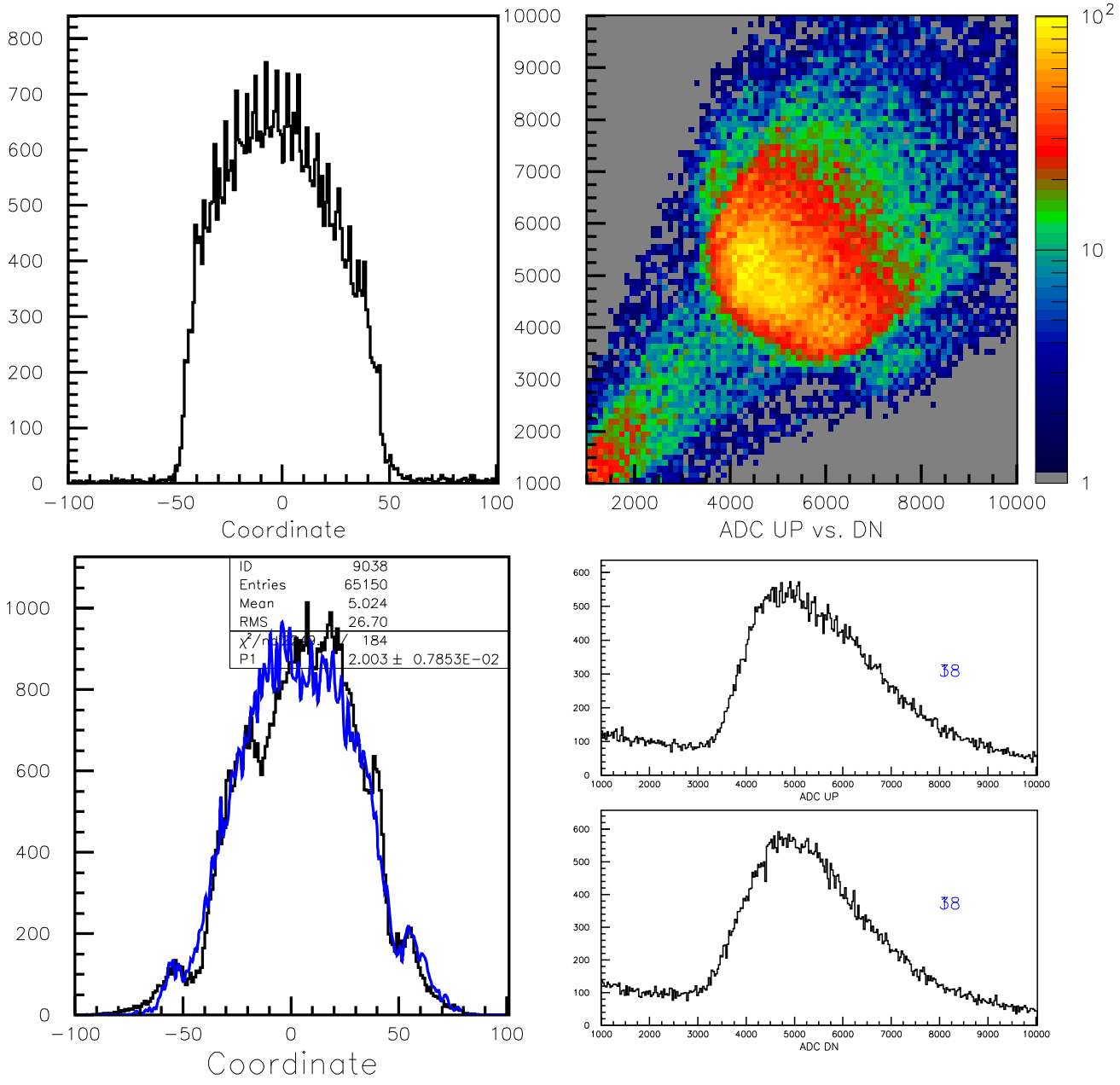

Figure 50: Data for counter #38.

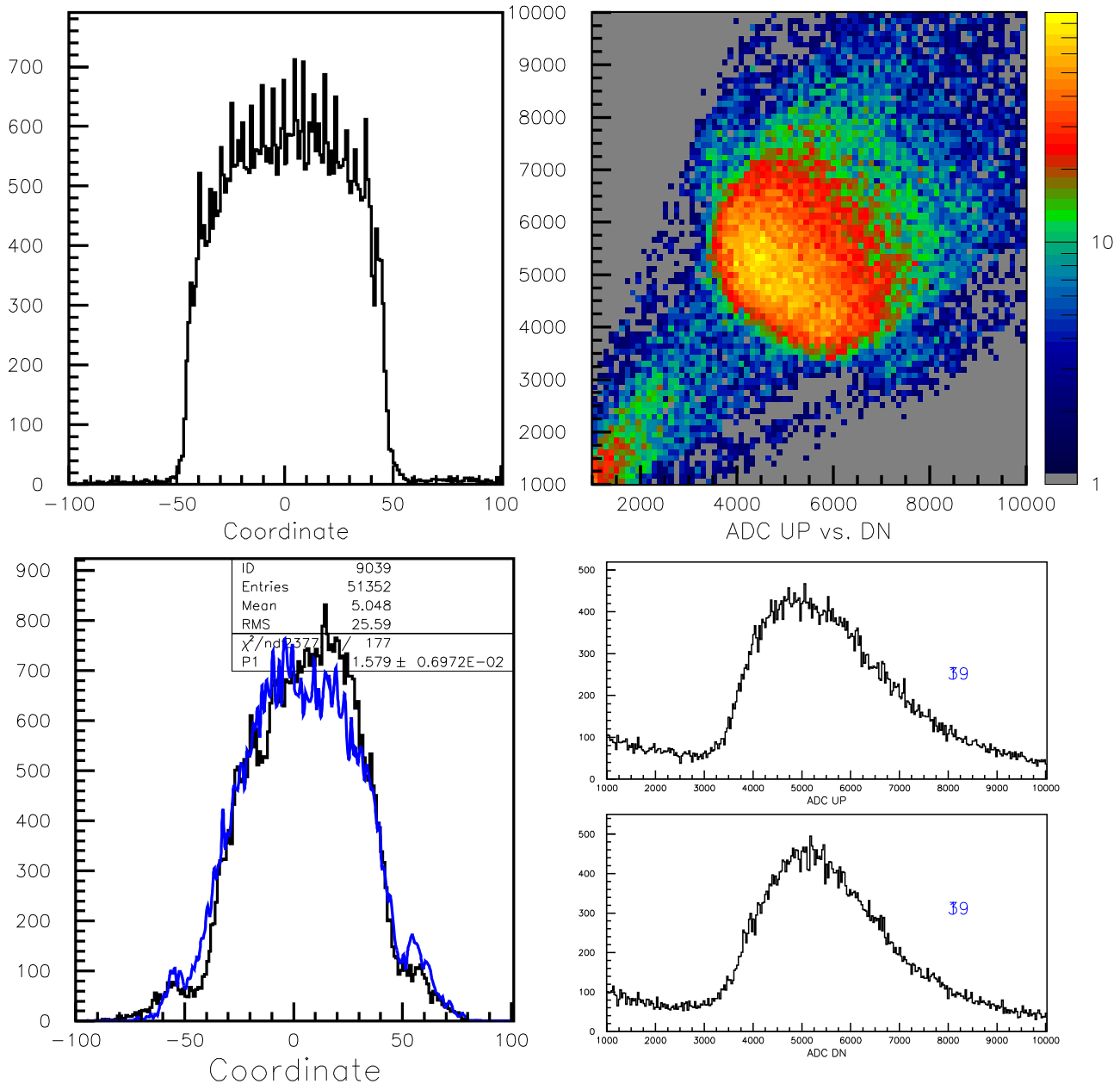

Figure 51: Data for counter #39.

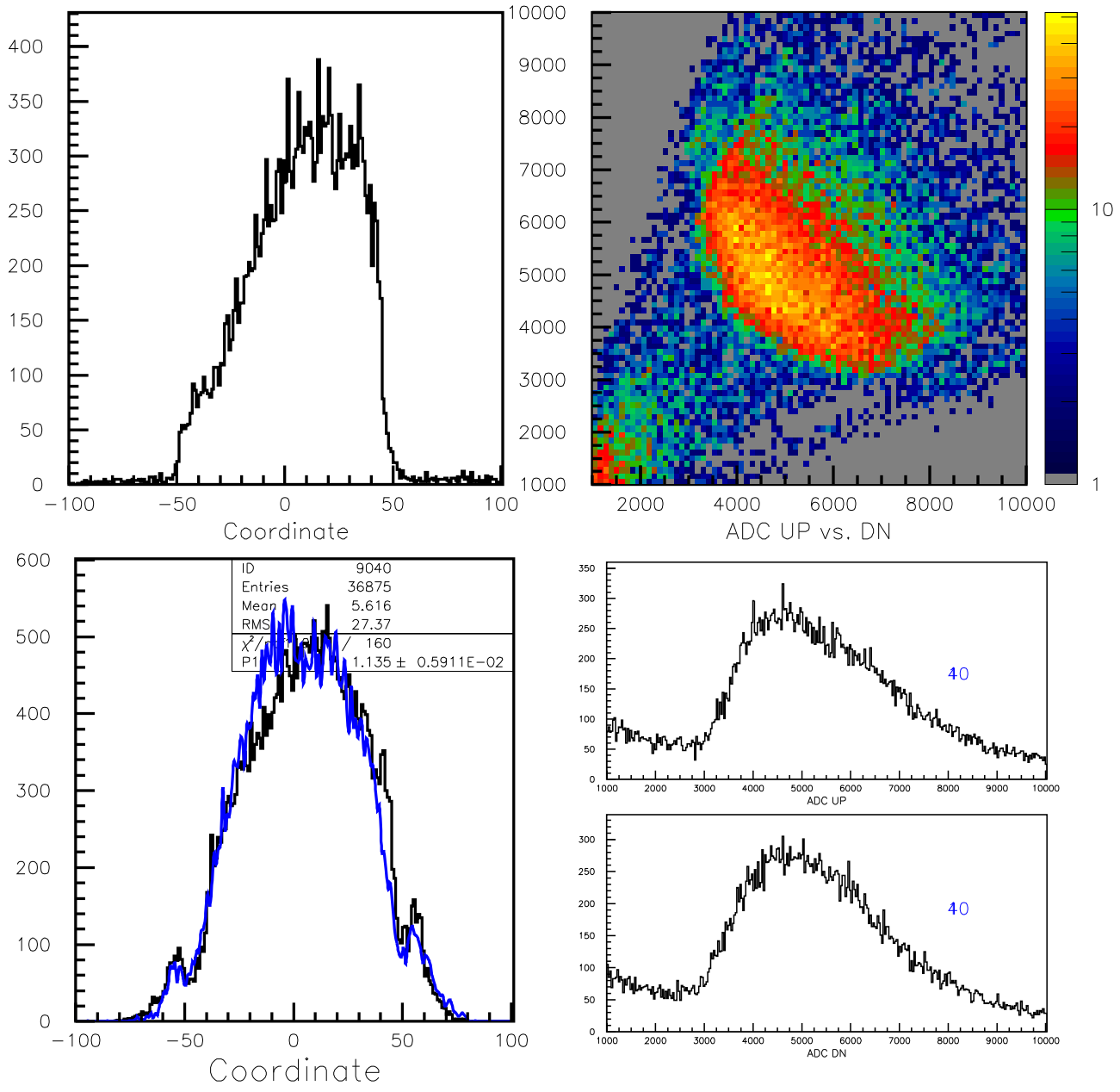

Figure 52: Data for counter #40.

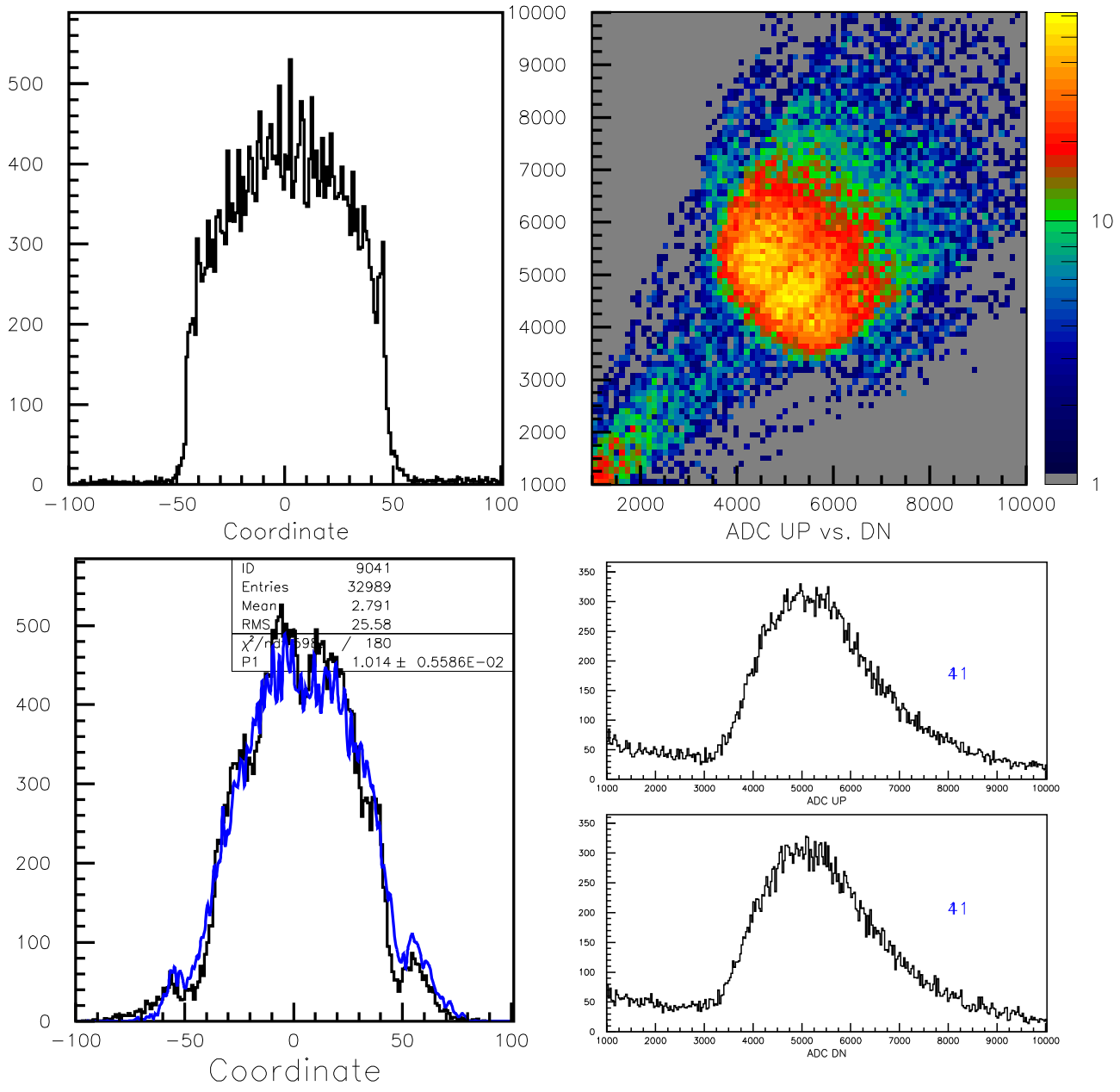

Figure 53: Data for counter #41.

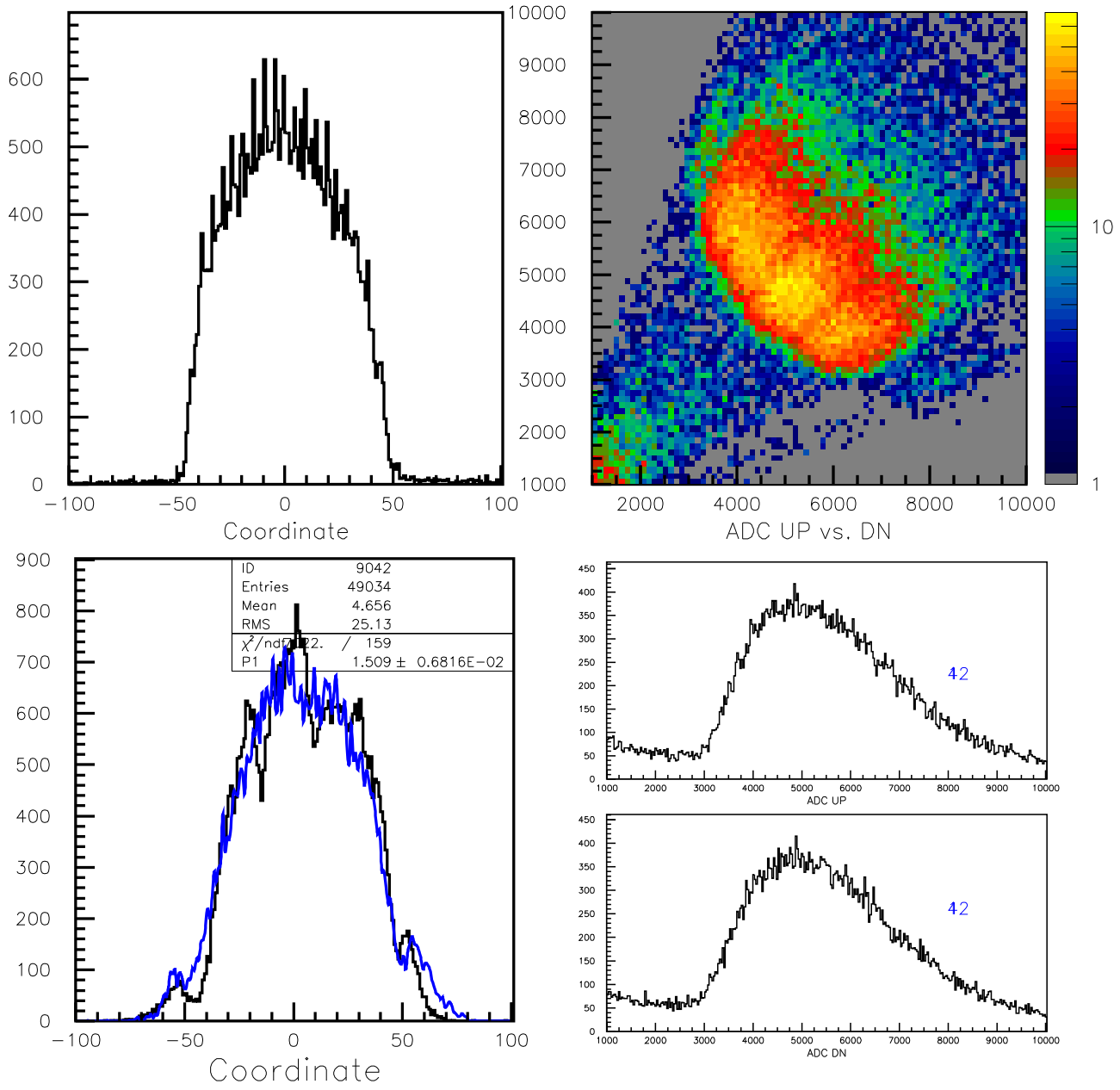

Figure 54: Data for counter #42.

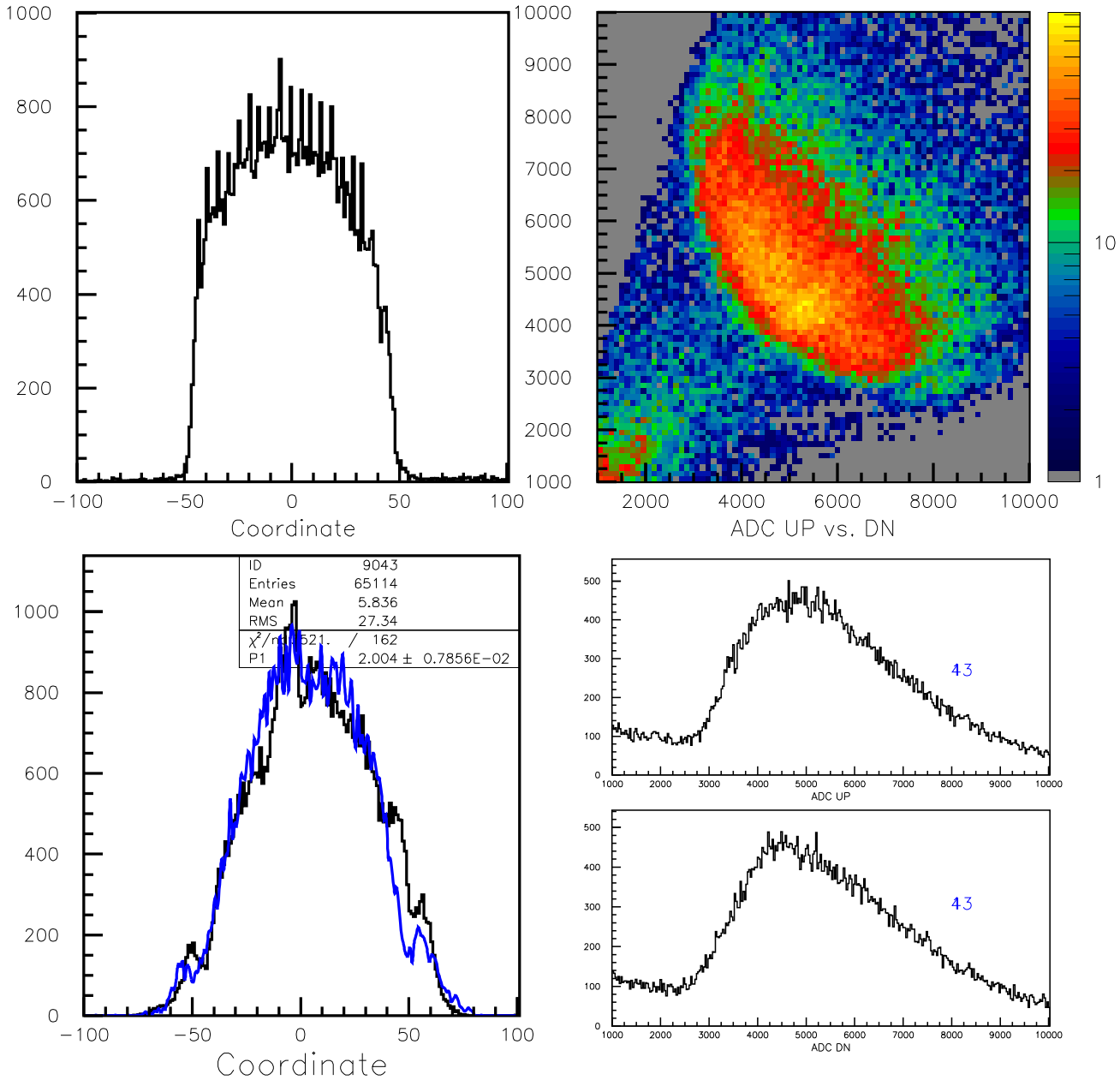

Figure 55: Data for counter #43.

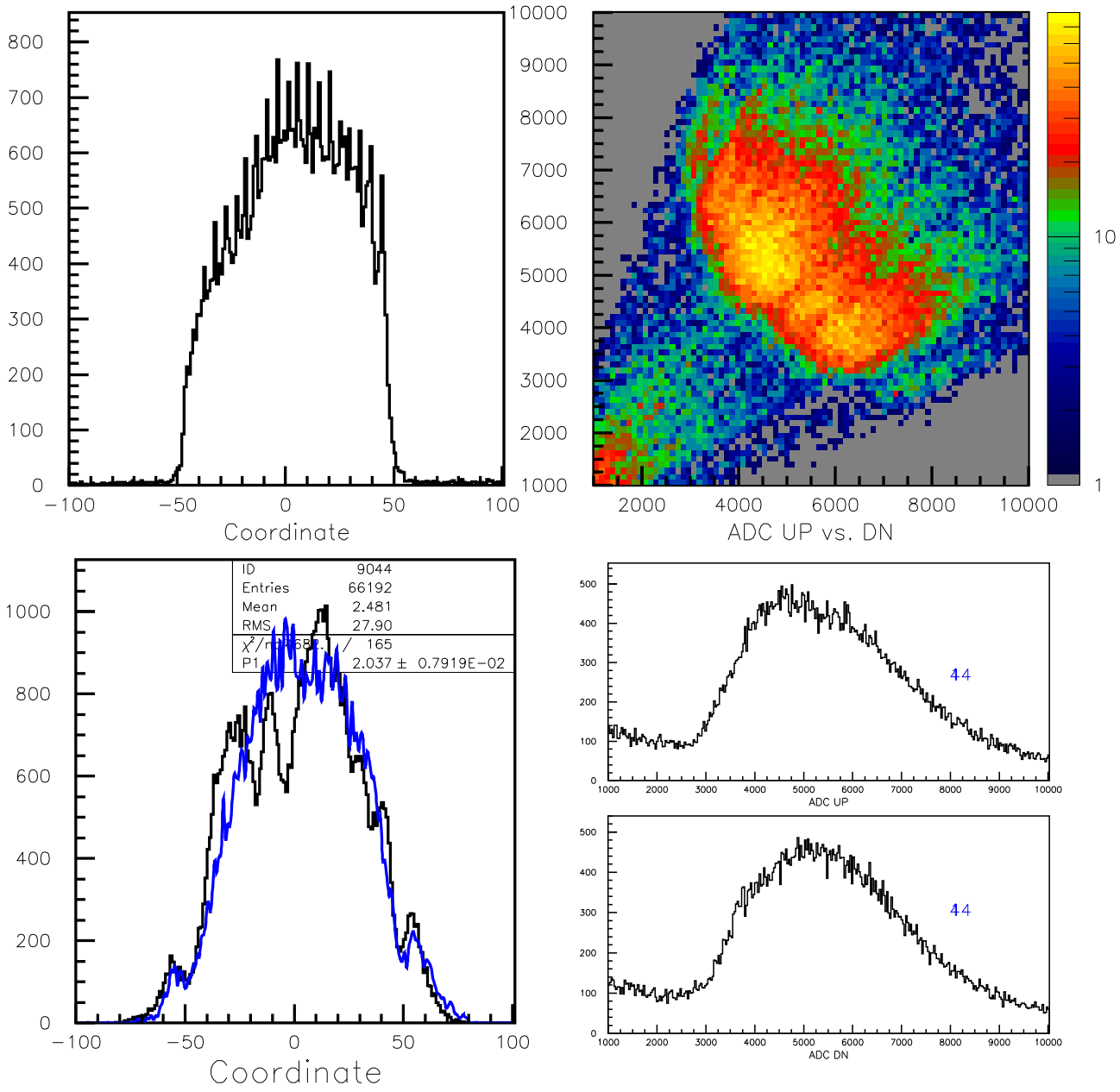

Figure 56: Data for counter #44.

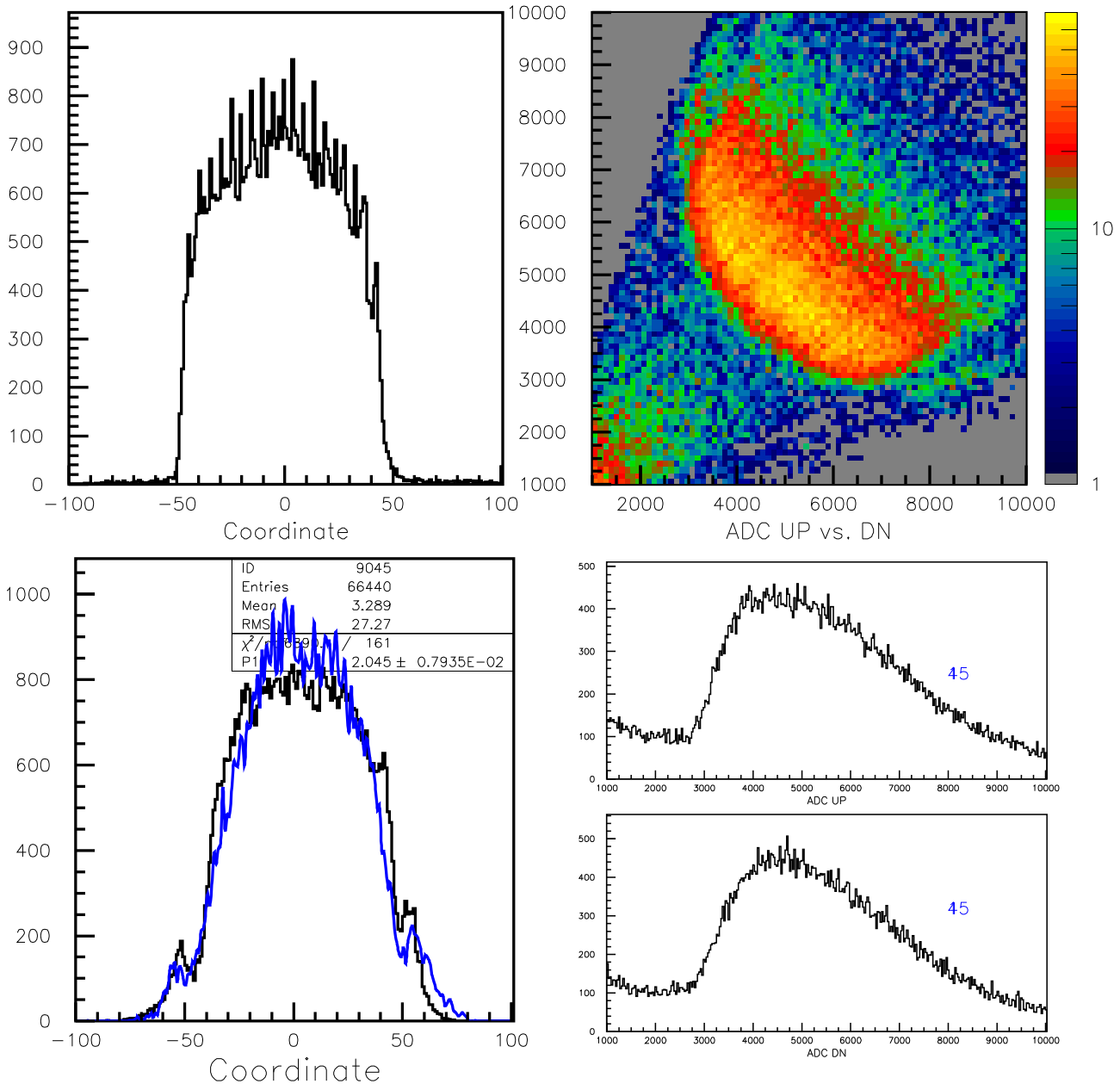

Figure 57: Data for counter #45.

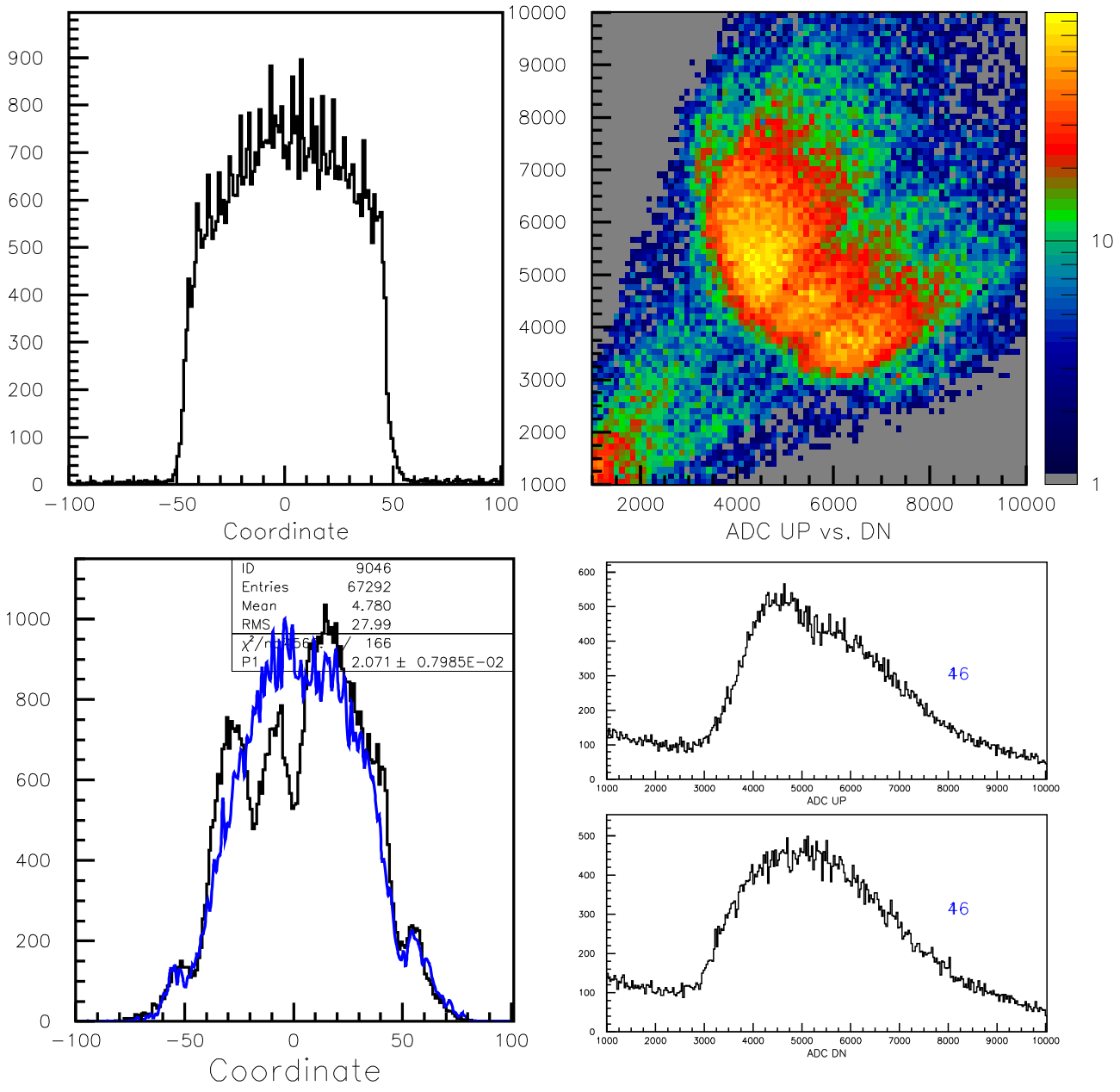

Figure 58: Data for counter #46.

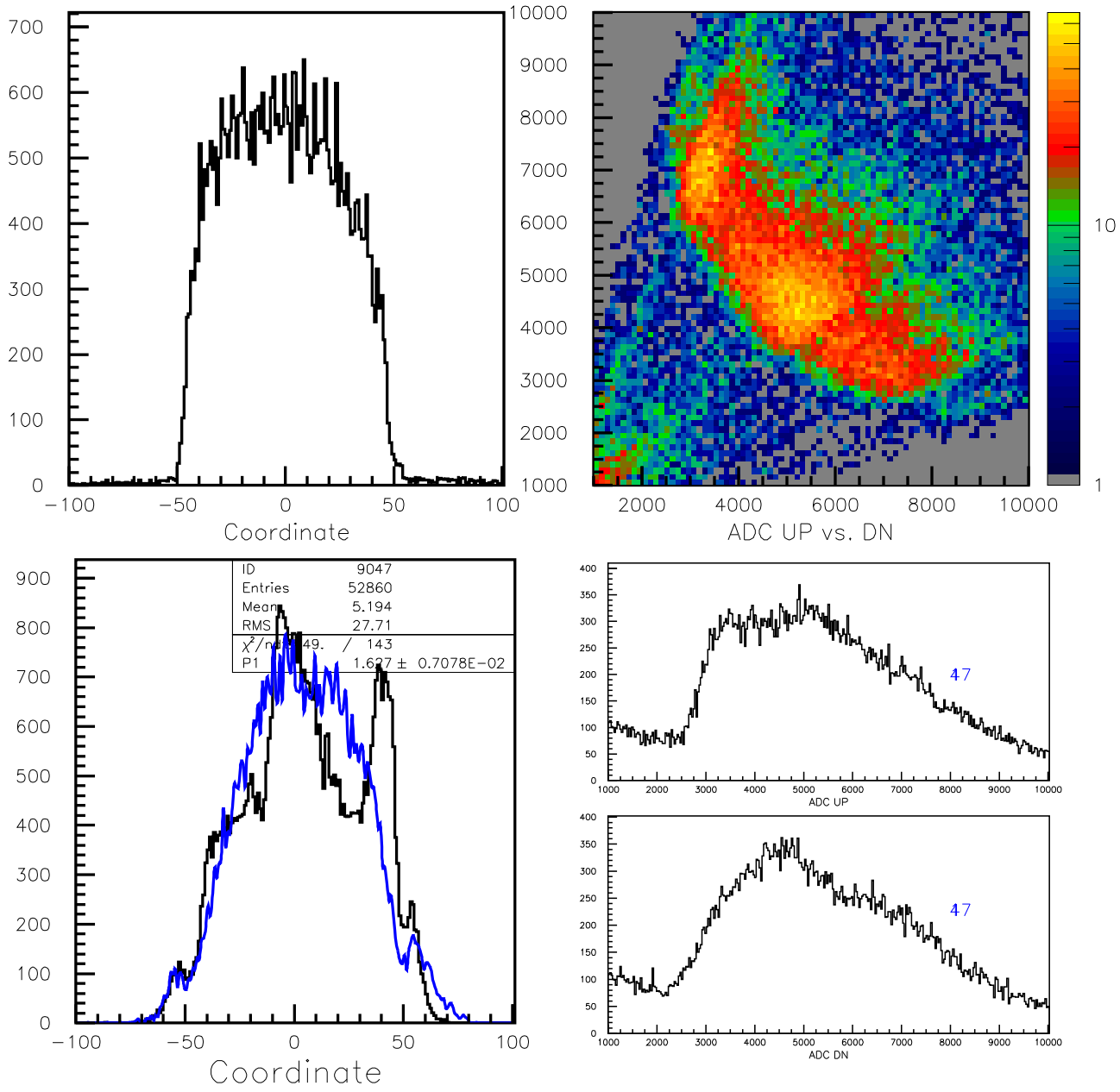

Figure 59: Data for counter #47.

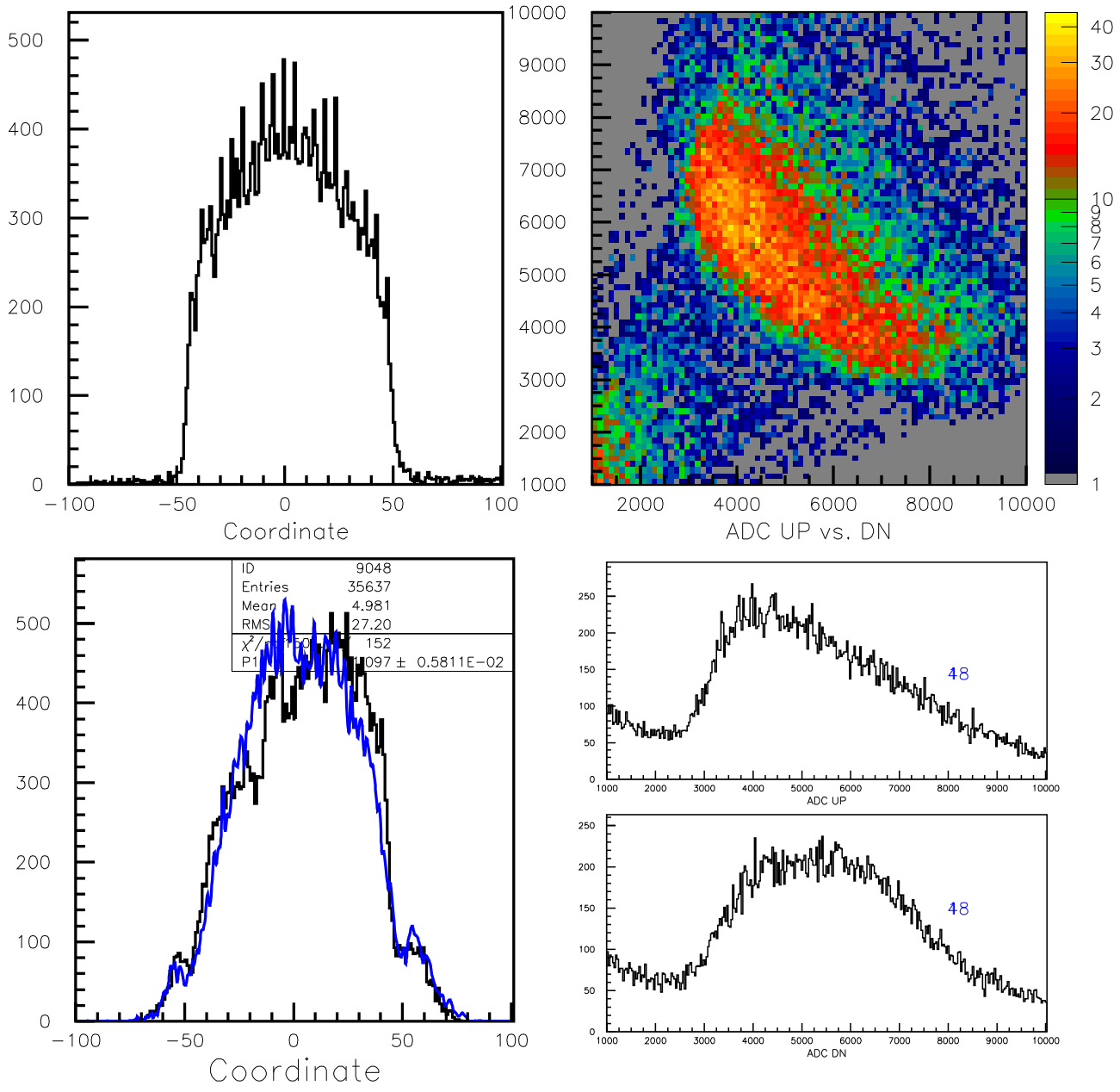

Figure 60: Data for counter #48.

4 Recommendations

Each of the counters in the CTOF cosmic ray test stand should, in the ideal case, give a comparable response in each of the higher-level and lower-level quantities shown. Counters that are different are candidates for further inspection due to problems from poor surface quality. Note that the timing resolutions measured show that the resolution for the counters with the high-pitch angle upstream light guide have slightly better resolution than for those with the low-pitch angle upstream light guide.

To date, four counters have been re-sanded and re-polished, #37, #44, #46, and #48. The before/after refinishing work showed significant performance improvements, but the data shows that in several cases, additional re-surfacing work is necessary. Since we resurfaced the four counters, we have worked to improve our polishing technique significantly.

In order to make decisions about the surface quality of the individual counters we have computed a quality factor for each counter. This quality factor was defined as:

$$\mathcal{QF} = \frac{10}{\chi^2_{coor}}, \tag{2}$$

where χ^2_{coor} is the χ^2 of the fit of the ADC-based coordinate distribution for the reference counter #17 to each of the other counters. This quality factor is plotted vs. counter number in Fig. 61. The counters highlighted in red represent those for which resurfacing is recommended based on the study of the data and the associated quality factor. This list is given by:

- Low-pitch angle design: #5, #7, #12, #13
- High-pitch angle design: #33, #44, #46, #47

While there are certainly surface quality issues in other scintillation bars beyond these, a somewhat arbitrary quality threshold had to be defined in order to keep the rework finite. Also note that during the resurfacing work on counters #37, #44, #46, and #48, only the scintillation bars were unwrapped. The VM2002 and Tedlar wrapping on the light guides were not removed. Thus we could not fully inspect the surface quality of the Acrylic light guides themselves. However, we could visually inspect the last 6 in of each light guide about the glue joints to the scintillation bars. The portion of the light guides that we could see did look of very good surface finish.

5 Conclusions

During cosmic ray studies of the CTOF counters, we found clear evidence of surface quality problems on the scintillation bars that likely affect all bars to some degree. The root cause for what gave rise to the crazing will likely never be fully known. However, we have presented the evidence of our findings to a wide range of experts at JLab (Elton Smith, Youri Sharabian, Stepan Stepanyan, Eugene Pasyuk) and at the scintillation bar manufacturer Eljen Technologies (Charles Hurlburt). The cause of the crazing is most likely due to one of two factors. The first is chemical poisoning due to the improper use of cleaning solvents

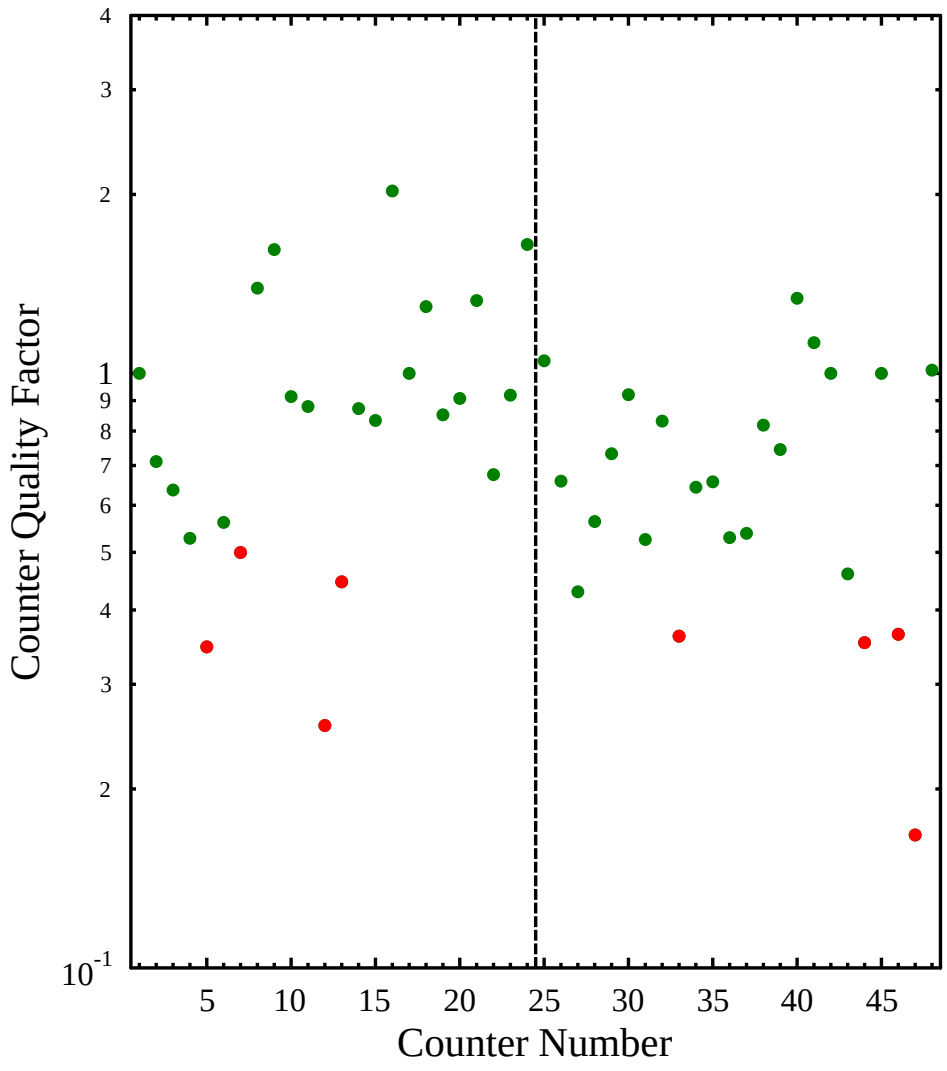

Figure 61: Plot of the counter quality factor vs. counter number. The red points are those counters that are defined to have the worst surface quality as given by this metric. See text for details. The vertical line separates the CTOF counters of the low-pitch angle design (#1 → #24) from those of the high-pitch angle design (#25 → #48).

(ethanol, methanol, acetone) and the second is due to stresses induced in the material during machining. While we cannot point to one or the other of these with absolute certainty, the best evidence suggests the crazing problems are linked to chemical poisoning. The worry regardless of the root cause of the crazing is that the micro-cracks will continue to propagate in the scintillation bars resulting in a slowly worsening performance with time. The best way to track this is to continue to study the performance of the CTOF scintillation bars between now and the end of spring 2016. In this way we can track the quality factor of the bars as a function of time to see whether or not the response is stable for both the bars that have been resurfaced and for the bars that have not been resurfaced.